Structural and functional analysis of cGMP dependent protein kinase I (cGKI) and LIM kinase 1 (LIMK1) engaged in BMP signaling crosstalk

Inaugural-Dissertation
to obtain the academic degree
Doctor rerum naturalium (Dr. rer. nat.)
submitted to the Department of Biology, Chemistry and Pharmacy
of Freie Universität Berlin

by
Alessandra Beltrami
from Udine, Italy

Berlin, May 2012

Research for this thesis was conducted from 2008 till 2012 under the supervision of Prof. Wolfram Saenger and Prof. Petra Knaus at the Institute for Crystallography at the FU Berlin. Most part of this work is the result of the collaboration with the Structural Genomics Consortium at the Oxford University, under the supervision of Dr. Alex Bullock.

This work was generously funded by the SFB449, the European Molecular Biology Organization and the Dahlem Research School.

1. Reviewer: Prof. Dr. Wolfram Saenger

2. Reviewer: Prof. Dr. Udo Heinemann

Date of the oral examination: 29.06.2012

Abbreviations

% (v/v)	volume of solute with respect to the final volume of the solution
% (w/v)	%(w/v) grams of solute per 100 ml solution
Å	Angstrom (10^{-10} m)
ActRI	Activin type I receptor
ActRII	Activin type II receptor
ADF	Actin depolymerizing factor
ADP	Adenosine diphosphate
ALK	Activin receptor-like kinase
ALP	alkaline phosphatase
BISCs	BMP induced signaling complexes
BMP	Bone Morphogenetic Protein
BMPRI	Bone Morphogenetic Protein type I receptor
BMPRII	Bone Morphogenetic Protein type II receptor
cGKI	cGMP-dependent protein kinase I
c-Src	Cellular sarcoma
Cdc42	Cell division control protein 42 homolog
cGMP	3'-5'-cyclic guanosine monophosphate
CID	Collision-Induced Dissociation
Co-Smad	Common Smad
c-Src	Cellular sarcoma
DEAE	Diethylaminoethyl
DLS	Dynamic Light Scattering
DSF	Differential scanning fluorimetry
DTT	dithiothreitol
ECM	extracellular matrix
EDTA	Ethylenediamine tetraacetic acid
ERK	Extracellular signal regulated kinase
F-actin	Filamentous actin
FBS	Fetal Bovine Serum
G-actin	globular actin
GDP	Guanosine diphosphate
GSK	glycogen synthase kinase
GST	Glutathione S-transferase
GTP	guanosine 5´-triphosphate
GTPase	Guanosine triphosphatase
HEPES	N-(2-hydroxyethyl)-piperazine-N'-2-ethanesulfonic acid,
I-Smad	Inhibitory Smad
IMAC	immobilized metal affinity chromatography
IPTG	Isopropyl β-D-1thiogalactopyranoside
ITC	Isothermal Titration Calorimetry
JNK	c-Jun N-terminal kinase
LATS1	large tumour suppressor 1
LB	Luria Bertani medium
LC-MS	liquid chromatography–mass spectrometry
LIMK	LIM kinase
MAP	Microtubule-associated protein
MAPK	Mitogen activated protein kinase

MAPKK	Mitogen activated protein kinase kinase
MAPKKK	Mitogen activated protein kinase kinase kinase
MES	2-(N-morpholino)ethanesulfonic acid
MH	Mad homology domain
MPD	2-Methyl-2,4-pentanediol
Ni-NTA	Ni^{2+} nitrilotriacetic acid
p38	38 kDa stress activated protein kinase
PAGE	polyacrylamide gel electrophoresis
PAH	pulmonary arterial hypertension
PAK	p21-activated kinase
PCR	Polymerase chain reaction
PDB	Protein data bank
PDZ	PSD95, DlgA, Zo-1
PEG	Polyethylene glycol
PEI	polyethyleneimine
PFCs	preformed complexes
PI3K	phosphoinsitide-3 kinase
PKC	Protein kinase C
PMSF	phenylmethanesulfonylfluoride
PP2A	Protein phosphatase 2A
R-Smad	Receptor-regulated Smad
Rac1	Ras-related C3 botulinum toxin substrate 1
RACK1	Receptor of Activated C Kinase 1
Rmsd	root mean square deviation
ROCK	Rho kinase
SDS	Sodium dodecyl sulfate
SEC	size exclusion chromatography
Sf	*Spodoptera frugiperda*
sGC	soluble guanylyl cyclase
SGC	Structural Genomics Consortium
SOC medium	Super optimal broth with catabolite repression
SPG system	succinic acid, phosphate, glycine system
SSH	Slingshot
TB	Terrific Broth
TCEP	Tris (2-Carboxyethyl) phosphine
Tctex-1	T-complex testis-expressed-1
TEV	Tobacco etch virus
TGF-ß	transforming growth factor ß
TKL	tyrosine kinase-like
Trb-3	Tribbles homolog-3
Tris	2-Amino-2-(hydroxymethyl)propane-1,3-diol
VSMCs	vascular smooth muscle cells

Acknowledgments

First of all, I would like to thank Prof. W.Saenger for giving me the possibility to work in his laboratory and for the support he gave me over the years, being always by my side.

I also would like to thank Prof. P.Knaus for sharing with me the SFB449 project on BMP signaling, and to introduce me to Dr. A.Bullock (SGC, University of Oxford). This collaboration was a fantastic scientific experience which made the results of this Ph.D. work possible.

A special thank deep from my heart to Dr. A.Chaikuad for being a fantastic postdoc, always available, patient and happy to answer all my questions about crystallization techniques, data collection, structure determination, validation…and so on and so on…☺

I kindly thank Prof. U. Heinemann who accepted to chair the thesis evaluation committee.

I am very grateful to the all Growth Factor Signaling group for welcome me as I was a part of the group, Eidarus Salah and Dr. P. Mahajan for the excellent training in the insect cell culture laboratory, Tracy Keates for her kindness and her fantastic good mood. Thanks to the all SGC members to make the Structural Genomics Consortium a special place to work.

I like to thank the all AG Saenger group members for the nice time we have spent together and that unfortunately will never be again.

An extraordinary thank to Sofia Banchenko for simply be herself and Gerburg Schwärzer for discussions and support.

Thanks so much to my "italian family" in Berlin over the years: Ester, Chiara, Mauro, Paola, Silvia, Santina, Daniele, Riccà, Marcello, Annamaria, Elena, Peppe, Giovà, Luciano, Alessandro and many many more.

Last, but not least, a special thank to my parents for encouraging me to follow my dreams and their constant support. And of course I say thank to my beloved husband Olaf for his unconditional love.

Table of Contents

1 Introduction

1.1 TGF-beta superfamily

The transforming growth factor ß (TGF-ß) superfamily, comprised of a large number of multifunctional cytokines, regulates a wide variety of biological responses in embryonic and mature tissues (Attisano and Wrana, 2002; Derynck and Zhang, 2003; Schmierer and Hill, 2007; Shi and Massague, 2003; ten Dijke and Hill, 2004; Wu and Hill, 2009). The TGF-ß superfamily includes more than 30 identified ligands that regulate an array of cellular processes including cell proliferation, lineage determination and differentiation, migration, adhesion and apoptosis. Non-functional TGF-ß signaling is involved in serious human diseases such as fibrosis, cancer and hereditary disorders such as pulmonary arterial hypertension (PAH) (Lane et al, 2000). This superfamily can be divided into three distinct branches: TGF-ß, Activins, and Bone Morphogenetic Proteins (BMPs).

BMPs were first discovered in the 1960s as osteoinductive proteins (Cheng et al, 2003; ten Dijke, 2006; Urist, 1965), but are now well known as multi-functional growth factors involved in organ development and tissue homeostasis (Chen et al, 2004; Hayashi et al, 2005; Yanagita, 2009). TGF-ß ligands bind with different affinities to BMP/TGF-ß receptors on the cell plasma membrane and initiate signaling cascades (Attisano and Wrana, 2002; Derynck and Zhang, 2003; Schmierer and Hill, 2007; Shi and Massague, 2003; ten Dijke and Hill, 2004; Wu and Hill, 2009).

1.2 BMP receptors

Members of the BMP family signal through two types of serine-threonine kinase receptors, which are required for signal transduction (Heldin et al, 1997; Derynck, and Zhang, 2003). Both receptors exhibit an extracellular ligand binding domain, a single transmenbrane domain and an additionally cytoplasmatic serine/threonine kinase domain.

Three receptors (BMPRIa, BMPRIb, Alk2) have been identified as BMP type I receptors, that are well conserved and show highly specific ligand binding. Mammalian BMP type I receptors show a molecular weight of about 50-55 kDa, and carry two characteristic motifs involved in signal transduction. The GS-box is a

glycine/serine-rich domain (-S_{216}-G-S-G-S-G_{221}-, positions according to BMPRIa) which is the target site for the phosphorylation of BMP receptor I and located at the N-terminal lobe of the kinase domain (Wrana et al, 1994). The second motif within the kinase domain is a small region of 8 amino acids called the L45 loop. It determines the specificity for the receptor-regulated Smads (R-Smads), which are phosphorylated by BMP receptor type I and shuttle the BMP signal directly into the nucleus (Feng and Derynck, 1997). Additionally, R-Smads carry the so-called L3 loop in their C-terminal MH2 domain, which comprises a sequence of 17 amino acids involved into the specific recognition of the L45 loop of BMP type I receptor.

Type II BMP receptors (BMPRII, ActRII and ActRIIb) also exhibit a similar structure to the type I receptors but feature higher glycosylation and show a molecular weight of about 75 KDa. Furthermore, the type II receptor kinase is constitutively active. After ligand binding type II receptor kinase phosphorylates the GS-box in the type I receptor and thereby activates BMP receptor type I kinase (Attisano et al., 1996; Wieser et al., 1993; Wrana et al., 1994).

Interestingly, BMPRII receptor occurs in two alternative splice variants, the short form (BMPRII-SF) and the long form (BMPRII-LF). BMPRII-LF exhibits a unique C-terminal cytoplasmic tail of 508 amino acids following the kinase domain encoded by exon 12 (Liu et al, 1995; Nohno, et al, 1995; Rosenzweig et al, 1995). The long form with the C-terminal tail is predominantly expressed in most types of cells tested for its presence, while the short form lacking the long C-terminal tail may be expressed only in certain types of cells (Foletta et al, 2003). It has been postulated that this region functions as a binding site for multiple adaptor proteins to regulate BMP signaling specificity.

The oligomerization pattern of BMP receptors is highly flexible and dependent on ligand modulation. Furthermore, the binding mode of BMP2 ligand can pave the way for two different signaling pathways: the Smad dependent or the Smad independent signaling. In the absence of ligand stimulation, BMP receptors are present as pre-existing homodimer and heterodimer complexes at the cell surface. The canonical Smad pathway is activated when ligands bind to so-called preformed complexes (PFCs) of BMPRI and BMPRII (Gilboa et al, 2000). Alternatively, ligands can bind first to the high affinity BMP type I receptor, which subsequently recruits the low

affinity BMPRII into the signaling complex. This alternative binding mode leads the formation of the BMP-induced signaling complexes (BISCs). It initiates Smad-independent signaling like activation of the MAPKs p38, Erk and JNK and PI3K/Akt signaling via BMP receptors themselves or via receptor interacting proteins. Thereby, the activation of the Tak1-Mkk3/6-p38 signaling cascade is well characterised and leads to the activation and/or expression of osteoinductive factors such as Runx2 and alkaline phosphatase (ALP) (Yamaguchi et al, 1999; 2010). Consequently, receptor interacting proteins regulate BMP signaling.

1.3 BMP receptor II interacting proteins

Proteins interacting with the BMPRII were classified into five different groups according to the assigned function in signaling, cytoskeleton regulation, metabolism, dubious function and hypothetical novel proteins. Moreover, Hassel et al. showed that the tail domain of BMPRII is a docking site for a certain number of proteins involved in Smad independent pathways such as FGF-dependent signaling (FGFR substrate), trafficking (Rab transferase), MAPK signaling (MOS and MAPKKK8), axon guidance (SemF) and protein kinase C (PKC)-dependent signaling (PKCß) required for apoptosis. Further studies have also identified more BMPRII-tail interacting proteins (Table 1.1), demonstrating that these interactors regulate both Smad dependent and independent signaling pathways. C-Kit, Trb-3, cGKI (§ 1.5) and PP2A associate with the tail domain of BMPRII enhancing Smad signaling (Bengtsson et al, 2009; Chan et al, 2007; Hassel et al, 2006; Schwappacher et al, 2009), whereas c-Src, Tctex-1, LIMK1 (§ 1.6) and JNK regulate the signal cascade trough the non-Smad pathway (Wong et al, 2005; Machado et al, 2003; Foletta et al, 2004; Lee-Hoeflich et al, 2004; Podkowa et al, 2010).

Table 1.2. Interacting partners of the BMP type II receptor, BMPRII.

BMPRII interacting protein	Description	Binding region on	Proposed function	Reference
Tctex-1	Dynein light chain carboxy-tail PPH mutations abolish	BMPRII-induced	Tctex-1 phosphorylation	(Machado et al, 2003)
LIMK1	Ser/Thr kinase	carboxy-tail	Activation of LIMK1 leads to actin remodelling and dendritogenesis	(Foletta et al, 2004; Lee-Hoeflich et al, 2004)
c-Src	Tyrosine kinase	carboxy-tail	PPH mutations affect interaction & BMP-induced phosphorylation of c-Src	(Wong et al, 2005)
Caveolin-1	Caveolae component	Kinase domain	Regulation of BMPRII localization	(Hartung et al, 2006; Ramos et al, 2006; Wertz and Bauer, 2008)
c-Kit	Receptor tyrosine kinase	carboxy-tail	Induces BMPRII phosphorylation, enhances BMP signaling	(Hassel et al, 2006)
Dullard	BMP receptor phosphatase	N/A	Promotes BMP receptor degradation during neural induction	(Satow et al, 2006)
RACK1	Adaptor protein	kinase domain	PPH mutations affect interaction with RACK1	(Zakrzewicz et al, 2007)
Trb-3	pseudokinase	carboxy-tail	Enhances BMP signaling by promoting Smurf1 degradation	(Chan et al, 2007)
TrkC	Receptor tyrosine kinase	outside the carboxy-tail region	Prevents BMPRI interaction, suppresses BMP signaling	(Jin et al, 2007)
cGKI	Ser/Thr kinase	carboxy-tail	Phosphorylates BMPRII, leads to amplification of BMP signaling	(Schwappacher et al, 2009)
NIPA1	Endosomal transporter	outside the carboxy-tail region	Promotes BMP receptor endocytosis to suppress BMP signaling	(Tsang et al, 2009)
PP2A	Smad1 linker phosphatase	carboxy-tail	Amplification of BMP signaling	(Bengtsson et al, 2009)
JNK	MAPK	carboxy-tail	Activation of JNK leads to microtubule stabilization & dendritogenesis	(Podkowa et al, 2010)

1.4 Roles of BMPRII in biological processes

BMPs regulate a certain range of cellular functions, which are involved in embryonic development from mesoderm formation to organogenesis. Within diverse species, BMPRII is ubiquitously expressed in almost all tissues during embryogenesis and in adulthood, suggesting an important role in many biological processes. The germline loss of function mutations in the bone morphogenetic protein receptor II (*bmprII*) gene have been identified on chromosome 2q33 (Deng et al, 2000). Mutations in the *bmprII* gene occur in patients with familial and sporadic pulmonary arterial hypertension (PAH), formerly known as primary pulmonary hypertension (PPH) and are twice as common in females than males. PAH is a dominant autosomal vascular disorder with an estimated incidence of 1 to 2 per million cases per year, which is characterized by abnormally high blood pressure (hypertension) in the pulmonary artery. Hypertension occurs when the blood vessel that carries blood from the heart to the lungs and vice versa narrows in diameter, thereby increasing the blood flow resistance through the lungs. Signs and symptoms, such as breathlessness, chest tightness, fainting spells, dizziness, ankles or legs swelling and a racing pulse, occur when the disease has already progressed beyond a mild stage. Indication suggests that *bmprII* may play important roles in the homeostasis of the pulmonary vascular system and also contribute to the maintenance of normal pulmonary vascular structure and function (West et al, 2004). Most of the BMPRII loss of function mutations promote cell division or prevent cell death, resulting in an overgrowth of cells in small arteries throughout the lungs.

1.5 cGMP-dependent protein kinases (cGKs)

BMPRII crosstalk pathways are assumed to be involved in the PAH phenotype; it was hypothesized that the loss of BMPRII function in vascular smooth muscle cells (VSMCs) is sufficient to effect pulmonary hypertension disease (West et al, 2004). Cyclic GMP-dependent protein kinase I (cGKI) plays an essential role in regulating cardiovascular and neuronal functions and was shown to interact with and phosphorylate the tail domain of BMPRII. It was also shown that overexpression of cGK recovers BMP deficient signaling resulting in PAH. cGK is a key mediator of the nitric oxide/cGMP signaling pathway. The synthesis of cGMP via nitric oxide

(NO)-sensitive guanylyl cyclases is highly regulated and dysfunction of these processes affects mainly vascular physiology. Signaling via cGMP and cGMP-dependent protein kinases (cGKs) plays a key role in vascular homeostasis, cellular permeability, cell survival, proliferation and in the regulation of the vascular smooth muscle cell (VSMC) phenotype. Moreover, it was demonstrated that cGKI enhances Smad signaling at multiple levels of the BMP cascade, first interacting with BMPRII and modulating the activity of both BMP receptors, enhancing the R-Smad phosphorylation, increasing the Smad signaling response and, at last, regulating specific gene transcription as Smad nuclear co-factor (Schwappacher et al, 2009).

1.5.1 NO and cGMP signal transduction

Nitric oxide (NO) is an uncharged free radical compound and an endogenous cell signal molecule, which has a pivotal role in vascular tone, insulin secretion and peristasis. NO also acts as a neuronal messenger in the nervous systems of vertebrates and invertebrates. It is involved in angiogenesis and plays an important role in the pathology of several inflammatory diseases (Dawson and Snyder 1994; Garthwaite and Boulton 1995; Müller 1997; Boehning and Snyder 2003; Garthwaite 2008).

The best known NO receptor is a soluble guanylyl cyclase (sGC), which gets activated by NO and converts guanosine 5´-triphosphate (GTP) to the second messenger 3'-5'-cyclic guanosine monophosphate (cGMP) (Friebe and Koesling 2003; Koesling et al, 2004; Krumenacker et al, 2004). cGMP was initially discovered in urine, shortly after cAMP discovery, and later on it was shown that cGMP is present in almost all types of cells. This second messenger has an important role in the regulation of many cell signaling events; in fact its targets are cyclic-nucleotide-gated ion channels, cGMP-regulated phosphodiesterases and protein kinase G leading to an increase or decrease of phosphorylated effector proteins (Krumenacker et al, 2004).

1.5.2 cGMP-dependent protein kinase I (cGKI)

The cGMP-dependent protein kinase is a key member of the AGC (cAMP-dependent, cGMP-dependent and protein kinase C) protein kinase family with whom it shares similar basic structural and functional properties. In fact, they share cytoplasmic

serine/threonine kinases that are regulated by secondary messengers such as cyclic nucleotides (cNTs) and are characterised by conserved phosphorylation sites that critically regulate their function. The cGK family is formed by two members. cGKI, is a soluble protein (Kuo and Greengard, 1972) mainly expressed in smooth cell muscle, platelets, cerebellum, hippocampus, neuromuscular junction end plate and kidney (Butt et al, 1993). cGKII is a membrane-bound enzyme identified in the epithelial cells of the intestine, brain and lung.

Two isoforms of cGKI have been described, type Iα (671 aa) and type Iβ (686 aa) that differ only in the N-terminal ~100 amino acids. cGKI is encoded by a single gene localized on chromosome 10q11.2, consisting of 17 exons coding the protein sequence common to both isoforms. Two exons were identified coding type Iα and type Iβ showing different expression patterns in various tissues (Ørstavik et al, 1997).

cGKI exists as a homodimer and is divided into three regions with the specific functions: an N-terminal dimerization domain, a regulatory cGMP binding domain and a catalytic kinase domain at the C-terminus (Figure 1.1).

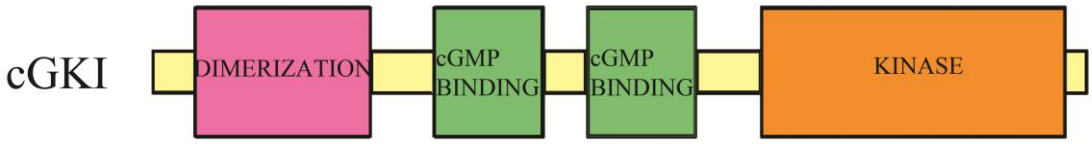

Figure 1.1. cGKI function structure.

The N terminal region includes the first 89 amino acids of type Iα and the first 104 of type Iβ isoform. The crystal structure of cGKIβ N-terminal domain was solved showing a dimerization/docking region (D/D) and an autoinhibitory sequence (Casteel et al, 2010). In fact, the N-terminal region contains a leucine/isoleucine zipper domain that allows dimerization through 5 helices characterizing two and a half pairs of coiled-coils. Only the first ~50 amino acids are ordered in the helices, which are given a smooth curvature. Interestingly, in cGKIβ D/D domain, leucines and isoleucines constitute the hydrophobic core participating in the interhelical hydrophobic interactions and it was demonstrated that the hydrophilic residues presented in the

coiled-coils core are directly involved in dimer formation and trimer inhibition (Gonzales et al, 1996).

Residues Arg26, Glu27, Glu29 and Glu31 form a highly electronegative patch on the N-terminal domain surface, which is not present on cGKIα, indicating a putative preformed and specific docking site for cGKIβ target molecules. The autoinhibitory domain within the N-terminal domain carries a substrate sequence, which is believed to inhibit the catalytic kinase activity in the dormant state. The crystal structure of the cGKIα tandem cyclic nucleotide-binding site (Osborne et al, 2011) has revealed a disulphide bond Cys117-Cys195 that, upon oxidation, may interfere with the interaction between the autoinhibitory domain and the catalytic kinase region enhancing enzyme activity. The molecular elongation occurs upon N-terminal dimerization and C-terminal catalytic domain following cGMP activation.

The regulatory region contains two tandem cGMP-binding sites. In cGK the N-terminal cGMP site has higher affinity and dissociates cGMP slowly, whereas the second cGMP binding-motif has lower affinity and dissociates faster. Other cyclic nucleotide kinases have an opposite arrangement of the high and low nucleotide binding affinity sites, suggesting slightly different modes of activation by cyclic nucleotides. The crystal structure of the cGKIα tandem cyclic nucleotide-binding shows two cGMP-binding sites separated by a long helix at the end of the first site. This structure showed that the examined cGMP-binding site exhibits a canonical cyclic nucleotide-binding fold built by eight β strands with the docking site for the phosphate binding cassette (PBC) between β-strands six and seven. This structure also suggests that there is no cGMP cooperative binding contributing to the regulation of the domain, since it seems there isn't direct communication between the two tandem cGMP-binding motifs.

The C-terminal catalytic domain is a serine/threonine kinase that contains ATP- and peptide-binding sites. It was demonstrated that the presence of cGMP increases considerably cGKI autophosphorylation, in fact, only the occupation of the slow binding affinity site is sufficient to stimulate the autophosphorylation of the enzyme (Smith et al, 1996). As mentioned above, the kinase activity is dependent on the occupation of the cyclic nucleotide-binding motifs, which allows a protein conformational switch where the autoinhibitory domain dissociates from the catalytic

region enabling the phosphorylation of target molecules (Chu et al, 1998 and Wall et al, 2003). A nuclear localization sequence was also identified within the C-terminal region of the enzyme, which is needed for cGMP-induced nuclear translocation of cGK (Gudi et al, 1997).

1.5.3 cGKI signaling

The BMP pathway is linked to numerous developmental disorders such as vascular diseases, cancer and fibrosis: a strict control at multiple levels is required. In 2004 several BMPRII associated proteins were identified, including cGKI (Hassel et al, 2004). In a well-characterized experiment, Schwappacher et al, for the first time, described the multiple role of cGKI in BMP signaling. It was, in fact, demonstrated through co-immunoprecipitation experiments, using different truncations of BMP type II receptor that cGKI interacts exclusively with the tail domain. cGKI does not need to be active to bind the BMPRII-tail but requires cGMP stimulation to switch to its active conformation and subsequently phosphorylates the kinase domain of BMPRII. This seems to support the transphosphorylation activity of BMP receptor type II and as a consequence enhance the activity of BMPRI and the Smad dependent signaling (Figure 1.2). Stimulation of HEK293T cells with BMP-2 showed a reduction of the cGKI-BMPRII interaction, suggesting a receptor conformational change, exerted by the ligand binding, which is the cause of cGKI dissociation in the cytoplasm. Afterwards, cGKI interacts with the activated R-Smads 1/5/8 and Smad4 forming a complex which translocates to the nucleus. There, cGKI interacts with the general transcription factor TFII-I and binds in a complex together with Smad1 and Smad4 to the promotor of the BMP target gene *Id1*. In consequence, the transcription of the *Id1* is enhanced (Schwappacher et al.). Thus, cGKI has a dual role in BMP signaling, it regulates BMPRII and Smad activity at the plasma membrane and modulates the expression of target genes after redistribution to the nucleus.

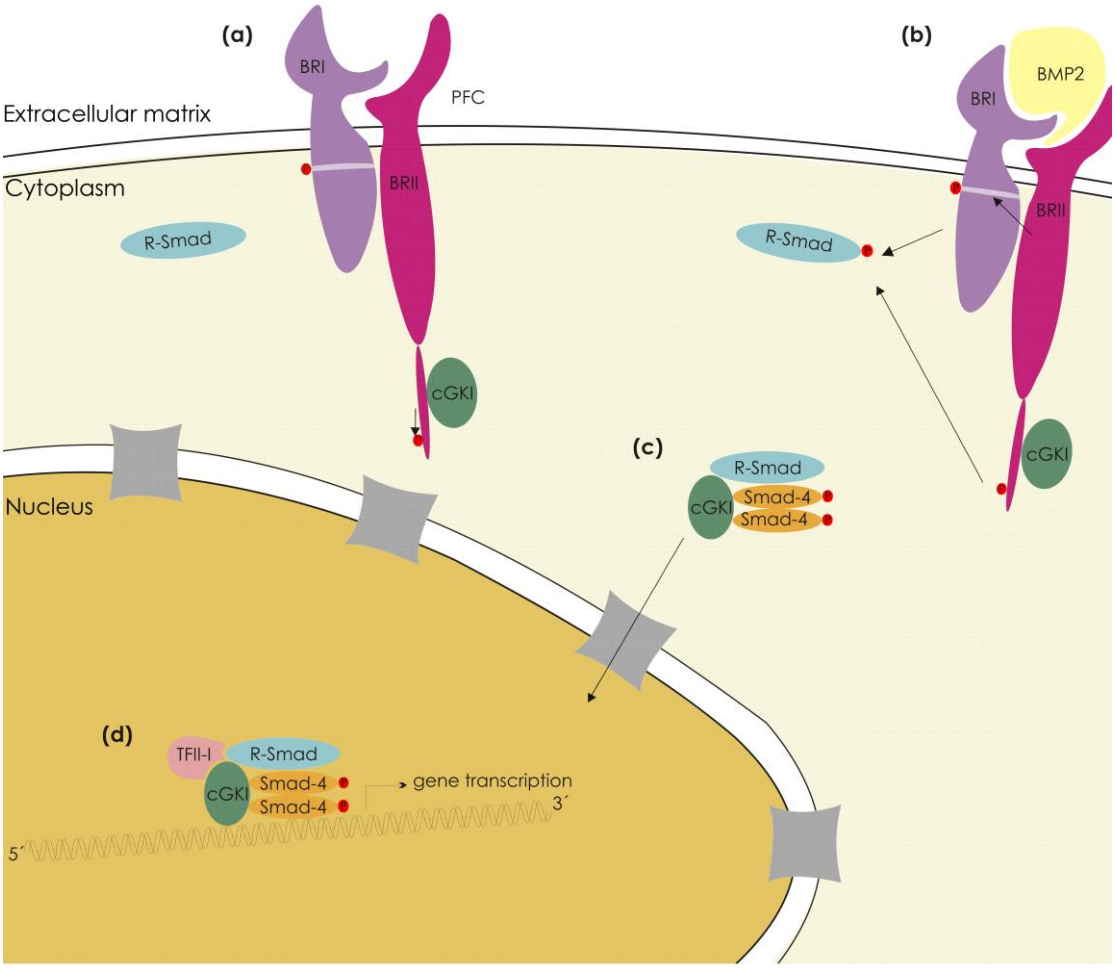

Figure 1.2. cGKI signaling. (A) cGKI interacts with BMPRII-tail and phosphorylates it modulating both BMPRII and BMPRI activity (B). After BMP2 stimulation, cGKI is released from the receptor and binds the complex formed by R-Smads and phosphorylated Smad4 (C) translocating into the nucleus and recruiting TFII-I (D).

1.5.4 cGKI signaling in diseases

NO/cGMP/cGKI signaling has a key role in cardiovascular health and disease and does not only contributes to beneficial effects but it may also be involved in potentially deleterious effects. The well-known mediator of the NO/cGMP/cGKI signaling is the activated cGKI that is believed to relax smooth muscle through different molecular targets and mechanisms (Hofmann, 2005). cGKI pathway is involved in vasculoproliferative disorders such as restenosis and atherosclerosis. Atherosclerosis is a consequence of multiple plaque formation within the arteries. These plaques result as cell deposits, which additionally accumulate lipids, calcium and/or fibrous connective tissue. Restenosis describes the reoccurance of an abnormal narrowing in a blood vessel forming an arterial blockage. The role of cGKI signaling

in vascular smooth muscle cells (VSMC) differentiation is still controversial. Interestingly, overexpressed cGK was assigned to an antiproliferative role in aortic VSMCs, which is able to restore the proliferative effect of BMPRII mutants on PAH. Besides the vascular system an excessive NO production is the major reasons for neurodegenerative pathogenesis such as Parkinson disease. Moreover, it has been suggested that an induced nitroxidative stress has a role in the degenerative processes observed in Alzheimer's disease.

1.6 LIM kinase (LIMK) proteins

Besides cGKI, LIMK1 also colocalizes with the BMPRII tail and is associated with many pathological processes such as tumour cell invasion and metastasis (Foletta et al, 2003). This interaction regulates the LIMK1-dependent phosphorylation of cofilin, which determines the polymerization of actin and induces dendritogenesis (Lee-Hoeflich et al, 2004).

LIM kinase family has been grouped in the tyrosine kinase-like (TKL) subfamily and is composed of only two members of serine/threonine and tyrosine kinases: LIM kinase 1 and LIM kinase 2 which were, respectively, identified in 1994 and 1995 (Mizukono et al, 1994; Okano et al, 1995). The LIMK family is highly expressed in embryonic and adult tissues; furthermore, LIM kinase 1 (LIMK1) is also widely expressed in brain, lung, stomach and testis (Foletta et al, 2004; Acevedo et al, 2006). They have an important role in several cellular functions such as cell cycle, migration and neuronal differentiation and are also involved in pathological processes such as cancer cell invasion, metastasis and in neurodevelopmental disorders. This kinase family has a certain number of partners modulating the phosphorylation or inactivation of their major substrate cofilin/ADF and, subsequently, mediating actin depolymerisation (Arber et al, 1998; Edwards et al, 1999). Inactivation of cofilin/ADF directly modulates the actin cytoskeleton and controls cell morphogenesis and motility (Bernard, 2007; Scott and Olson, 2007).

1.6.1 LIM kinase organization

The LIM kinases share a unique structural organization of signaling domains, with two amino-terminal LIM domains, a central PDZ domain connected to a proline/serine rich region and a carboxyl-terminal kinase domain (Figure 1.3). The LIM and PDZ domain names derive from the initial letters of the proteins where they were first identified: Lin-11, Isl-1, Mec-3 and PSD95, DlgA, Zo-1, respectively. These domains form two repeated zinc fingers, which are cysteine/histidine rich regions coordinating zinc ions. LIM domains play multiple roles through regulation of the kinase activity (Nagata et al, 1999), modulation of protein-protein interactions (Hiraoka et al, 1996) and by putative protein-DNA interaction (Nishiya et al, 1998). The PDZ domain also functions as a site for protein-protein interaction, and it furthermore contains two leucine-rich nuclear exports signals (NES) that influence nuclear/cytoplasmic translocation (Yang et al, 1998; Yang and Mizuno, 1999).

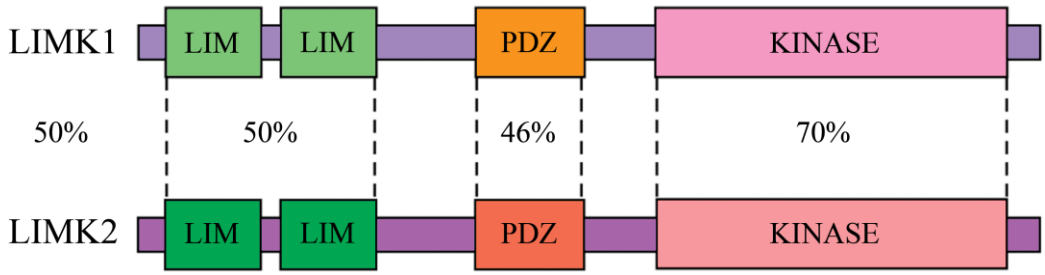

Figure 1.3. LIM kinase protein structure. LIM kinase proteins contain two LIM domains. The domain alignment between LIMK1 and LIMK2 is shown, and the percentage of amino acid similarity is indicated.

Moreover, another nuclear localization sequence is founded between the PDZ and the kinase domain on both LIMK1 and LIMK2 and a second additional sequence is present only in LIMK2, proposing an active nuclear function (Goyal et al, 2006). LIMK1 and LIMK2 share 50% overall sequence identity, with 50% identity in the LIM domains, 70% in the kinase domain and a little less then 50% in the PDZ domain (Figure 1.3). Both kinases are dual serine/threonine and tyrosine kinases containing the unusual diagnostic sequence motif DLSNDHN instead of DLKXXN for serine/threonine kinases and DLAARN or DLRAAN in case of a tyrosine kinase.

1.6.2 LIMK regulators

LIMKs are regulated by different upstream signaling pathways, chiefly acting downstream of Rho GTPases and modulating actin cytoskeleton stability via cofilin/ADF to control cellular motility and morphogenesis (Figure 1.4).

The first function that affects control of the cytoskeleton is associated with the potential of the N-terminal LIM and PDZ domains to influence the LIMK kinase activity. The amino terminal domains have also been shown to interact with the kinase domain thereby limiting the kinase activity of LIMK1 (Lee-Hoeflich et al, 2004). Inactivation by deletion or mutation of the LIM and PDZ domains enhances the kinase activity, suggesting that the N-terminal region acts as a constitutive autoinhibitor (Nagata et al, 1999).

1.6.2.1 Autophosphorylation and transphosphorylation

It has been reported that LIMK1 undergoes autophosphorylation on serine and tyrosine, but perhaps not on the regulatory site of threonine 508 in the kinase activation loop (Proschel et al, 1995). A T508V mutant, in fact, retains autophosphorylation activity, suggesting that phosphorylation occurs elsewhere (Kobayashi et al, 2006). Currently, the autophosphorylation sites and their regulation mode have still to be determined.

Moreover, LIM kinase levels and activity are regulated by Heat shock protein 90 (Hsp90), which promotes their transphosphorylation upon homodimerization (Li et al, 2006). The interaction between Hsp90 and Pro394 of LIMK1 induces the formation of LIMK1 homodimeric complexes, which increase the phosphorylation levels of LIMK1 and also its activation.

1.6.2.2 Positive activity regulators

The Rho family of GTPases contains several signaling proteins, including RhoA, Rac1 and Cdc42, which are involved in cytoskeleton regulation. These proteins together with their downstream effectors modulate LIMK activity (Figure 1.4). LIM kinases were shown to be phosphorylated in the kinase activation loop on Thr508

(LIMK1) and Thr505 (LIMK2) by the Rho effector Rho kinase (ROCK), p21-activated kinases (PAKs: PAK1, PAK2, PAK4) and myotonic dystrophy kinase-related Cdc42-binding kinase (MRCKα) (Figure 1.4).

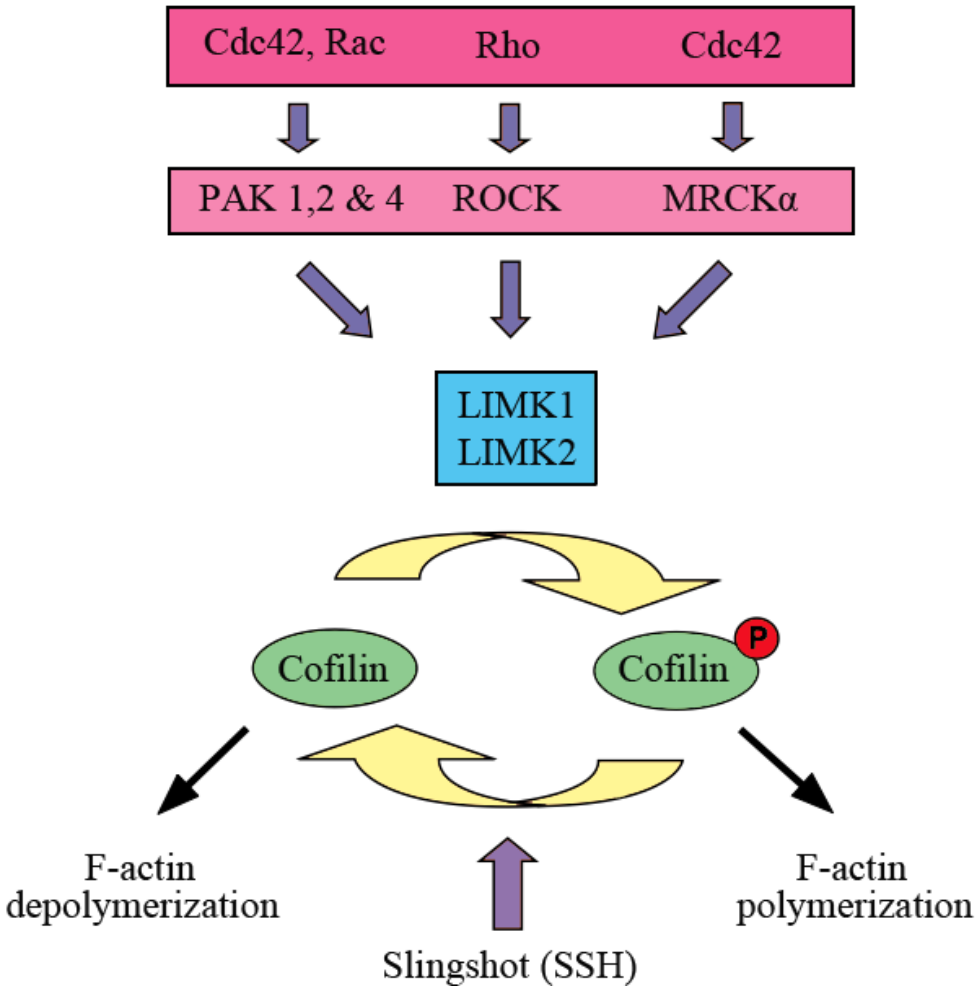

Figure 1.4. LIM kinase signaling pathways. LIMK is part of the signaling network that regulates actin dynamics by integrating signals from Rho GTPases: Cdc42, Rac1, RhoA, and effector proteins: PAK, ROCK and MRCKα. LIMK phosphorylates cofilin at Ser3 and renders it inactive. Slingshot (SSH) is a phosphatase that dephosphorylates and re-activates cofilin.

It was shown that the constitutively activated Rac1 and Cdc42 increased the interaction between PAK1 and LIMK1. PAK1 enhanced LIMK1 kinase activity by direct phosphorylation on the activation loop (Edwards et al, 1999). PAK4 can also phosphorylate LIMK1 and shows a higher affinity than PAK1 (Dan et al, 2001). Interestingly, PAK4 has a dual role in LIMK regulation; first, it phosphorylates LIMK and stimulates its ability to phosphorylate cofilin, resulting in the accumulation of

actin polymers; second, PAK4 inactivates the slingshot phosphatase SSH-1 by phosphorylation, which dephosphorylates LIMK1 increasing cofilin activity (Soosairajah et al, 2005). SSH-1 is strongly dependent on the presence of F-actin. PAK2 was also shown to induce a significant increase of LIMK and cofilin phosphorylation (Misra et al, 2005). ROCK and MRCKα have been reported to phosphorylate and activate both LIMK1 and LIMK2 (Sumi et al, 2001). Unlike the well characterized mechanism of LIMK1 activation through Thr508 phosphorylation, in vascular endothelial growth factor (VEGF) cells, LIMK1 has been reported to be activated by MAPK activated protein kinase-2 (MK-2) mediated phosphorylation on Ser323 (Kobayashi et al, 2006). The kinase upstream of MK-2, p38, was also able to phosphorylate LIMK1 on serine 310 despite interfering with LIMK1 activity.

1.6.2.3 Negative activity regulators

LIMK1 is the only kinase acting on cofilin, which can be activated by caspase cleavage. Truncated LIMK1, formed upon cleavage on caspase 3 type site Asp-Glu-Ile-Asp (DEID), shows an elevated kinase activity resulting in membrane blebbing. Proteolysis of LIMK1 occurs also via proteasome-mediated degradation mediated by the RING finger E3 ubiquitin ligase Rnf6 in axonal growth cones of hippocampus neurons (Tursun et al, 2005). The large tumour suppressor 1 (LATS1) is a factor able to indirectly modulate cofilin activity by direct interaction with LIM domains leading to a reduction of cofilin phosphorylation by LIMK1 (Yang et al, 2004).

1.6.3 LIMK1 in development and disease

LIM kinases have an important role in different cellular processes such as cell migration, cell cycle and neuronal differentiation. Aberrations in the fine-tuning of LIMKs activity could be proved in the Williams syndrome, a rare genetic disorder that is characterized by learning difficulties or mild to moderate retardation (Meyer-Lindenberg et al, 2006; Li et al, 1998) and in pathological processes like cancer and HIV.

Cancer cell metastasis is a process that begins with local invasion of nearby tissues. The ability of metastatic cells to move through tissues requires the reorganization of

the actin-myosin cytoskeleton that will occur by extracellular matrix (ECM) remodelling to create a path of increased movement from the primary site (Olson and Sahai, 2009). It has been proposed that LIMK1 regulates actin dynamics and plays a central role in tumour cell invasion and metastasis. In fact, LIMK1 has been found to be overexpressed in tumour cell lines (Yoshioka et al, 2003), prostate tumours (Davila et al, 2005) and breast cancer tumours (Bagheri-Yamand et al, 2006). Furthermore, Scott and colleagues have shown that LIMK activity has a pivotal role in the cellular processes contributing to the cell movement via ECM degradation, demonstrating that LIMK inhibition blocks cell invasion (Scott et al, 2010).

Most viral pathogens require the cytoskeleton to enter the host and for intracellular transport. In HIV-1 infection, the virus binds the blood resting CD4 T cells and initiates a process of actin polymerization and depolymerization. Even if the virus-mediates actin polymerization in HIV-1 infection is still unknown, it has been suggested that LIMK1 is the main regulator controlling the actin dynamics involved in this infection process (Manetti, 2011). HIV-1 binding to CD4 and CXCR4 activates LIMK1 and triggers actin polymerization that promotes the clustering of coreceptors and virus interaction. Following viral entry, cofilin is activated leading to the formation of filamentous actin, which may facilitate the viral DNA anchorage for reverse transcription (Vorster et al, 2011).

1.7 Aims of the project

Among the BMP/TGFβ receptors, the cytoplasmic domain of BMPRII features a long C-terminal tail that forms a docking site for the cGKI and LIMK1 kinases. Mutations in the tail promote pulmonary arterial hypertension (PAH), but do not impair known BMP signaling outputs. Coexpression of cGKI with BMPRII-tail mutants can rescue some effects of PAH through the BMP signaling pathway, suggesting that the downstream activity of cGKI is as an important regulator of PAH and vasodilation. LIMK1 also colocalizes with the BMPRII tail and is associated with many pathological processes such as tumour cell invasion and metastasis.

My Ph.D. project aims to solve the crystal structures of cGKIβ and LIMK1 at high resolution by X-ray crystallography to investigate the structural basis of PAH and cancer metastasis. From these structures we hope to gain insights on better understanding on how cGKIβ restores BMP signaling and LIMK1 regulates actin polymerization through the phosphorylation of cofilin. We expect to identify and validate the key residues of BMPRII-tail docking sites for cGKIβ and LIMK1, which will provide insight into the complexities of BMP signaling mechanisms. Furthermore, using enzymatic assays we aim to determine binding modes and specificity of small molecule inhibitors that define therapeutic targets, generating new prospectives for drug development in cancer and against rare autosomal diseases such as PAH.

2 Materials and methods

2.1 Molecular biology

2.1.1 Ligation independent cloning

The plasmids used in this work are modified vectors, which allow expression of the putative proteins fused with a TEV cleavable N- or C-terminal His_6-tag (PAK4 has an alternative GST-tag).

Table 2.1. Plasmids used in this work.

Plasmid	Target	tag
pNIC28-Bsa4	LIM-LIM-PDZ	N-term
pNIC-CTHF	LIM-LIM	C-term
	Cofilin1	C-term
pGEX-6P2	PAK4	N-term
pFB-Lic-Bse	cGKI	N-term
	LIMK1	N-term

Ligation-independent cloning was developed for the directional cloning of PCR products without the need for restriction enzyme digestion or ligation reactions. The fragment amplification oligonucleotides have additional poly-nucleotide tails complementary to the tails used for vector, permitting the creation of single strand-ends with T4 DNA polymerase. The desired targets were amplified by PCR from cDNAs obtained from the mammalian gene collection. The templates were diluted to an optimal concentration of 2.5 ng/µl, the forward and reverse primers to a concentration of 10 µM each and aliquoted into a 96-well plate followed by the already prepared master mixture to each well separately. The typical master mixture reaction composition is described in table 2.2.

Table 2.2. Reaction mixture for PCR.

Reactant	For 1 reaction
10 x Pfx buffer	5 µl
10 x PCR enhancer	5 µl
50 mM MgSO4	1 µl
10 mM dNTP mix	1.5 µl
Platinum Pfx	0.4 µl
Water	33.1 µl
Primers (10 µM)	1.5 µl
Template DNA (approx. 50 ng)	2.5 µl

The PCR was performed using the following standard touchdown reaction to avoid production of multiple products:

Table 2.3. Touchdown PCR program.

Reaction	Temperature	Time	Cycles
Denaturation	94°C	5 min	
Denaturation	94°C	30 sec	
Annealing	68°C,	30 sec	5 cycles
Elongation	68°C	1-3 min	
Denaturation	94°C	30 sec	
Annealing	68°C,	30 sec	5 cycles
Elongation	68°C	1-3 min	
Denaturation	94°C	30 sec	
Annealing	55°C,	30 sec	5 cycles
Elongation	68°C	1-3 min	
Denaturation	94°C	30 sec	
Annealing	50°C,	30 sec	20cycles
Elongation	68°C	1-3 min	
Elongation	72°C	10 min	
Pause	15°C	hold	

A small aliquot of the amplified product, usually 3-5 µl, was then checked by electrophoresis on a 1% (w/v) agarose gel (as described in § 2.1.2). The vector was cut with a single restriction enzyme, (BseRI or BsaI depending on the vector) for 2-3 hours at 50 °C in a heating block and then incubated with T4 DNA polymerase (NEB) in the presence of the specific dNTPs for 30 minutes at 22°C to generate the specific

vector-compatible overhangs. The T4 DNA polymerase was deactivated for 20 minutes at 70°C in a thermocycler. PCR products were purified with a QIAquick purification kit (Quiagen). Complementary overhangs were created by treating the PCR products with T4 DNA polymerase for 30 minutes at 22°C in the presence of complementary dNTPs to those used with the vector. Again, the enzyme was inactivated by heating for 20 minutes to 70°C in a thermocycler. The annealing was performed by incubating 1 µl of treated plasmid with 2 µl of treated insert for 5-10 minutes at room temperature. The total amount of DNA was determined spectrophotometrically at 260 and 280 nm using a NanoDrop instrument (Thermo Scientific) and was estimated considering that $1OD_{\lambda 260}$ corresponds to 50 µg/ml double strand DNA or 0.15 mM (in nucleotides).

2.1.2 Agarose gel electrophoresis

DNA samples were analysed on a 1.0 % agarose gel in 1X TAE buffer (40 mM Tris Acetate, 1 mM Ethylenediamine tetraacetic acid (EDTA), pH 8.0) containing 3 ml of SYBR® safe DNA stain 10,000X (Invitrogen). The electrophoresis was performed by applying a voltage of 80 V for 30/60 minutes in 1X TAE buffer. The DNA bands on the gel were visualized under UV-light.

2.1.3 Transformation with competent cells

The DNA plasmid was used to transform *E.coli* MACH1, or Rosetta competent cells. An aliquot of 50 µl competent cells were thawed, incubated with 50 ng of purified DNA on ice for 15 minutes, then heat-shocked at 42°C for 45 seconds to enable transformation. The cell suspension was chilled briefly on ice, then 100 µl of SOC medium was added and the plates sealed with porous adhesive film and incubated with shaking for at least 1 hour at 37°C. Transformants were selected on LB agar plates supplemented with the appropriate antibiotic through incubation at 37°C over night. Single colonies were tested by colony PCR by repeating the following thermal cycle 25 times: initial denaturation 94°C for 5 min, then 94°C for 30 sec 50°C for 30 sec, 72°C for 1-3 min x25, the reaction was kept at 72°C for 5 min and at the end was cooled at15°C.

2.1.4 Bacmid production

Bac-to-Bac® technology relies on the generation of recombinant baculovirus by site-specific transposition in *E. coli*. The gene of interest, previously cloned into a pFastBac™ vector, has to be transformed into DH10Bac™ competent *E. coli*, which contains a parent bacmid with a *lac*Z-mini-*att*Tn7 fusion. The transposition then occurs between the elements of the pFastBac™ vector and the parent bacmid.

10-15 µg/ml of recombinant DNA were incubated with 20 µl of DH10Bac cells in a 96-well PCR plate on ice and left for 30 minutes before heat shock treatment for 45 seconds in a 42^{o}C water bath. The sample was cooled on ice for 5 minutes. Subsequently 900 µl of pre-warmed 2xLB medium were added to each well of a 96-deep well block, which was covered with a porous seal and placed in a micro-expression shaker (Glas-col) at 37°C shaking at 700 rpm for 5 hours. The cultures were diluted 1:10 into LB medium; 50 µl of the dilution was spread onto the DH10Bac selective plates and incubated at 37°C for 48 hours. White colonies, which contain the recombinant DNA, were picked for the amplification of the recombinant bacmid by growth in 1ml 2xLB medium with 50 µg/ml kanamycin, 7 µg/ml gentamycin, and 10 µg/ml tetracycline at 37°C overnight at 700 rpm in a micro-expression shaker (Glas-col). The next day the bacmid DNA was extracted with the Plasmid Miniprep Kit (Qiagen) and resuspended in 50 µl TE buffer. The DNA concentration was measured using the NanoDrop (Thermo Scientific), as previously described. Afterwards to confirm the transposition, a PCR was set up using M13-Bac specific forward and reverse primers. The amplified product was visualised on 1.0 % (w/v) agarose gel by electrophoresis.

2.1.5 Transfection and infection of insect cells

Once the correct bacmid was produced, it was used to transfect Sf9 insect cells grown to mid-log phase (~ 2 x 10^6 cells/ml). For initial virus preparation, 24 or 96 well blocks were used. In a 96 well microliter plate 10 µl of the recombinant bacmid was gently pipetted into 50 µl of serum free Grace's insect cell medium (Gibco®) and 50 µl of a mixture of 5 ml Grace's medium (Gibco®) and 0.3 µl of cellfectin. Plates were then incubated at room temperature inside a laminar flow hood for 45 minutes. The reaction mixture was diluted with 100 µl of Grace's insect cell medium (serum free).

Separately, Sf9 mid-log phase cells were diluted to ~ 2 x 10^5 cells/ml and 1 ml was incubated per well in 24 well tissue culture plates in the presence of cellfectin, for an hour at 27°C. In parallel, an untreated cell control was also prepared. After that, the medium was removed from the wells, which were washed once with 1 ml of Grace's insect medium, and afterwards incubated with 200 µl of the recombinant bacmid (preincubated into the 96 well microliter plates) and 200 µl of Grace's insect medium for 5 hours at 27°C. Later the transfection mixture was removed and 700 µl of SF900 II insect medium (Gibco®) containing 2% (v/v) FBS and antibiotics (50 U penicillin and 50 µg streptomycin per ml of medium) were added into 24-deep-well blocks and subsequently incubated at 27°C for 72-96 hours. After a minimum time of 72 hours the transfected cells were compared under the microscope with the controls to look for signs of infection. Infected cells are larger and deformed or elongated compared to the uninfected ones; this morphology cell change can take up to 96 hours or more. When cells were properly transfected they were moved to a 96-deep-well block and centrifuged at 1,500 x g for 20 minutes at room temperature. The supernatant was collected and stored at 4°C as P_0 viral stock, protected from light. Further amplification of the virus to generate P_1, P_2 and P_3 virus were all carried out using the same protocol incubating 3 ml of Sf9 insect cells grown to mid-log phase with 120 µl of the previous virus stock generation at 27°C for 48 hours shaking in a micro-expression shaker incubator. The 24-deep-well blocks were then centrifuged at 1,500 x g for 20 minutes at room temperature, the supernatant collected and stored at 4°C generating the new viral stock.

2.2 Protein expression

2.2.1 Small scale bacterial expression

1 ml of an overnight starter culture, prepared by inoculating 10 ml of LB media with the specific antibiotic and an aliquot of a glycerol stock, was used to inoculate 250 ml volume (4X 50 ml for each construct) flasks of selective LB or TB media at 37°C incubator overnight shaking at 160 rpm. Once the cultures reached OD_{600}= 0.5, the incubator temperature was reset to 18°C; upon reaching 18°C the cell density was typically OD_{600}= 0.8. At this point, 0.5 mM IPTG was added and the cultures left shaking for overnight protein induction. The next day each 4X 50 ml sample was

pooled to a total volume of 200 ml of cells for each construct. Cells were harvested by centrifugation, at 12,000 rpm for 40 minutes, using a JLA 16.250 rotor (Beckman Coulter). The supernatant was removed and the cells transferred on ice. If the desired proteins were designed for expression with a fused His_6-tag then the pellets were resuspended into binding buffer (50 mM Hepes pH 7.5, 0.5M NaCl, 5% glycerol, 5 mM imidazole, 1mM TCEP/1:2000 Protease inhibitor). Cell lysis was performed by sonication using the following parameters: amplitude = 35%, time = 5 minutes, pulser = 5 seconds on and 5 seconds off. Each sonic extract was transferred to 2 ml labelled eppendorfs and centrifuged at 14,000 rpm for 40 minutes. To check the expression of the putative proteins, 10 ml BioRad columns were used packed with 500 µl of 50% (v/v) Ni-NTA slurry. 2 ml supernatant fractions for each construct were loaded on the resin, pre-washed with 5 volumes of water and binding buffer. The flow-through was collected and the resin was washed with 2 ml of binding buffer and then wash buffer, containing 50 mM Hepes pH 7.5, 500 mM NaCl, 5% Glycerol, 30 mM Imidazole, to remove the impurities. The samples were eluted with elution buffer at high imidazole concentration (50 mM Hepes, 500 mM NaCl, 5% Glycerol, 250 mM Imidazole, pH 7.5), 10 µl of each fraction was loaded on an SDS-PAGE gel to check whether the protein was soluble expressed.

In the specific case of PAK4, where the protein was expressed as a GST fusion, the collected pellets were resuspended with a binding buffer without imidazole. Columns were packed with a similar amount of 50% glutathione sepharose resin slurry, which was washed through with water and binding buffer. The supernatant was applied to the matrix and washed with 5ml of binding buffer, and the protein was eluted with 300 µl of elution buffer (50 mM Hepes pH 7.5, 300 mM NaCl, 5% Glycerol and 15 mM reduced glutathione).

2.2.2 High throughput small-scale baculo expression

The rapid analysis of recombinant baculovirus constructs is very useful to direct the target protein expression in insect cells and screen which of the analysed constructs is the best to scale up. To analyse the virus expression it is necessary to incubate 3 ml of mid-log phase Sf9 cells in four 24-deep-well blocks in the presence of 120 µl of virus stock for 48 hours at 27°C in a micro-expression shaker (Glas-col) at 450 rpm. The

blocks have to be centrifuged at 1,500 x g for 25 minutes, the supernatant discharged and the pellets resuspended into 0.4 ml of 50 mM Hepes pH 7.5, 500 mM NaCl, 5% glycerol shaking at 800 rpm for some minutes. The suspension has to be transferred to a 96-deep-well block and 1ml of lysis buffer (50 mM Hepes pH 7.5, 500 mM NaCl, 5% glycerol, 1% CHAPS, 10 mM imidazole, 1mM TCEP, 1 µl of antiprotease cocktail and 20U benzonase per ml buffer) added to lyse the cells that are shaked for 30 minutes. To check whether the proteins are insoluble, 50 µl of the suspension were heated for 10 minutes at 98°C in the presence of 10 µl of loading buffer, then spinned at 10,000 x g for 15 minutes and loaded on a SDS Page gel. The remaining suspension in the block had to be centrifuged at 1,500 x g for 30 minutes at 4 °C and the supernatant transferred in a new block. As before, 50 µl were taken and analysed on an SDS-PAGE gel as soluble fraction. All constructs expressed in baculovirus were designed to carry a His_6-tag, for that reason the expression yield was only checked using Nickel resin. In the new block 100 µl 50% Ni-NTA slurry, pre-equilibrated in 50 mM Hepes, 500 mM NaCl, 5% glycerol, pH 7.5, were added and incubated for half an hour to let the proteins specifically bind to the beads. Afterwards the putative proteins needed to be eluted: the mixture of supernatant and resin were transferred into 96 well filter block for purification, placed on the top of a 96-deep-well block to collect the waste. Once the flow-through had been collected, the resin was washed with 0.4 ml of binding and wash buffer (50 mM Hepes pH 7.5, 500 mM NaCl, 5% glycerol in addition to 10 mM and 30 mM imidazole, respectively). The block was centrifuged for 1 minute at 700 x g to discharge all the residual liquid. 80 µl of a 500 mM imidazole concentration buffer was added to the wells and incubated for 5 minutes. Subsequently, the block was centrifuged at 700 x g for a minute to elute the proteins. The protein expression was examined by SDS-PAGE. When the expression of a putative protein was successfully reached, then it was scaled up in a large scale insect cell production. Sometimes the expression levels of a heterologous gene may vary significantly; it is useful to try to optimize the expression conditions. Four parameters have to be considered: different infection times (48, 72 and 96 hours), two Sf9 cells concentrations ~ 2 x 10^6 and ~ 3 x 10^6 cells/ml, three volumes of initial virus stock (20, 40 or 80 µl), and in the case of LIMK1, expression also used an alternative cell line such as High Five.

2.2.3 Bacterial expression

All the bacterial constructs were transformed in Rosetta expression cells and used to pre-inoculate a culture as fresh colony from a selective LB agar plate or from a frozen glycerol stock. 50 ml pre-inoculum was grown overnight in LB medium treated with antibiotics and the following morning 8 ml of it were used to inoculate 1 liter autoclaved LB or TB selective media in a 2 liter flask. The cultures were grown at 37°C in a shaking incubator at 170 rpm until the optical density at 600 nm reached 0.5; the incubator temperature was then lowered to 18°C. When the incubator temperature reached 18°C, the OD_{600} nm for the cultures was typically 0.8 and protein overexpression can be induced by the addition 0.5 mM IPTG, as final concentration, to the flasks in a shaking incubator for 12-18 hours. The next day the cells were harvested by centrifugation at 9,000 rpm for 15 minutes, using a JA 8.1 rotor (Beckman Coulter). The cells were transferred to ice and resuspended in 20 ml of Lysis Buffer (50 mM Hepes pH 7.5, 500 mM NaCl, 5% glycerol, 5 mM imidazole, 0.5 mM TCEP, 1:2000 Protease inhibitor) and immediately processed or frozen in liquid nitrogen and stored at -80°C.

2.2.4 Baculoviral expression

Healthy cells are an important condition in successful protein expression, and for this reason insect log-phase cells had to be maintained with >95% viability. Generally, cells were passaged every 1-2 days and splitted 1:1 or 1:2. Sf9 cells were seeded at the approximate density of 2.0 x 10^6 cells/ml and Pen/Strep (Invitrogen) solution was added on a final dilution of 1:1000 to avoid bacterial contamination. Depending on the virus stock concentration, 1-2 ml of virus stock solution were added for each 100 ml of solution. The flasks were incubated at 27°C for 48-72 hours with shaking set at 100 rpm. A standard scale up of 4 to 8 liters infection was prepared.

2.2.5 Cell lysis

For all constructs, cell lysis was accomplished by sonication. Different conditions were used according to cell origin; in case of bacterial cells 35% of amplitude was used for 10 minutes with 5 seconds pulser on and 8 seconds off. Since insect cells are

more soft than bacterial cells, shorter sonication time was necessary, and all samples were lysed using 2 minutes sonication at 35% of amplitude for only 2 minutes using 5 seconds pulser on and 8 seconds off. The cell debris was spun down at 21,500 rpm in a JA 25.50 rotor (Beckman Coulter) for 1 hour; afterwards the supernatant was generally filtrated with 0.8 or 1.2 µm diameter filters.

Lysis buffer: 50 mM Hepes, 500 mM NaCl, 5 mM Imidazole, 5% Glycerol, 0.5 mM TCEP 1:1000/2000 protease inhibitor SET V (Calbiochem), pH 7.5.

2.3 Protein purification

2.3.1 IMAC purification

Nickel affinity chromatography was performed at 4°C either on a Ni-NTA column or in a rotation batch.

In column

4-6 ml of 50% Ni-NTA slurry were put in a 1.5 x 10 cm column. The resin was equilibrated in water and then in binding buffer. The lysate supernatant was applied by gravity flow onto the Ni-NTA column, which was afterwards washed with 50 ml of binding buffer and wash buffer to remove unspecifically bound proteins. The desired protein was eluted with a step gradient of imidazole (50-250 mM) in 4 x10 ml volume fractions.

In batch

10 ml of 50 % Ni-beads (pre-equilibrated in water and then binding buffer) were incubated with the protein supernatant for 1 hour on a rotation platform at 4°C and then pelleted at 800 x g for 10 minutes and the supernatant was removed. Subsequently, the beads were washed twice with 50 ml of binding and wash buffer. The slurry was applied onto the column and eluted by applying 10 ml portions of eluting buffer with an increasing imidazole concentration. 10 µl of each fraction was mixed with the SDS loading dye, boiled for 5 min, and loaded onto an SDS-PAGE

gel. Fractions corresponding to the correct protein molecular weight were pooled and concentrated to 5 ml using an Amicon Ultra-15 filter with an appropriate size cut-off.

2.3.2 Nickel rebinding

A Ni-rebinding step was performed to remove minor contaminants and to separate the untagged protein from the fused one, usually right after a size exclusion chromatography. 0.5 ml 50% Ni-NTA slurry was applied onto a BioRad polypropylene disposable drip column, washed and equilibrated with binding buffer. The collected fractions were applied onto the column under gravity flow. In the absence of the cleavable His_6-tag, the desired protein was collected by washing the beads with a further 3 ml of binding buffer and 8 ml of wash buffer. Contaminants were mostly separated, as judged by SDS-PAGE analysis, by a subsequent elution containing 250 mM imidazole.

The following buffers were used:

Binding buffer: 50 mM Hepes, pH 7.5, 500 mM NaCl, 5% glycerol, 5 mM Imidazole, pH 7.5.

Wash buffer: 50 mM Hepes, pH 7.5, 500 mM NaCl, 5% glycerol, 30 mM Imidazole, pH 7.5.

Elution buffer: 50 mM Hepes, pH 7.5, 500 mM NaCl, 5% glycerol, 50-100-150-250 mM Imidazole, pH 7.5.

2.3.3 TEV cleavage

To remove the His_6-tag the concentrated fractions were diluted with 10 ml of binding buffer and incubated together with 10 mM DTT and 0.1 mg of TEV protease at 4°C.

2.3.4 Size exclusion chromatography (SEC)

Protein targets were further concentrated to 3 ml and purified by SEC on 16/60 HiLoad Superdex 75 or 200 (Ge Healthcare) run on ÄKTA-Express. The column was previously equilibrated with typical gel filtration buffer, composed of 50 mM Hepes,

pH 7.5, 300 mM NaCl, 5% glycerol and 0.5 mM TCEP. The experiment was performed at a constant flow of 1ml/min. Fractions were analysed on SDS PAGE gel and pooled together.

2.3.5 Ion exchange

Different ion exchange chromatography runs were performed in the case of some constructs, with the goal to remove contaminants.

Nucleic acid removal with DEAE cellulose (DE52, Whatmann), for example, was applied to all constructs expressed in *E.coli*. 10 g of resin was suspended in 50 ml of 2.5 M NaCl, and then applied onto a 2.5 x 20 cm column. The resin was then equilibrated with 50 ml of the canonical binding buffer prior to loading the sample. The supernatant was first applied onto the column by gravity flow, which was followed by a wash with 50 ml wash buffer. The column flow-through and wash were directly applied onto a Ni-NTA column.

Anion and cation exchange columns, HiTrap SP HP and HiTrap QP HP (GE Heathcare), respectively, were used to remove unspecific contaminants still present after the Ni-rebinding step. The protein was concentrated to 5ml and combined with 45 ml low salt buffer to reduce ionic strength. The diluted protein was then loaded onto the pre-equilibrated column and eluted with a gradient from buffer A to buffer B (high salt).

Generally after this purification step most proteins were pure enough to be concentrated for crystallization trials or to be stored at -80°C, after stabilization with 25% glycerol and flash freezing in liquid nitrogen.

2.3.6 Desalting chromatography

Proteins from -80°C storage or proteins which could not be exposed to overnight dialysis because they precipitated, were thawed and applied onto a PD10 desalting column (GE Heathcare). The protein was typically eluted in 50 mM Hepes, 300 mM NaCl, 5% glycerol and 0.5 mM TCEP, pH 7.5.

2.4 Protein characterization

2.4.1 SDS-PAGE

The purity and integrity of the recombinant proteins were assessed by denaturing gel electrophoresis. Protein samples were run on precast gels (Criterion XT Bis-Tris Gel, 4–12%, 26-well, BioRad) composted of a stacking and resolving part of 4% and 12% acrylamide, respectively in 5X XT MES buffer (BioRad).

2.4.2 Intact Mass (Native)

Masses were determined by LC-MS TOF, using an Agilent LC/MSD TOF system with reversed-phase HPLC coupled to electrospray ionisation and an orthogonal time-of-flight mass analyser. Proteins were desalted prior to mass spectrometry by rapid elution off a C3 column with a gradient of 5-95% isopropanol in water with 0.1% formic acid.

2.4.3 MSMS (Phosphorylation mapping)

Protein samples were digested by trypsin and chymotrypsin; phosphopeptides were determined by Collision-Induced Dissociation (CID) and Electron Transfer Dissociation (ETD) using Ion Trap. The data were analysed using BioTools and the Mascot server database. This work was performed by Dr. Rod Chalk (SGC, Biotechnology).

2.4.4 Kinase assay

Two kinase assays were set up. One has the purpose to test the kinase activity of the putative kinases, while in the second experiment, kinetic properties were measured with consensus peptide substrates.

<u>Radioactive assay</u>

1 µg of recombinant cGKI was incubated with 25 µM of cGMP and supplemented with kinase buffer containing ATP. Reactions of cGKI in the presence of the kinase

inhibitor were set up as well. Then, phosphorylation was initiated by the addition of 1 μCi (γ-^{32}P) ATP (Hartmann Analytics) and the samples were incubated at 30°C for 30 minutes. The proteins were separated on SDS-PAGE and transferred to nitrocellulose membrane. The phosphorylated proteins were detected using X-ray films. Subsequent immunoblotting with the respective antibodies monitored the protein amounts. This experiment was performed together with Eva Heining (AG Knaus, FU Berlin).

Coupled assay

The phosphorylation reactions were measured using a coupled assay in which ADP production was coupled to NADH oxidation by pyruvate kinase (PK) and lactate dehydrogenase (LDH) and assumed a molar extinction coefficient for NADH. The progress was monitored following fluorescence decrease in NADH every 8 seconds for 10 minutes. The experiment was performed at room temperature using a 96-well plate format in 50 μl reactions containing 50 mM Hepes, 100 mM NaCl, 1 mM $MgCl_2$, 0.1 mM $MnCl_2$, 1 mM phosphoenolpyruvate, 0.1 mM NADH, 15 U/m pyruvate kinase and 30 U/m lactate dehydrogenase. The protein concentration varied between 50 and 200 nM. ATP and/or cGMP were added to the reaction at 1 mM final concentration and the consensus peptides were used as substrates at a concentration range from 10 to 200 μM or 200 μM to 1.5 mM, according to the peptide type.

2.4.5 Peptide array

A peptide array-based method was addressed to study protein–protein interactions. The SPOT technique is a widespread peptide-array technology, which is able to distinguish semi-quantitatively the binding affinity of peptides, therefore its intention is to define protein-protein interactions within one array. Our purpose was to investigate interactions between BMPRII-tail and full length cGKI, as well as BMPRII-tail and LIMK1 LIM-LIM-PDZ domain. Peptide syntheses of BMPRII-tail were performed at the Institut für Medizinische Immunulogie, Charité-Universitätsmedizin Berlin under the supervision of Dr. Carsten Mahrenholz. The tail region was immobilized on a cellulose membrane as overlapping 15-mer peptides with a shift of 3 amino acids on different identical membranes (for the recombinant

proteins and to check the cross-reactivity of the respective antibodies). Using the results of a previous peptide array addressed to study the BMP receptor II tail/full length cGKI interaction an alanine walk was also performed. For this experiment 3 amino acids in the putative peptides were subsequently mutated to alanines with the goal of identifying if any specific sequence is required for the binding. The matrices were washed with ethanol once for 5 minutes and three times for 5 minutes with Tris-buffered saline [TBS: 50 mM Tris-(hydroxymethyl)-amino-methane, 50 mM NaCl, 2.7 mM KCl, adjusted to pH 8 with HCl/ 0.05%]. To eliminate non-specific binding, the membrane-bound peptide arrays were blocked for two hours with blocking buffer [casein-based blocking buffer concentrate (Sigma-Genosys), 1:10 in TBS containing 5% (w/v) sucrose], and then washed with TBS (3×10 min). Subsequently, the membranes were incubated with the recombinant protein concentrated at ~ 5μM for 1 hour in TBS blocking buffer and detected by antibodies. Upon washing for 30 minutes with TBS, analysis and quantification of peptide-bound recombinant protein were carried out using a chemiluminescence substrate and a Lumi-Imager. Analysis and quantification of spot signal intensities were executed with the Genespotter software. The spot signal was calculated from a circular region around the spot centre detected on the image. The background signal for each spot was determined with a safety margin to this circular region.

2.4.6 Differential scanning fluorimetry (DSF)

Differential scanning fluorimetry is a chemical screening method to assess stability and detect ligand binding. Since the stability of a protein is related to its Gibbs free energy of unfolding, which is temperature-dependent, and can be increased in the presence of a ligand, by reducing its propensity to unfold or aggregate. In fact, when the temperature increases the Gibbs free energy of unfolding decreases and becomes zero, reaching the melting temperature (Tm). This indicates that the folded and unfolded protein concentrations are at equilibrium. If a ligand binds specifically to the folded state of a protein the free energy of binding contributes to an increase in Gibbs free energy, which results in an increase in the Tm (Figure 2.1). The difference between the Tm of the native protein alone and when the ligand is added, is referred to as the Tm shift; this is a guide to the affinity of the interaction. A fluorescent dye

with high affinity for hydrophobic residues, which are exposed on unfolded protein, is used to monitor the change in fluorescence of the protein-bound dye during heating. Purified samples were buffered in 10 mM Hepes buffer pH 7.5, 500 mM NaCl at a final concentration of 2μM in 20μl volume. The fluorophor SYPRO Orange (Invitrogen, Carlsbad, CA) was added as a fluorescent probe at 1 in 1000 dilution. Protein and 10 mM concentration ligands were then assayed in 96-well PCR microplates (ABGene, Surrey, U.K.) in the RT-PCR devices (Stratagene Mx3005p). The temperature was raised with a step of 1°C per minute, from 25°C to 95°C. Fluorescence readings were taken at each interval and plotted as a function of temperature by using an SGC internally developed software package. These experiments were done under the supervision of Dr. Frank Niesen and Dr. Oleg Fedorov (SGC, Chemical Biology).

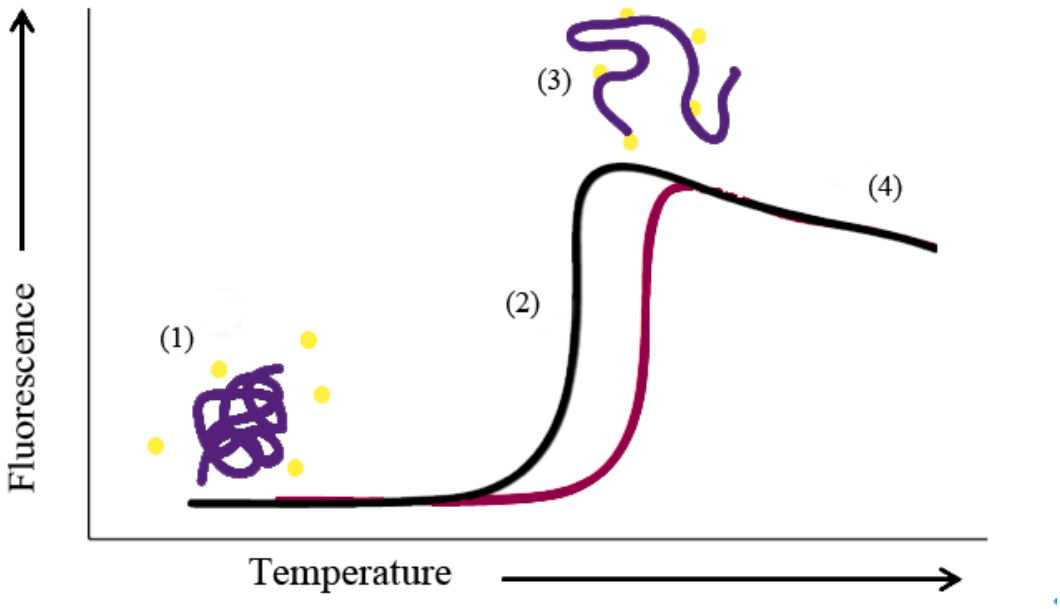

Figure 2.1. Cartoon representation of DSF. (1) The dye binds weakly to the folded protein giving poor fluorescence. (2) Reaching of the Tm. (3) The dye binds preferentially to unfolded protein with exposed hydrophobic regions giving the highest level of fluorescence. (4) Sloping baselines are expected as fluorescence intensity decreases with increasing temperature. The black curve represents the apo-protein, the purple curve the protein bonded to the small molecule.

2.4.7 Dynamic light scattering (DLS)

Dynamic Light Scattering is also known as "photon correlation spectroscopy" (PCS) or "quasi-elastic light scattering" (QELS). This technique uses the scattered light to determine the size of particles or molecules. If the spherical particles in Brownian motion are illuminated with a monochromatic light beam, such as a laser, this causes the variation of the light intensity, which is related to the size of the particle. Using the Stokes-Einstein relation (Equation 2.1), it is possible to derive a size distribution for the sample, where the size is given by the "Stokes radius" or "hydrodynamic radius" (R_H) of the protein particle, which depends on mass and conformation.

$$R_H = \frac{k_B T}{6\pi\eta D}$$

Equation 2.1.

k_B is the Boltzmann constant (in J K^{-1}), D the diffusion coefficient (in m^2s^{-1}), T the temperature in Kelvin and η the viscosity. If temperature and viscosity are maintained constants, small particles move and tumble faster then large ones, rapidly incrementing the scattering function changes.

Usually conformational homogeneity increases protein self-assembly into ordered crystals, which is required for crystallographic studies. Dynamic light scattering is a method to check the presence of very small amounts of aggregated protein (<0.01% by weight). The aim of this experiment was to identify suitable buffer/additive conditions for stabilization of the kinase domain of LIMK1. The protein at 1 mg/ml was incubated in different buffer conditions at 12-µl volume. The DLS experiment was performed at room temperature. The experiments were performed at room temperature under the supervision of Dr. Melanie Vollmar (SGC, Crystallography).

2.4.8 Limited proteolysis

Limited proteolysis and subsequent mass spectrometric analysis was applied to detect globular folded domains in the full-length cGKI. The target protein was concentrated at 1mg/ml. Protease trypsin stock solution (1mg/ml) was diluted in 50 mM Hepes,

300 mM NaCl, 2 mM $CaCl_2$, 5 mM DTT, pH 7.5 at different sample/ protease ratios. The digestion reactions were carried out by incubating 0.5, 1, 2, 4 and 10 μg of trypsin in 20 μl final volume at room temperature. Proteolysis was stopped by addition of 10 μl of stop buffer (2 mM PMSF, 10 mM EDTA) after 0, 15, 30 and 60 minutes. Each reaction was analysed by SDS-PAGE gel and mass spectrometry.

2.4.9 Isothermal Titration Calorimetry

Purified proteins were extensively dialyzed against ITC buffer (50 mM Hepes, 150 mM NaCl and 0.5 mM TCEP, pH 7.5). ITC experiments were conducted on a VP ITC microcalorimeter instrument (MicroCal Inc) at 15°C. During each experiment about 1.4 ml of titrand (LIM-LIM and LIM-LIM-PDZ) were titrated with 20 injections of the titrant (the peptide). The injection spacing was 150 seconds, which allowed complete requilibration. ITC data were analysed with the processing software based on Origin 7.0 supplied by MicroCal. ITC is a thermodynamic technique that directly measures the heat released or absorbed during a biomolecular binding event. Binding stoichiometry (N), enthalpy (ΔH), and binding constants (Ka) were determined by fitting the data to a one-site binding model. For each experiment the free energy change (ΔG) and the entropy change were calculated according to the equations:

$$\Delta G = -RTln(Ka)$$

Equation 2.2

$$\Delta G = \Delta H - T\Delta S$$

Equation 2.3

where R is the gas constant (1.9872 cal/$K^{-1}$$mol^{-1}$) and T the temperature in Kelvin at which the experiment was performed.

2.4.10 Buffer screen

The buffer screen was designed by Dr. Opher Gileadi (SGC, Genome Integrity and Repair) and aims to identify any buffer condition that preserves a protein in solution without precipitation. The experiment is very simple: protein precipitation is measured on a 96 well sitting drop crystallization plate, using different buffer conditions such as pH, salt, additives, metals and detergents in the well reservoirs. 50 nl of the desired protein were mixed with 200 nl of screen solution using a crystallization robot. The plate was incubated at 20 °C and inspected within 24 hours. According to the drop quality, clear solution or precipitate, a score of 1 or -1, respectively, was assigned. A final score was calculated using the Excel correlation function.

2.5 Crystallization experiments

2.5.1 Crystallization

Crystallization was performed at the SGC, using the vapour-diffusion sitting drop method, taking advantage of a Mosquito (TTP Labtech) robotic crystallization device. The robot was programmed to set up 150-200 nl-scale vapour diffusion sitting drop crystallization experiments in 96-well plates containing 20 µl of reservoir solution. For initial trials several sparse matrix screens were used, including commercial screens such as Hampton Crystal Screens I/II and Hampton Index screen (Hampton research), as well as homemade screens named LFS4, JCSG4 and BCS2. Protein was mixed in a 3:1, 2:1 and 1:1 volume ratio with the reservoir solutions. Crystallization plates were incubated at 4°C or 20°C and regularly inspected over a period of two months using a Minstrel™ HT crystal imaging system (Rigaku).

2.5.2 Microseeding

Microseeding is a technique used to introduce nucleation sites at low protein saturation, where the growth is optimal but nucleation improbable, by supplementation of a small amount of seeds into crystallization drops. To prepare a seed stock, a number of small crystals was crushed and mixed with the stabilization buffer, and then the solution was collected into a seed bead tube (Hampton). The

solution was initially diluted with 40 µl of the stabilization solution, and the tube vortexed in pulse, 2 seconds on and 10 seconds off to avoid heat, for 10 times. The seed stock was further diluted 3 times with the stabilization solution prior to the use in crystallization experiment, where 20 nl of the diluted seed stock was added into crystallization drops.

2.5.3 Data collection and structure determination

Crystals were cryoprotected with the respective mother liquor supplemented with as suitable cryosolution prior to flash-frozen in liquid nitogen. High resolution datasets were collected at beamline I03 of Diamond Light Source. The data was indexed, integrated and scaled using the programs MOSFLM (Leslie, 2006) and SCALA (Evans, 2006), respectively. The phase problem was solved by molecular replacement using the program PHASER (McCoy et al, 2005). Density modification and NCS averaging were performed with PARROT (Zhang et al, 1997), and the improved phases were used for automated model building with ARP/wARP (Perrakis et al, 1999). Model refinement was carried out using REFMAC5 (Murshudov et al, 1997). The program COOT (Emsley & Cowtan, 2004) was used for model building and visual inspection of electron density map. Optimal TLS groups calculated by the TLSMD server (Painter & Merritt, 2006) were used in the last refinement step. Structure was validated for geometric correctness using MOLPROBITY (Davis et al, 2007). Figures and topology diagrams were generated using MOLSOFT ICM-Pro (Abagyan et al, 1994).

3 Results

3.1 Characterisation of cGKIβ

3.1.1 Expression

The full length cGKIβ was initially expressed in *E. coli* Rosetta using many different vectors, but unfortunately showed no soluble expression. A cell-free expression system based on wheat germ extract was also tested; the putative protein was successfully expressed but the yield was too poor for crystallization trials. To overcome such limitations, human cGKIβ was overexpressed by employing the Baculovirus Expression Vector System in Sf9 insect cell lines (§ 2.2.2). All baculovirus plasmid constructs were cloned by the Structural Genomics Consortium (SGC) prior to this study and available as P3 viruses. The expression induced an N-terminal $(His)_6$-tag and a TEV protease recognition sites for tag cleavage. Since the addition or deletion of one single domain can drastically change the physicochemical properties of a protein, several constructs, including multi-domains, were tested for soluble expression (Table 3.1). During this PhD work, other groups were able to offer new structural insights solving the structure of some domains of cGKI: the dimerization region (Casteel et al, 2010) and the tandem cyclic nucleotide-binding site (Osborne et al, 2011). Constructs in wells A1 and A6 (Table 3.1) were initially expressed in a large scale seeding Sf9 cells at the density of 2×10^6 cells/ml, as it was described in § 2.2.4. Following guidance from a limited tryptic digestion experiment, the construct in well A2, containing both the cGMP-binding sites and the kinase domain was also tested. The full length protein, from well A1, was the only cGKIβ construct that can be expressed in a sufficient yield, about 1 mg per litre of culture, for crystallographic studies. Cells were harvested as described in material and methods and the resuspended pellet was used either fresh or was frozen in liquid nitrogen and then stored at -80°C.

Table 3.1. Expression testing of cGKIβ constructs harvested 48 hours after baculoviral infection of 50ml Spodoptera frugiperda (Sf9) cell culture and purified by Ni-sepharose pull down.

Well	Construct a.a.	Domains	Mass in KDa	Expression
A1	Met1-Phe686	Full length	80.414	medium
A2	Ser102-Phe686	2cGMP-binding sites +Kinase	68.839	low
A3	Glu123-Phe686	2cGMP-binding sites +Kinase	66.437	none
A4	Met134-Phe686	2cGMP-binding sites +Kinase	65.047	none
A5	Arg192-Phe686	2cGMP-binding sites +Kinase	58.888	none
A6	Asp208-Phe686	cGMP-binding site +Kinase	57.093	low
A7	His224-Phe686	cGMP-binding site +Kinase	55.170	low
A8	Gln238-Phe686	cGMP-binding site +Kinase	53.459	low
A9	Ser246-Phe686	cGMP-binding site +Kinase	52.5489	low

3.1.2 Purification

All tested constructs of cGKIβ were present in the supernatant fraction after cell disruption and centrifugation of the cell debris. The purification process needed to be optimized to establish an efficient protocol. In fact, insect cell lysate is often viscous due to nucleic acid contamination, and difficult to handle, especially if it has to be loaded on chromatography columns. To avoid this inconvenience, polyethyleneimine (PEI) can be added to the cell lysate to precipitate nucleic acids prior to centrifugation. In the case of the examined cGKIβ constructs, this additional purification step was harmful since the proteins were precipitating together with the PEI. Nucleic acid removal with DEAE cellulose was also ineffective. Cell debris was

filtrated and applied either to a gravity Ni-NTA column or in batch and purified through IMAC (§ 2.3.1). The His-tag was removed from the fusion protein by TEV enzymatic cleavage, and the protein was further purified by size exclusion chromatography (SEC) S200 (Figure 3.1A). The tag free protein was, then, separated from uncleaved protein by a second run of IMAC chromatography using a Ni rebinding gravity column (Figure 3.1B).

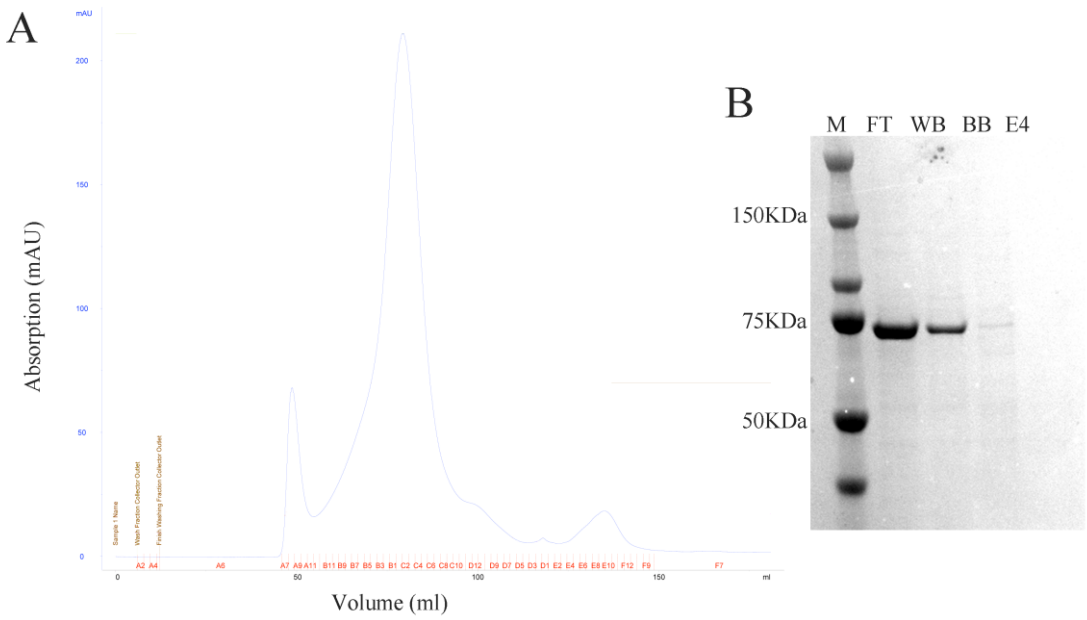

Figure 3.1. Size exclusion elution profile and SDS-PAGE of the Ni-rebinding column. The protein was monitored at 280 nm (blu curve). cGKIβ purity was checked by SDS-PAGE. The gel shows the marker (M), gel filtration elution fractions (B4-C4), which were collected as flow trough, (FT) the washings with an imidazole gradient (5 mM, 30 mM and 250 mM).

A total of three purification steps were necessary to obtain a protein purity ideal for crystallization trials. During the purification steps, the intact mass of all constructs was analysed by liquid chromatography–mass spectrometry (LC-MS) to see whether the length of the cloned sequence and an additional ~80 Da corresponded to a singularly occupied phosphorylation site.

3.1.3 Identification of cGKI ligands

The Structural Genomics Consortium had a collection of ~700 small molecule kinase inhibitors that were available for screening in this study. It has been shown that ligands increase the success rate of protein crystallization, perhaps by reducing protein flexibility, or the propensity to unfold, aggregate, or degrade under proteolysis (Vedadi et al, 2006; Niesen et al, 2007). Differential scanning fluorimetry (DSF) was used to identify cGKIβ ligands.

Table 3.2. Tm shifts measured for the short kinase cGKIβ domain (A6).

Compound n°	cGKIβ (A6) Tm	Compound SGC	Compound description
1	16	K00207a	Staurosporine
2	13.07	K00611a	
3	9.68	K00606a	
4	7.66	K00545	Indirubin E804
5	7.02	K00244	GSK inhibitor XIII
6	7	K00604a	
7	6.96	K00225a	JAK Inhibitor I
8	6.94	K00204	BIM 9
9	6.88	K00608a	
10	6.82	K00232	Staurosporine Aglycone
11	6.4	K00609a	
12	6.22	K00605a	
13	6.12	K01844a	
14	5.99	K00077a	K252a
15	5.88	K00963a	Cdc7/CDK9 inhibitor
16	5.82	K00937a	
17	5.49	K01779a	
18	5.42	K00084b	H-89
19	5.39	K00476a	BIM
20	5.38	K00071	Ellipticine
21	5.31	K00610a	

In this thermal shift assay, inhibitor binding is detected by an increase in the protein's thermal stability, which is proportional to the binding affinity. To identify a kinase inhibitor for use in crystallization of cGKIβ several thermal melting experiments were set up (as described in § 2.4.6). In particular, two constructs were analysed, the kinase domain (A6) and the full length protein (A1), using available kinase inhibitor screening library plates (Table 3.2 and 3.3).

Table 3.3. Tm shifts measured for the full length cGKIβ (A1) construct.

Compound n°	cGKIβ (A1) Tm	Compound SGC	Compound description
1	16	K00207a	Staurosporine
2	3.85	K02698a	PI 3-K Inhibitor VIII
3	2.94	K00963a	Cdc7/CDK9 inhibitor
4	2.59	K00982a	GW8510
5	2.27	K00071	Ellipticine
6	2.24	K00983a	AZD 7762
7	2.03	K02717a	
8	1.27	K02671a	Keratinocyte Differentiation Inducer
9	1.22	K02703a	Reversine
10	1.16	K00967a	

Interestingly, the examined constructs showed different compound affinity; some compounds indicated higher Tm shift for the kinase domain rather the full length cGKIβ. For example, the Cdc7/CDK9 inhibitor (K00963a) indices a Tm shift of 5.88 °C when it binds to the kinase domain and only 2.94°C to the full length protein (Table 3.2 and 3.3). This behaviour can be explained postulating that the dimerization/docking region together with the two tandem cGMP-binding sites of the full length cGKIβ would influence the accessibility at the ATP-pocket for inhibitor binding. Furthermore, analysis of the denaturation curves of the full length protein in the presence of cGMP and the kinase inhibitor, shows that cGMP changes the unfolding profile. In fact, a shoulder is present on the curve of the full length cGKIβ incubated with its cofactor cGMP, probably reflecting a conformational change in the

first cGMP-binding domain, while this is not observed with ligand presence, such as staurosporine (Figure 3.2.).

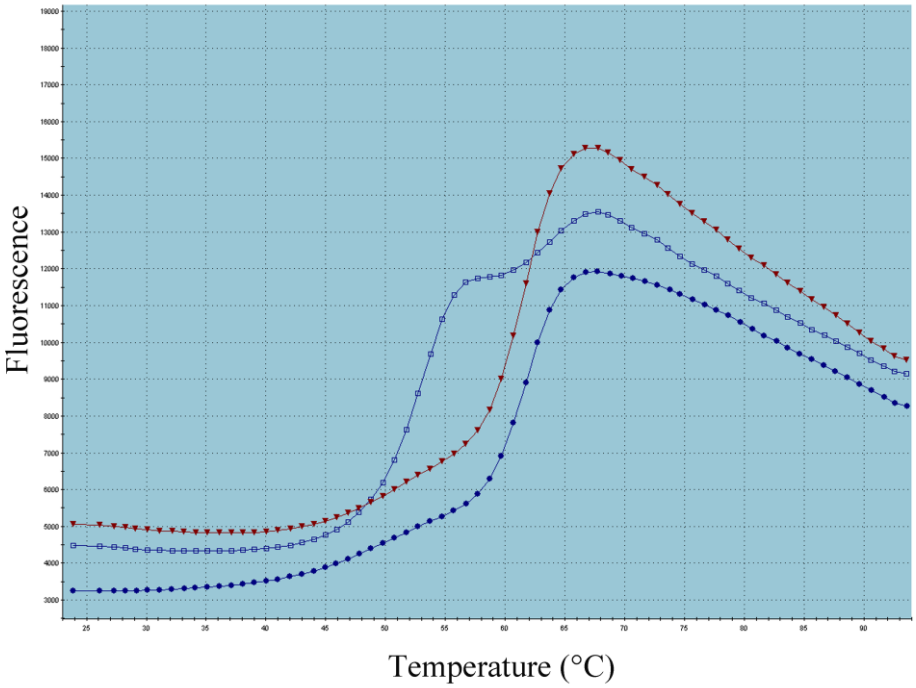

Figure 3.2. Comparison of full length cGKIβ dissociation curves under cGMP effect. The curve in blue represents the apo-cGKIβ fluorescence emission signal recorded as a function of temperature. The thermal shift of the enzyme in complex only with the small molecule staurosporine is represented by the red curve. cGKIβ in presence of cGMP (cyan) goes under a kinetic change, probably, in proximity of the first cGMP binding domain shown by a shoulder on the curve.

From the inhibitors that were screened for potency against the full length cGKI, staurosporine (K00207a), PI 3-K Inhibitor VIII (K02698a) and AZD 7762 (K00983a), giving Tm shifts of 16°C, 3.85°C and 2.24°C, respectively, where chosen to proceed with crystallographic studies (Figure 3.3). K00983a was used instead of K00963a, K00982a and K00071 for the simple reason that it was the only one available in sufficient quantity at the time and the Tm differences between the compounds were insignificant.

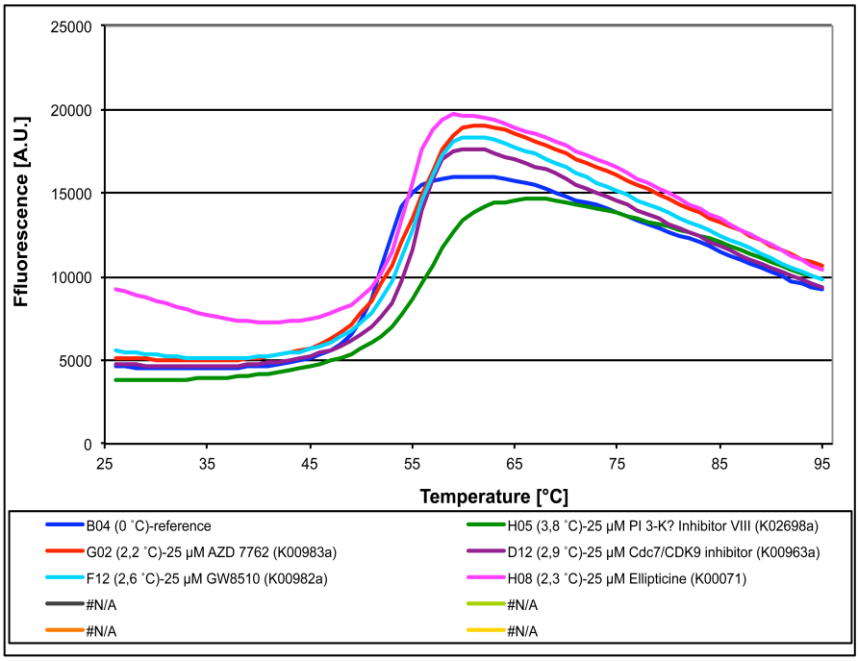

Figure 3.3. DSF analysis of cGKIβ. Example plot of cGKIβ unfolding curves with several different inhibitors measured by Sypro Orange fluorescence.

The high conservation of the ATP pocket in human kinases presents a major challenge for the design of selective kinase inhibitors. The DSF data available in the SGC provides coverage across a large part of the kinome.

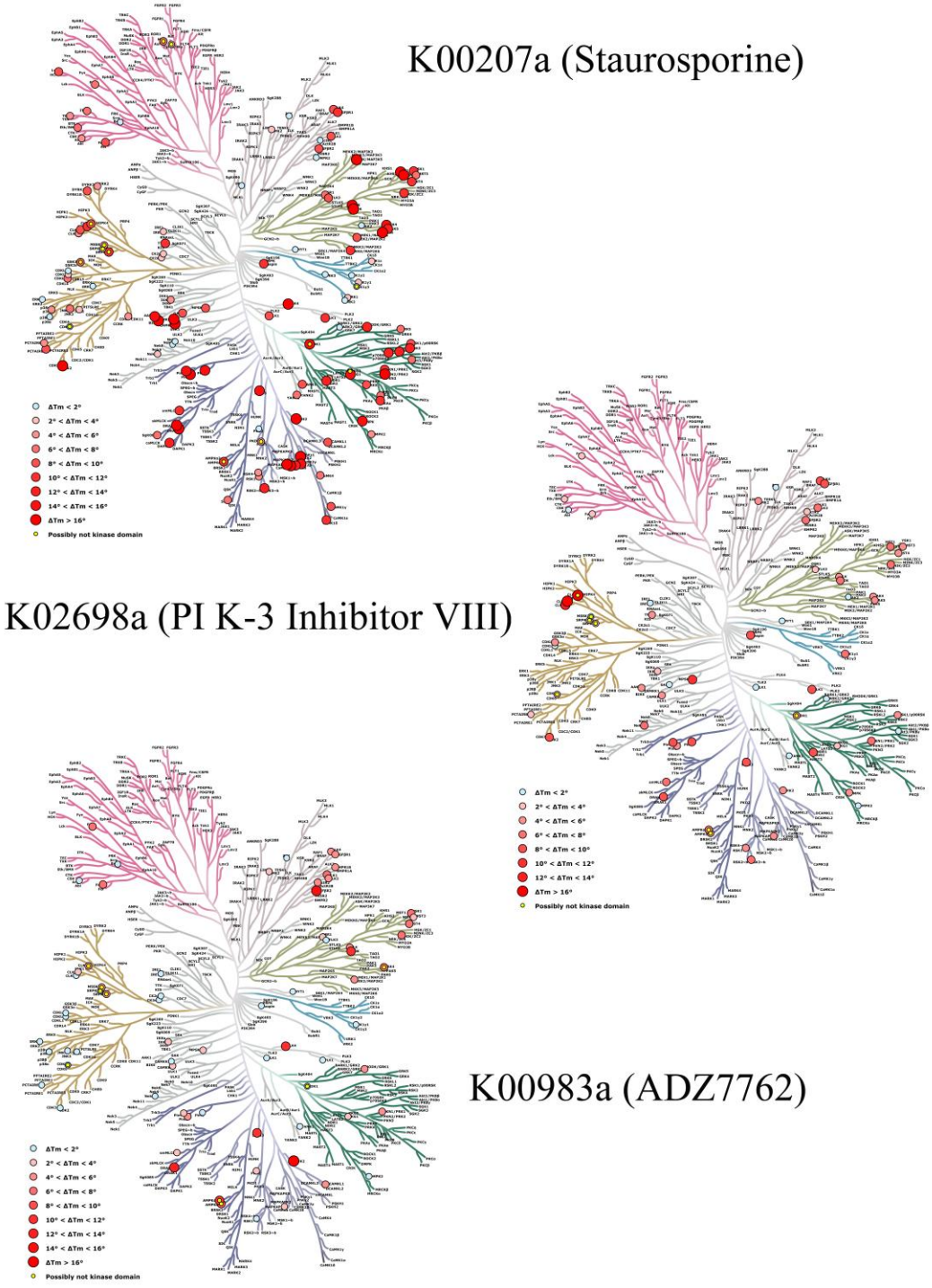

Figure 3.4. Selective kinase inhibitors interaction for cGKIβ. Kinases found to bind are marked with a colour scale based on ΔTm shift (from cyan to red to the highest Tm shift).

It is important to compare the activity of the identified cGKI hits with their activity across the kinome to determine their specificity (Figure 3.4). This was conducted by analysis of historical data held in SGC databases. As expected K02698a and K00983a were more selective than staurosporine and for this reason these inhibitors were considered of higher interest for initial crystallization trials.

3.1.4 Identification of amino acids in BMPRII that interact with cGKI

To further define the binding of cGK1 to BMPRII a cellulose-bound peptide SPOT (pepscan) array was prepared. To this end, the amino acid sequence of the human BMPRII cytoplasmic tail domain (amino acids 500-992) was covered by an array of cellulose-bound 15-mer peptides, each overlapping in sequence by 3 amino acids. All incubation and washing steps were carried out under gentle shaking and at room temperature. The membrane was washed as described in § 2.4.5. At the time of this experiment an expression system for the full length cGKIβ was not yet established. Therefore, a recombinant full length human cGKIβ protein (ORF NP_006249.1, 1-686 a.a.) with an N-terminal GST-tag was purchased (Abnova). The membrane containing the peptide array was incubated with the GST-tagged cGKIβ and washed extensively. The bound protein was detected by anti-GST antibodies bound to HRP-conjugated secondary antibody (Santa Cruz). A first peptide array identified a main interacting region that covers the initial N-terminal region of BMPRII-tail (amino acids 556-594) and a central shorter region (amino acids 798-813). A second peptide array was performed to define these sequences further. The identified regions were divided into different 15-mer peptides. Three amino acids were mutated in alanines and overlapped in full sequence of each peptide. The goal was to investigate whether any of this amino acids residue is critical for the protein-protein interaction and can be identified as a pivotal docking site for cGKIβ. This pepscan overlay assay identified a two main sequences, which lost cGKI interaction: those are EKNRNSI and VTVTM (BMPRII amino acids 581-587 and 800-804, respectively). It was then decided to synthetize peptides at least 10 amino acids long for further characterization: GEKNRNSINY (KP0157) and EPHVVTVTMNN (KP0158).

3.1.5 Characterisation of cGKI flexibility

Flexible regions are undesirable for crystallization. Due to identify stable protein domains, different constructs of cGKIβ from the kinase domain to the full length protein were investigated by limited tryptic digestion. For some constructs, purification was poor, for example, due to poor protein yield or aggregation. To identify stable fragments of the full-length cGKIβ protein that may have the best chance of producing well ordered crystals, a limited proteolysis was performed as described in § 2.4.8. The masses of protein fragments produced by the tryptic digestion were measured by time of flight mass spectrometry. Interestingly, cGKI gave rise to a stable fragment of 65.33 kDa. Fitting of the mass to the cGKI sequence was carried out using the program PAWS and tryptic cleavage sites. This showed that the cGKIβ fragment encompassed residues 121-587 (Figure.3.5). Thus, the protease removed most of the N-terminal portion that carries the leucine/isoleucine zipper domain (Takio et al., 1984). On the basis of the above considerations, it was decided to also start the purification of a cGKIβ construct lacking the N-terminal autoregulatory domain. Unfortunately, the corresponding protein had the tendency to aggregate making its purification difficult.

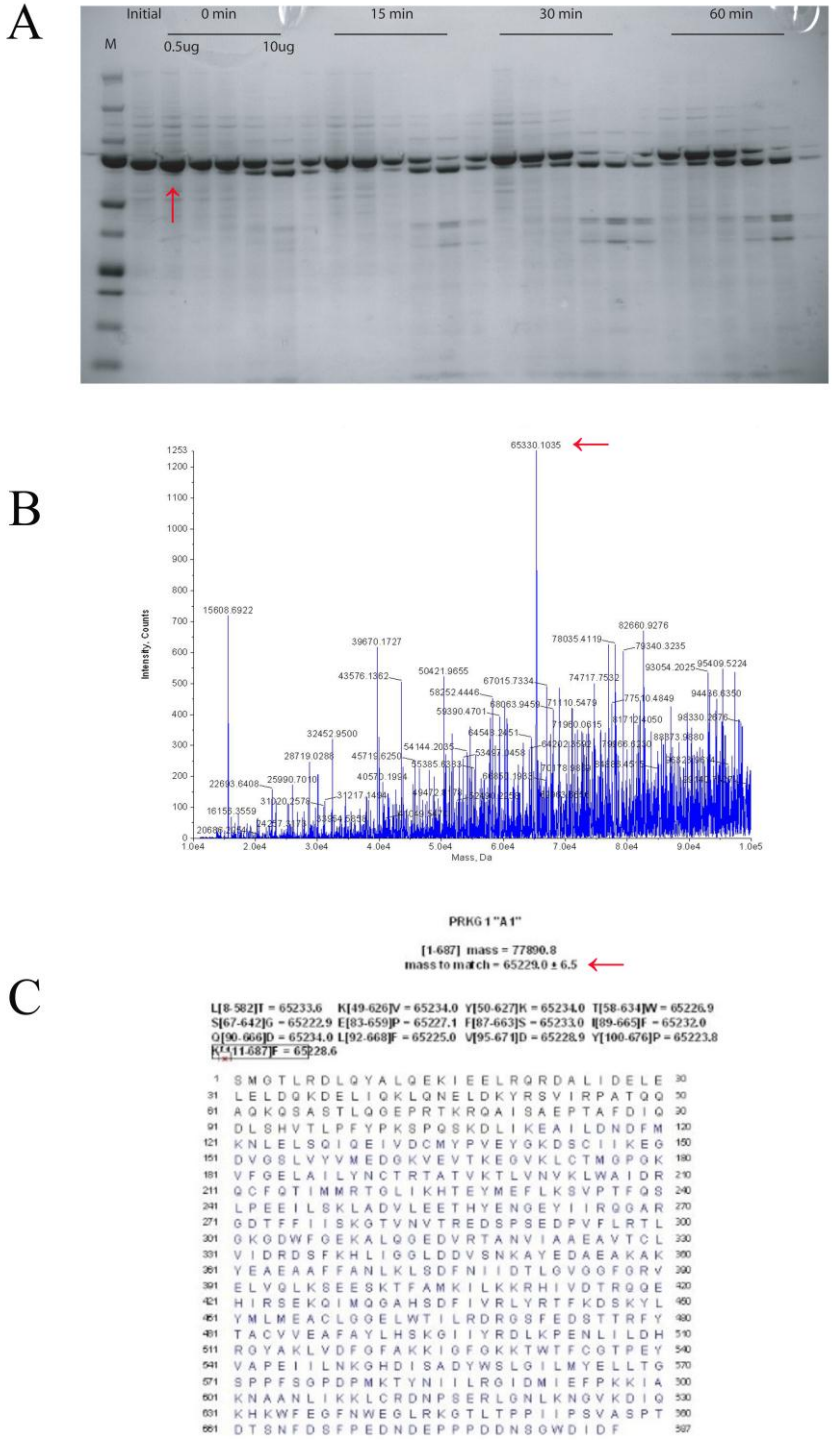

Figure 3.5 Limited tryptic digestion of cGKIβ. (A) SDS-PAGE analysis of a limited proteolysis experiment using the cGKIβ full length protein. A similar digestion pattern was observed under different trypsin concentrations and incubation times revealing a common stable product. (B) Intact mass (LC-MS) of cGKIβ incubated with 1mg of trypsin. (C) Identified sequence from the PAWS mass fitting (blue sequence matches the stable fragment sequence).

3.1.6 Characterisation of cGKIβ Activity

To verify that the expressed cGKIβ proteins were functional, protein kinase assays were performed testing for autophosphorylation of cGKI as well as substrate phosphorylation. cGKIβ constructs that could be expressed and purified with good yield were analysed by LC-MS, a radioactive kinase assay and a NADH coupled assay. Interestingly, the intact mass of both cGKIβ A1 and A6 (see Table 3.1) was 80 Da above the predicted mass, indicating full occupation of a single phosphorylation site (Resing et al, 1995), and suggesting cGKIβ kinase activity. To confirm the activity of the recombinant full length cGKIβ, it was subjected to an *in vitro* phosphorylation assay using γ-^{32}P-ATP. The experiment was set up as described in § 2.4.4. The enzyme was also tested in the presence of the identified kinase inhibitors K00207a, K02698a and K00983a to validate their cGKI inhibition. Incorporated ^{32}P was detected by autoradiography. The input of fusion protein was visualized by immunoblotting using α-cGKI antibody.

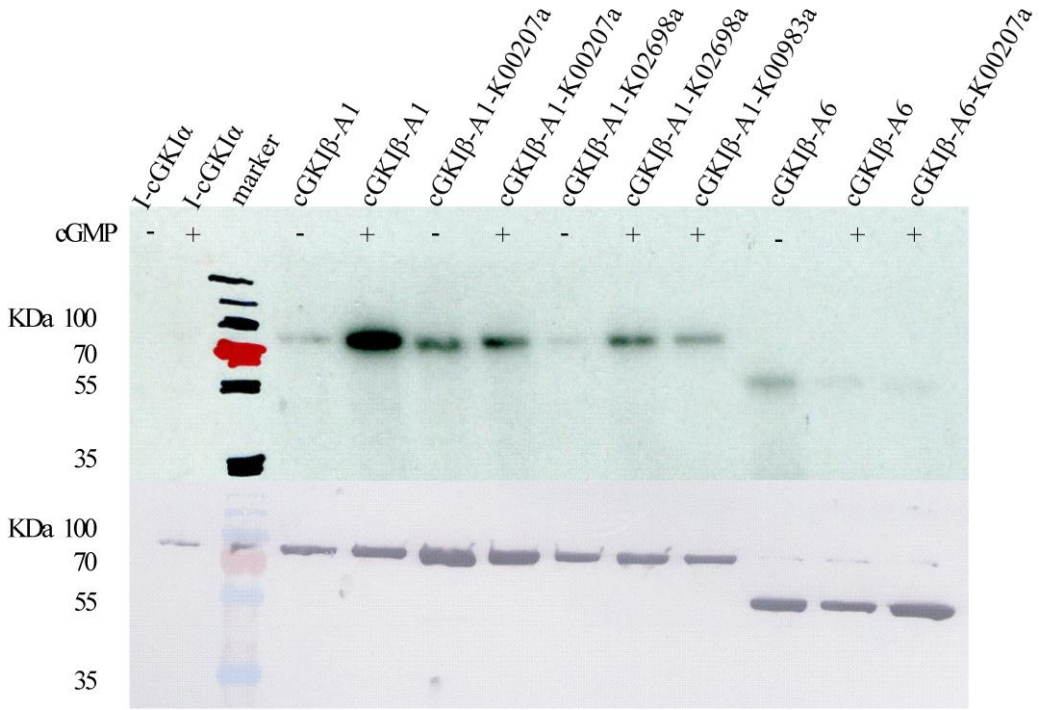

Figure 3.6. Phosphorylation study of cGKIβ full length (A1) and kinase-cGMP domain (A6).

Figure 3.6 demonstrates that cGKIβ showed very strong autophosphorylation in the presence of cGMP, but very little in its absence. Autophosphorylation was also tested in the presence of the kinase inhibitors. Since the signal intensities are much weaker in the inhibited samples it is possible to assert that K00207a, K02698a and K00983a are able to prevent cGKIβ autophosphorylation.

The specific activity of recombinant cGKIβ was further demonstrated using a NADH coupled assay, as described in § 2.4.4. As expected, cGKIβ enzymatic activity was totally dependent on the presence of its cofactor cGMP; in fact, there was no activity with ATP alone.

3.1.7 Crystallization trials with cGKIβ

Crystallization trials of cGKIβ were undertaken with different constructs and ligands. Good expression and purity was achieved for the kinase domain with one cGMP binding domain (A6) as well as the full length protein (A1). These were tested in crystallization using a vapour diffusion set up using several commercial sparse matrix screens taking advantage of a Mosquito (TTP Labtech) robotic crystallization device. For simplicity the protein concentration, sparse matrix screens and incubation temperatures are reported in Table 3.4. In all experiments the desired protein was mixed in 2:1, 1:1 and 1:2 ratios with the reservoir solution to give 150 nl final volume drop. Crystallization plates were incubated at 4°C and 20°C and inspected regularly over a period of two months using a Minstrel™ HT crystal imaging system (Rigaku).

Table 3.4. Crystallization experimental conditions for cGKI short and long form.

Construct	Concentration	Compound	Compound concentration	Screen	Temperature
cGMP-binding site +Kinase (A6)		K00207a	1 mM	LFS4	20°C
	20 mg/ml	cGMP	2 mM	JCSG4	
Full length (A1)	14 mg/ml	K00207a	1 mM	BCS2	20°C
				HCS	
Full length (A1)	14 mg/ml	K00983a	1 mM	HIN	20°C
				LFS4	
Full length (A1)	15 mg/ml	K02698a	1 mM	JCSG4	20°C
				BCS2	
Full length (A1)	14 mg/ml	K00207a	1 mM	JCSG4	20°C
		chymotripsin	1:1000		
Full length (A1)	6 mg/ml	K00207a	1 mM	LFS4	20°C
				JCSG4	
Full length (A1)	9 mg/ml			LFS4	20°C
				JCSG4	
				HIN	
				HIC	
Full length (A1)	9 mg/ml			LFS4	4°C
				JCSG4	
				HIN	
Full length (A1)	11 mg/ml	K00983a	1 mM	LFS4	4°C
		cGMP	2 mM	JCSG4	
				HIN	
Full length (A1)	12 mg/ml	K02698a	1 mM	LFS4	4°C
		cGMP	2 mM	JCSG4	
Full length (A1)	12 mg/ml	K02698a	1 mM	HIN	20°C
		cGMP	2 mM	HIC	
Full length (A1)	8.4 mg/ml	K02698a	1 mM		
		cGMP	2 mM	cGKI-sp-z001	20°C
		consensus peptide	1 mM		

Egg-shaped crystals appeared for the full length protein in a condition containing 0.1 M SPG (succinic acid, phosphate and glycine buffer mix), 30 % (w/v) MPD, pH 8, incubated at 20°C (Figure 3.7A), which unfortunately dissolved by the time they were removed from the imager for crystal mounting. Taking advantage of this information, an optimization follow up, cGKI-sp-z001, was designed covering a pH range from 7.2 to 8.8 of SPG system and spanning from 37-70 % MPD (§ 7.2.1). A skin crystal was obtained in condition 0.1 M SPG pH 8.8, 70% (w/v) MPD (Figure 3.7B), it was cryoprotected in mother liquor supplemented with 10% glycerol. The crystal was tested at the Diamond Light Source synchrotron, but showed no protein diffraction pattern. These conditions remain of interest for optimization, but due to time constraints (and success with other projects) they have not been investigated further in this study.

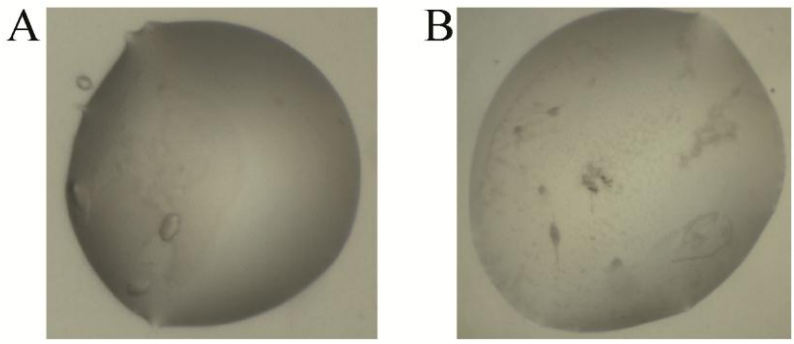

Figure 3.7. Crystallization of cGKIβ. (A) Small egg shape crystals grown in 0.1 M SPG system, 30 % (w/v) MPD, pH 8, incubated at 20°C. (B) Skin crystal grown in 0.1 M SPG, 70% (w/v) MPD, pH 8.8.

3.2 LIMK1

LIMK1 has emerged as an important drug target in cancer. Furthermore, its coexpression with the tail domain of BMP receptor II is associated with several other pathological processes. Since LIMK1 is formed by more than one domain, which are implicated in different and specific functions, it was decided to focus the attention on these different constructs: the kinase domain, implicated in tumour cell invasion and metastasis; the LIM-LIM-PDZ and the LIM-LIM domains involved in the binding with BMPRII long cytoplasmic tail.

3.2.1 Characterisation of the LIMK1 Kinase domain

The kinase domain of LIMK1 is the catalytic region of the enzyme, which determines its activity against cofilin and control over actin polymerization. It is therefore of great interest to determine the first LIMK1 kinase domain structure and to establish protocols for the co-crystallization of LIMK1 kinase inhibitors with potential application in cancer models.

3.2.1.1 LIMK1 kinase expression screening

Many different constructs of the kinase domain were designed and cloned by the Structural Genomics Consortium (SGC) prior to this PhD project. The proteins were expressed as N-terminally His_6-tagged proteins in Sf9 insect cell lines (§ 2.2.2). An initial small scale expression test was performed, showing that only 3 of the 11 engineered constructs were soluble expressed in high yields (Table 3.5).

Table 3.5. Expression testing of LIMK1 constructs harvested 48 hours after baculoviral infection of 50ml Spodoptera frugiperda (Sf9) cell culture and purified by Ni-sepharose pull down.

Well	Construct a.a.	Mass in KDa	Expression
A1	Ser271-Asp647	45.515	medium
A2	Ser271-Ser637	44.502	high
A3	Ser271-Gly627	43.190	low
A4	Asp317-Asp647	40.946	medium
A5	Asp317-Ser637	39.933	low
A6	Asp317-Gly627	38.621	low
A7	Glu322-Asp647	40.418	medium
A8	Glu322-Ser637	39.405	medium
A9	Glu322-Gly627	38.092	low
A10	Pro330-Asp647	39.475	high
A11	Pro330-Ser637	38.462	high
A12	Pro330-Gly627	37.149	none

These three constructs were expressed in large scale and purified according to the protocols described in material and methods § 2.2.4, but two of the constructs failed to yield protein. An additional expression test was pursued to explore different virus concentrations, infection times and cell density, with the goal to optimize the

expression of 5 constructs (in wells A2, A5, A7, A10 and A11). The best expression was obtained by incubating 2ml of the P3 virus of construct Pro330-Ser637 (well A11) per 100 ml Sf9 cells at the density of 2 x 10^6 cells/ml for 72 hours at 27°C under shaking. Protein yields of human LIMK1 kinase domain averaged ~ 3 mg/L InsectXpress medium.

3.2.1.2 Purification of the LIMK1 kinase domain

The purification of the human LIMK1 kinase domain construct A11 was a limiting and challenging step. The protein had a tendency to aggregate and precipitate, precluding the purification of sufficient material for crystallization trials. To establish a successful purification protocol other experiments had to be performed to solve these problems, in particular to identify a kinase ligand (using DSF screening), optimum pH, salt concentration or buffer additive (using dynamic light scattering, DLS) that would provide protein stabilization. LIMK1 was very sensitive to proteolysis during purification; to prevent protease degradation a high amount of protease inhibitor (1:1000, Calbiochem® Protease Inhibitor Cocktail Set III, EDTA-Free) was needed during cell disruption and in all purification steps. Nucleic acid removal by PEI or DEAE cellulose binding as a pre-purification step also enhanced the precipitation of the protein. For this reason, this step was avoided with the consequence that the soluble lysate was highly viscous.

LIMK1 kinase domain was first purified by nickel affinity chromatography, initially using a drip column under gravity flow, but later performed in batch to due to problems with the column clogging. Using this method it was possible to minimize the loss of LIMK1 protein. After this step, the tag was removed by TEV enzymatic cleavage, and the untagged protein was further purified by size exclusion chromatography (SEC) (Figure 3.8 A and B). The cleaved (untagged) protein was separated from any remaining uncleaved protein by a second run of IMAC chromatography using a small Ni-rebinding column (Figure 3.8C). Following this procedure, the protein still contained minor contaminants and was unsuitable for crystallization. The protein was therefore further purified by cation exchange chromatography on a HiTrap SP column, knowing that the theoretical pI of the cleaved protein is 9.55. Finally, a desalting chromatography step was applied to

obtain the optimal buffer and salt concentration for the monomeric protein prior to crystallization trials. This purification protocol was established after several optimization attempts to obtain the stable enzyme in solution. The intact mass of the LIMK1 kinase domain was analysed by liquid chromatography–mass spectrometry (LC-MS) at each purification step, and always matched the theoretical mass of the construct (Figure 3.8D).

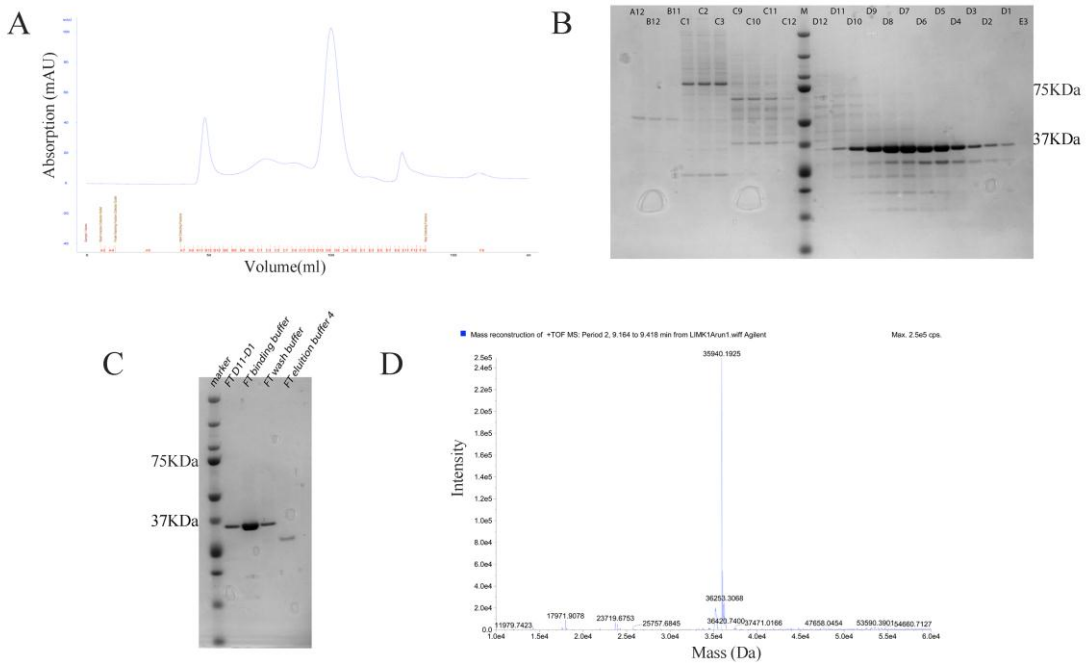

Figure 3.8. Purification profile of LIMK1. (A) Size exclusion elution protein profile was monitored at 280 nm (blu curve) and checked on SDS-PAGE (B). The purity was checked by SDS-PAGE. The fractions of the main peak were pooled and run on a Ni-rebinding gravity column. LIMK1 purity and correct size were controlled under SDS-PAGE (C) and LC-MS (D).

3.2.1.3 Identification of LIMK1 inhibitors

To stabilize the protein and increase the success of protein purification and crystallization, 96 different kinase inhibitors were screened against the purified LIM kinase 1 domain using a differential scanning fluorimetry (DSF) assay. Figure 3.9 shows the strongest inhibitor hits: 31 compounds were identified that bound the target protein as shown by shifting the melting temperature (Tm) between 2 and 8 degrees (Table 3.6).

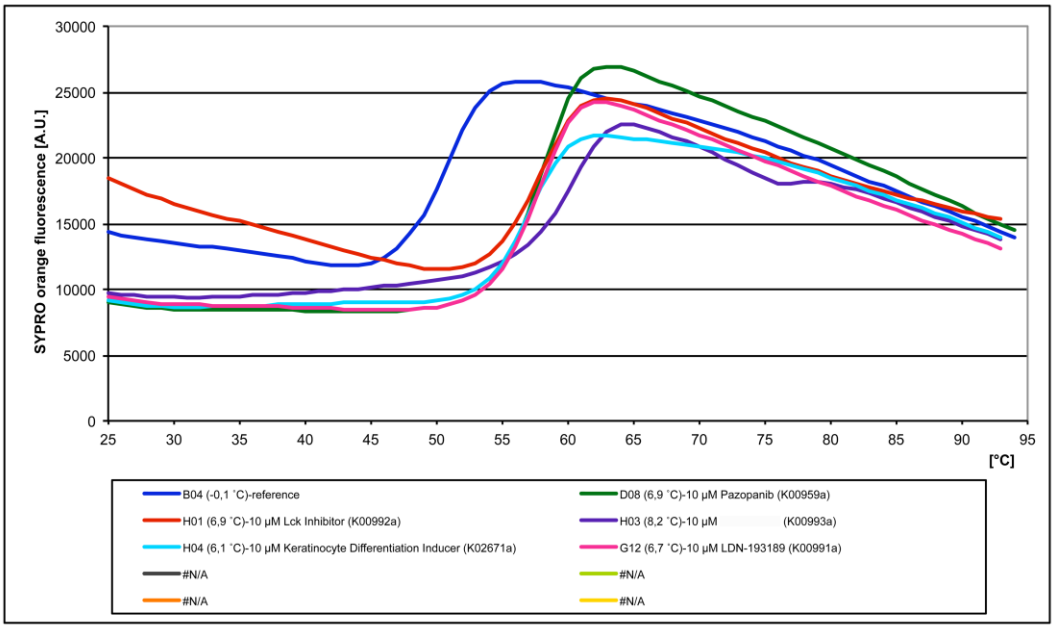

Figure 3.9. DSF analysis of LIMK1. (A) Example fluorescence unfolding curves for LIMK1 in the absence and presence of selected kinase inhibitors.(B) Plot summarizing the Tm shifts for different inhibitors.

The highest Tm shifts were observed for compound K00993a and reversine, which induced Tm shifts of 8.19°C and 8.11°C, respectively. Staurosporine, which gave a Tm shift of only 3.94°C, was also included in crystallization trials, since its known promiscuity suggested that its binding was likely. The structure of the LIMK1 kinase domain was later solved in the presence of staurosporine (PBD 3S95) as described in § 2.5.3. However, it is clearly not the most potent or specific inhibitor identified for LIMK1. From the DSF screening assay the compound K00993a appeared to be the best kinase inhibitor identified for LIMK1 and would be of interest for further chemistry as part of a structure-activity relationship (SAR) study to optimize its activity. From the experience of the SGC, the Tm shift of >8°C is equivalent to an inhibitor IC50 of 100 nM or less. Furthermore, K00993a showed excellent selectivity across the kinome (Figure 3.10).

Table 3.6. Kinase inhibitors selective compounds for LIM kinase 1.

Compound n°	LIMK1 Tm Shift	Compound SGC ID	Compound description
1	8.19	K00993a	
2	8.11	K02703a	Reversine
3	6.89	K00959a	Pazopanib
4	6.88	K00992a	Lck Inhibitor
5	6.66	K00991a	LDN-193189
6	6.12	K02671a	Keratinocyte Differentiation Inducer
7	4.9	K00779a	Flt3 Inhib III
8	4.85	K00984a	BX-795
9	4.68	K02698a	PI 3-K Inhibitor VIII
10	4.59	K00982a	GW8510
11	4.22	K00979a	GSK-3 Inhibitor XVI
12	3.94	K00207a	Staurosporine
13	3.81	K00994a	Dovitinib
14	3.62	K00968a	
15	3.58	K00956a	Axitinib
16	3.16	K00059	Aloisine A
17	3.07	K00986a	Compound 66
18	3.02	K00954a	CVM-O5-149-3

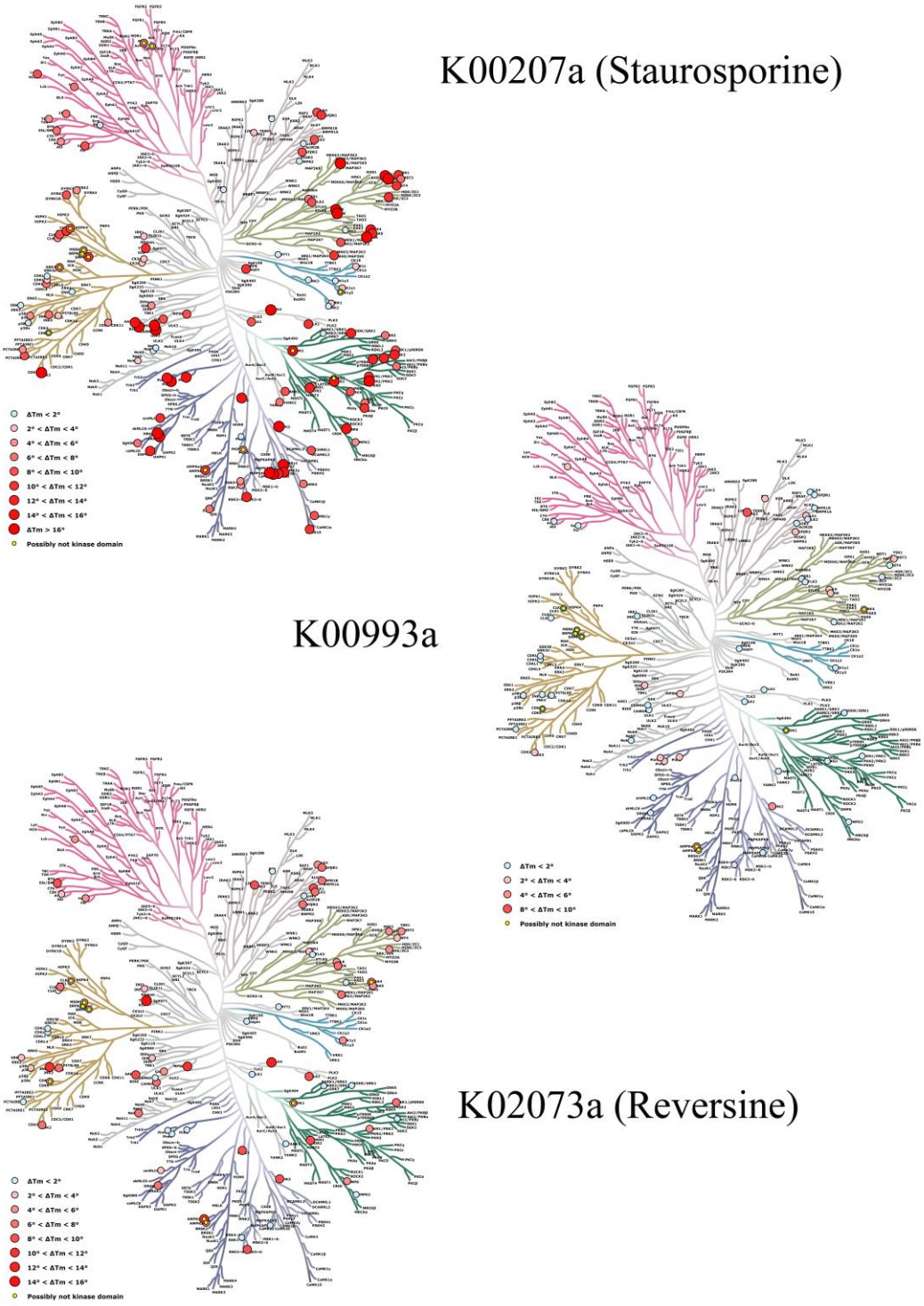

Figure 3.10. Selective kinase inhibitors interaction for LIM kinase 1. Kinases found to bind are marked with a colour scale based on ΔTm shift.

3.2.1.4 Dynamic light scattering test for monodispersity

The identification of buffer conditions that maintain a protein in a soluble, monodispersed state, is generally a prerequisite for successful crystallization trials. The optimization of critical buffer components is often a time- and protein-consuming process. Monodisperse protein particles are the ideal building blocks of stable crystal lattices. To determine the appropriate conditions for monodisperse LIMK1, a dynamic light scattering (DLS) experiment was performed testing different conditions, such as detergent choice, salt concentration and the presence of sugars. The protein was concentrated to 5mg/ml and then diluted 1:5 into buffer conditions (Table 3.7) as different salt, pH, sugar conditions, were tested at room temperature in 12 μl final volume solutions. A desirable result of a DLS experiment is a narrow size distribution and a monodisperse sample. 2 compounds improved the solubility of LIMK1 and were subsequently added to all purification buffers. These were 1 mM EDTA and the amino acid mix of 50 mM Arginine, 50 mM Glutamate (Figure 3.11). In addition, the presence of glycerol helped to maintain the soluble state, while the pH in use was already optimal. The tested solutions were the following:

Table 3.7. Buffer condition tested in the DLS experiment.

	Buffers
1	Control (GF Buffer only)
2	GF Buffer pH 6.2
3	GF Buffer pH 8.2
4	750 mM NaCl
5	100 mM KBr
6	100 mM Li_2SO_4
7	1 mM EDTA
8	50 mM Arg/Glu
9	5% Sucrose
10	10% PEG400
11	10% glycerol
12	10% Ethylene Glycol

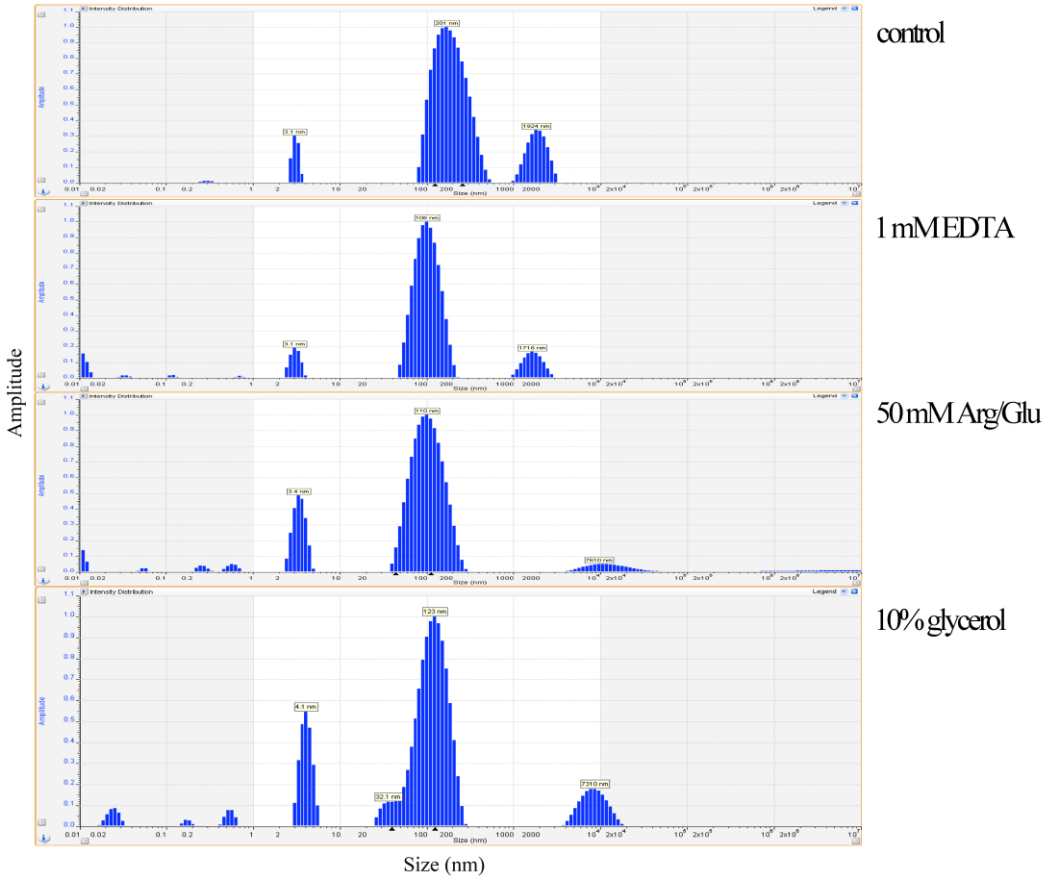

Figure 3.11. Size distribution of LIMK1 determined using dynamic light scattering.

3.2.1.5 Demonstration of LIMK1 kinase activity

To confirm that the purified protein was functional, a NADH coupled assay was performed. In this assay ADP release by a kinase reaction is coupled to NADH oxidation by pyruvate kinase (PK) and lactate dehydrogenase (LDH), as described in § 2.4.4. The results demonstrate kinase activity of the LIMK1. As shown in Figure 3.12, the line slope of the enzyme in the presence of ATP, represented in green, is negative since the initial ATP has been used to produce ADP, that consequently transformed NADH in NAD^+ decreasing the fluorescence signal. Similarly, the initial kinetic rate increased when LIMK1 was incubated in the presence of cGKI consensus peptide (RKRSRAE), cyan line in Figure 3.12, although this it is not the specific substrate.

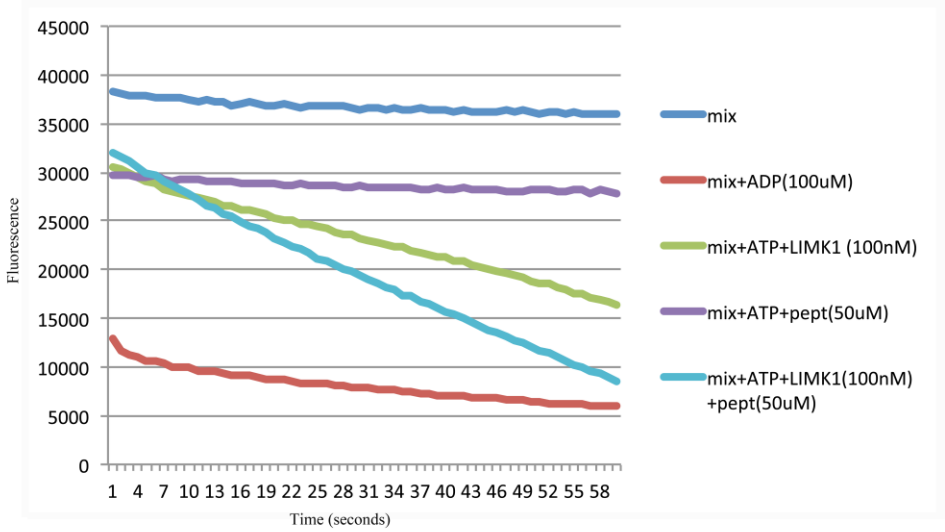

Figure 3.12. NADH coupled assay layout showing on the X axis the time in second and on the Y axis the fluorescence intensity. The red line was a control experiment proving the maximal response to ADP.

3.2.1.6 Crystallization screening

Crystallization of LIMK1 was achieved by vapour diffusion using the sitting drop method as described in § 2.5.1. The initial crystallization was carried out by incubating 10 mg/ml of the apo-enzyme with 1 mM final concentration of three potentional inhibitor identified by DSF, such as K00993a, reversine and staurosporine. The sparse-matrix screens showed that the protein crystallized in complex with staurosporine under several JCSG4 screen conditions, with crystals appearing after 24 hours incubation at 20° C. Analyses of the compositions of some promising conditions showed that effective precipitants were organic molecules, such as MPD, Jeffamine-M600 and PEG3350, and inorganic (Table 3.8). Four lead conditions were selected based on the chemistry of the precipitate agent and a single follow up optimization screen in a 96 well plate format was designed. This was to limit the amount of protein used and also to initially explore if these conditions would be good to reproduce crystals reliably.

Table 3.8. Selected conditions that merited follow up.

JCSG4 screen	Condition
E8	1M Na/K PO_4, 0.1M acetate, pH 4.5
F3	20% MPD, 0.1M Tris, pH 8.0
F4	20% Jeff-M600, 0.1M Hepes, pH 7.5
H8	25% PEG3350, 0.2 NaCl, 0.1M Bis-Tris, pH 5.5

3.2.1.7 Optimization of initial crystals

Optimization of initial crystallization conditions was performed by incremental steps (Figure 3.13). At first all four selected conditions were further explored their efficacy in LIMK1 crystallization by broadly varying the main precipitants and salts concentrations and pH. The first and the second follow-up screens LIMK1A-sp-z001 and LIMK1A-sp-z002 were made (§ 7.2.2 and 7.2.3). Although various inhibitors were used, only staurosporine was shown to be an effective ligand that enabled LIMK1 crystallization in these two follow up screens. Tiny cubic crystals of LIMK1/staurosporine grew in several different MPD- and Jeffamine-M600-based conditions from the LIMK1A-sp-z001 screen, and after implementation of microseeding (see § 2.5.2) in the crystallization experiment these conditions were shown to yield crystals reproducibly.

The third follow up screen, LIMK1A-sp-z003, was then designed to explore a wider and finer range of MPD and Jeffamine-M600-based conditions (§ 7.2.4). At this stage of the experiment, it was shown by DLS that 1 mM EDTA would improve LIMK1 monodispersity and subsequently, 1 mM EDTA was included in the purification buffers (except IMAC) for further crystal screening. The crystals obtained in this optimization screen from both MPD- and Jeffamine-based conditions were similar in their morphologies and growth rate. Typically the drops remained clear for four days before small egg shape crystals formed in conditions B7 and F4. Crystals required approximately a week to grow to the final size. Viable crystals obtained in 24% MPD, 100mM Tris pH 7.2 were cryoprotected in 30% MPD and 10% glycerol.

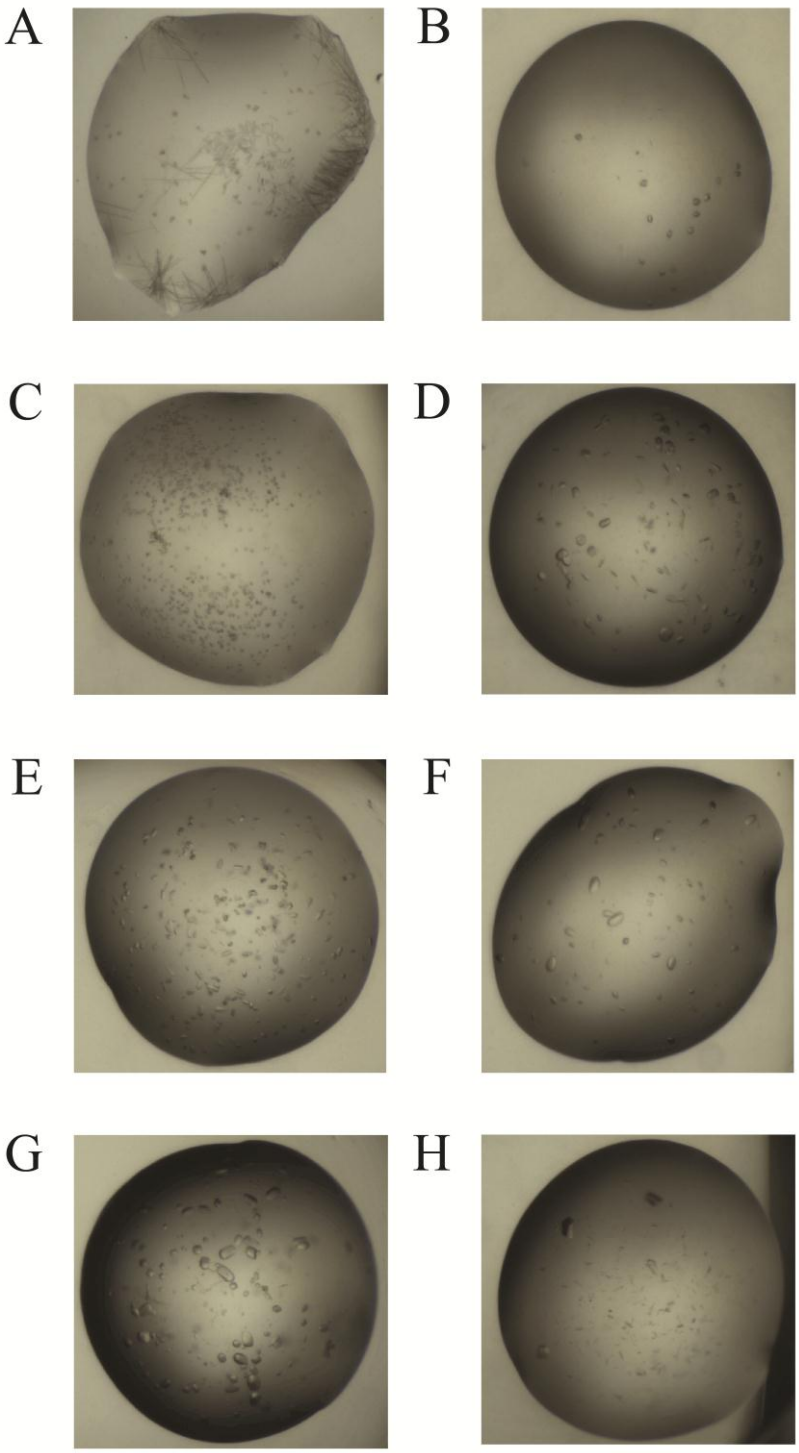

Figure 3.13. Crystals of LIMK1 kinase domain in complex with staurosporine grown in: (A) 20% Jeff-M600, 0.1 M Hepes, pH 7.5; (B) 14% Jeff-M600, 0.1 M Hepes, pH 7.0; (C) 14% Jeff-M600, 0.1 M Hepes, pH 7.9; (D) 15% MPD, 0.1 M Tris, 1 mM EDTA, pH 7.0; (E) 15% Jeff-M600, 0.1 M Bis-Tris Propane, pH 6.5; (F) 15% Jeff-M600, 0.1 M Bis-Tris Propane, 1 mM EDTA, pH 6.5; (G) 15% MPD, 0.1M Tris, 1 mM EDTA, pH 7.0; (H) 24% MPD, 0.1 M Tris, 10 mM Phenol, 1 mM EDTA, pH 7.2.

The X-ray diffracting quality was tested at the Diamond Light Source synchrotron, however the diffraction was poor with a streaky pattern visible to 6 Å resolution. To further improve the crystal quality, the Additive Screen from Hampton research was considered, and each additive at 2 µl was mixed with 18 µl of the previous condition as a base condition (24% MPD, 100mM Tris pH 7.2) to make up 96 reservoirs. Crystallization of the protein using the additive screen was performed at a LIMK1 concentration of 8 mg/ml mixed with 1.5 mM staurosporine. A change in the crystal morphology was apparent in one condition in a drop mixing protein and reservoir at 3:1 volume ratio, in which the crystals appeared to be a cube (Figure 3.13H) with sharper edge compared to previous LIMK1 crystals (Figure 3.13G). This condition contained 10 mM phenol as an additive. Crystals were cryo-protected using the same cryoprotectant as previous.

Apart from attempts to grow the LIMK1-staurosporine complex crystal, the results of the crystallization of the LIMK1 with the other two small inhibitors were less successful with only crystalline precipitates of the LIMK1-reversine (K02703a) and LIMK1-K00993a complexes obtained in a few JCSG4-screen conditions after application of streak seeding (Figure 3.14). Another follow up screen was designed according to the previous conditions. LIMK1A-sp-z004 was generated using 3 different PEGs and salts (§ 7.2.5). To advance the crystal structure of LIMK1 in complex with reversine (K02703a) and K00993a, screens using the condition, which generate the diffracting crystal, 24% MPD, 100 mM Tris pH 7.2, 10 mM Phenol. The enzyme at 6.5 mg/ml was mixed with 1mM of the two inhibitors and mixed 3:1, 2:1 and 1:1 in 200nl sitting drop grown at 20°C, giving crystalline precipitate as well. Unfortunately, no improvement of crystals of these two complexes was obtained.

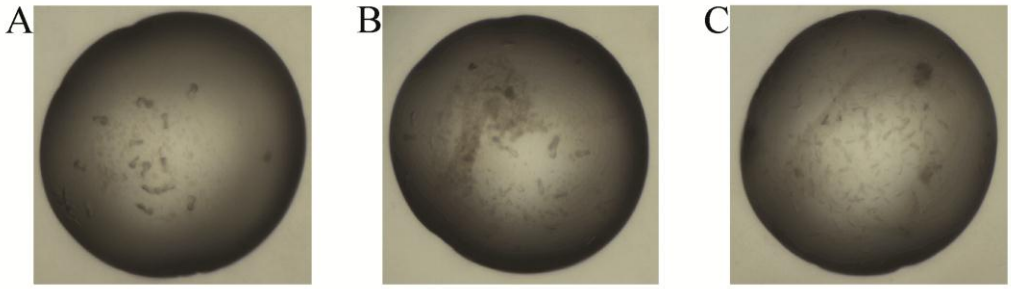

Figure 3.14. Crystalline precipitate and microcrystals of LIMK1 kinase domain in complex with K00993a grown in: (A) 14% MPD, 0.1 M Tris, pH 7.7; (B) 14% MPD, 0.1 M Tris, pH 8.0; (C) 17% MPD, 0.1 M Tris, pH 8.3.

3.2.1.8 X-ray diffraction data collection and Structure determination

A complete X-ray diffraction dataset was collected from a single crystal using monochromatic radiation at wavelength of 0.976 Å at Diamond Light Source synchrotron, beamline I03 and the PSI PILATUS 6M detector system. The reflections were indexed into a *c*-centered monoclinic spacegroup and integrated with MOSFLM (Leslie, 2006). Scaling and merging were performed using the program SCALA (Evans, 2006) and the final resolution of the dataset was truncated to 1.65 Å. Detailed data collection statistics are reported in Table 3.10.

The structure was solved by molecular replacement (MR) using the data between 1.65 and 44-Å resolution and the program PHASER (Read, 2001). To choose a search model, the sequence of LIMK1 kinase domain was used as an input for sequence homology searching against sequences of known structures using EBI Blast server (Figure 3.15). It was observed that the LIMK1 kinase domain has more than 30% sequence identity with human tyrosine kinases (Table 3.9). Two structures chosen as initial search models were the c-Src kinase (pdb id 1YI6) and the human Epha3 kinase (pdb id 2QO9). However, since the protein kinase fold typically consists of two lobes – a smaller amino-terminal lobe (N-lobe), and a larger carboxyl-terminal lobe (C-lobe) – and they are highly flexible depending on activation states, both c-Src and Epha3 structures were further sub-divided into two domains for two rounds of molecular replacement. As a result, the input search models were i) the superimposed C-lobes of the kinases (c-Src, aa 345-533 and Epha3, aa 707-904) and ii) the superimposed N-lobes (c-Src, aa 285-338 and Epha3, aa 608-699).

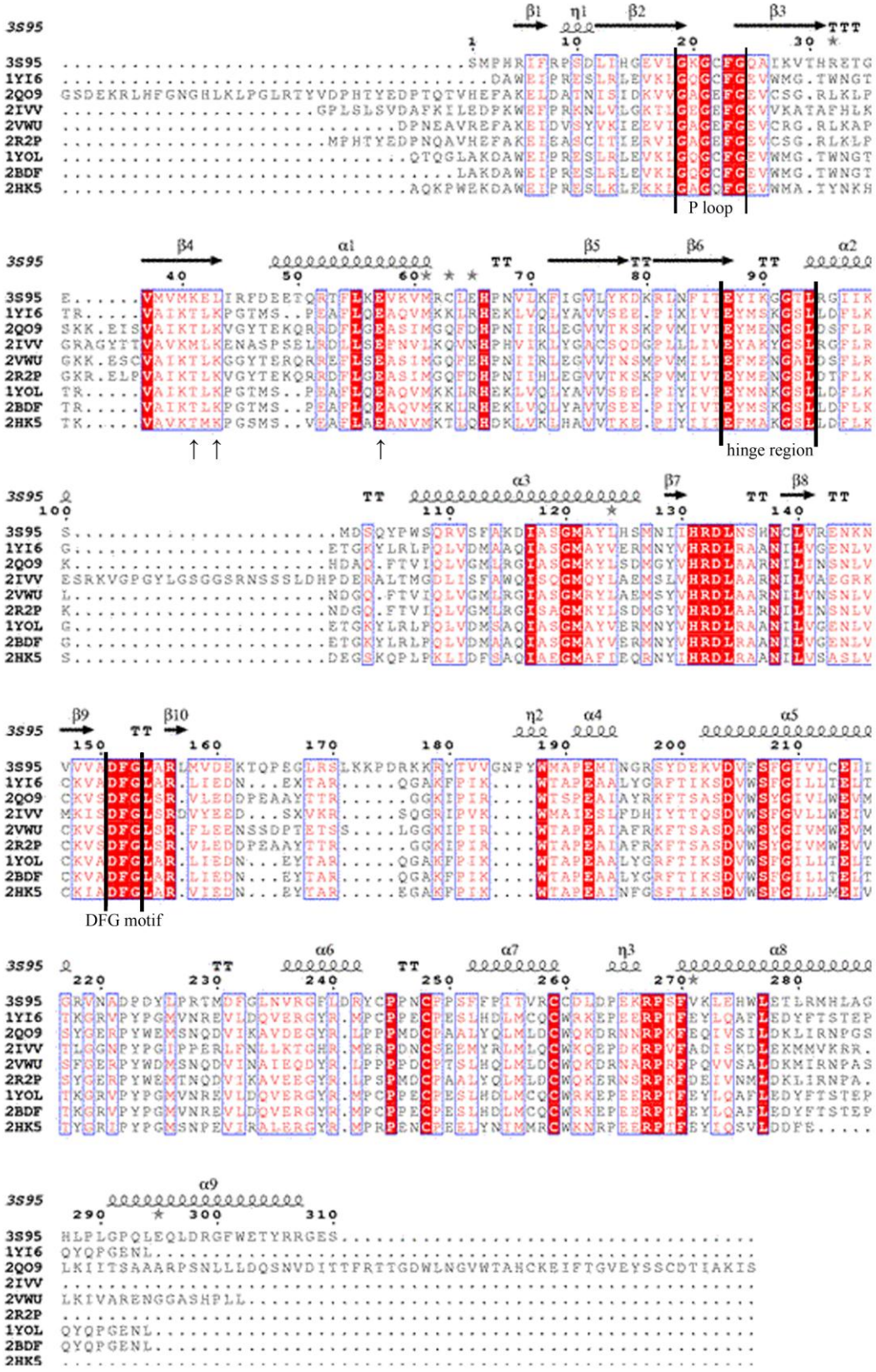

Figure 3.15. Multiple sequence alignment of LIMK1 with sequential and structural homologs. Sequence identities are highlighted in red background and similarities are shown as red letters. Helices are displayed as spirals and β-strands as arrows. Arrows indicate the Lys (β3) and Glu (αC) involved in the conserved salt bridge. The residues numbering is given according to LIMK1 primary sequence. The sequence comparison was performed with the program CLUSTALW (Goujon et al, 2010) and graphically represented with the program ESPript (Gouet et al, 1999).

Table 3.9. Comparison of LIMK1 kinase domain with known protein structure using DALI (Holm and Sander, 1993).

Protein	PDB	Z-score	rmsd	LALI[1]	LSEQ[2]	IDE[3]
c-Src tyrosine kinase	1YI6	27.0	2.8	251	276	32
Epha3 tyrosine kinase	2QO9	27.9	2.5	250	277	29
RET tyrosine kinase	2IVV	29.2	2.2	248	283	31
Ephb4 tyrosine kinase	2VWV	25.6	2.6	240	255	30
Epha5 tyrosine kinase	2R2P	28.1	2.5	255	283	28
c-Src tyrosine kinase	1Y0L	25.6	2.6	240	255	30
c-Src tyrosine kinase	2BDF	27.2	2.2	246	273	33
Hck tyrosine kinase	2HK5	26.9	2.3	243	269	32

[1]lengh of the aligned sequence; [2]total length of sequence; [3]% of identical residues.

First, the MR was performed using the C-lobe search model, and two molecules were found. After fixing this initial solution, two molecules of the N-lobe search model were placed in the structure, and the final solutions showed two molecules of the kinase in the asymmetric unit. Density modification with applications of non-crystallographic symmetry (NCS) and solvent flattening was performed and showed an improvement of calculated phase as observed from an increase of the figure of merit (FOM) from 0.391 to 0.751. This improved phase was used as an input for the automated model building using Arp/Warp program, and a total of 510 amino acids of LIMK1 (269 and 241 residues for chain A and B, respectively) were initially built. This output model was used as a starting model for further manual model building using COOT, alternated with refinement using REFMAC5 (Murshudov et al., 1997) in the CCP4 suite. Optimal TLS refinement was performed in the last refinement stages using parameters generated by the TLSMD server (Painter & Merrutt, 2006). Refinement statistics of the final model are reported in Table 3.10. The model was validated with MOLPROBITY (Davis et al, 2007), and it shows excellent geometry with all residues fitting into either the most favoured or allowed regions of Ramachandran plot (Figure 3.16).

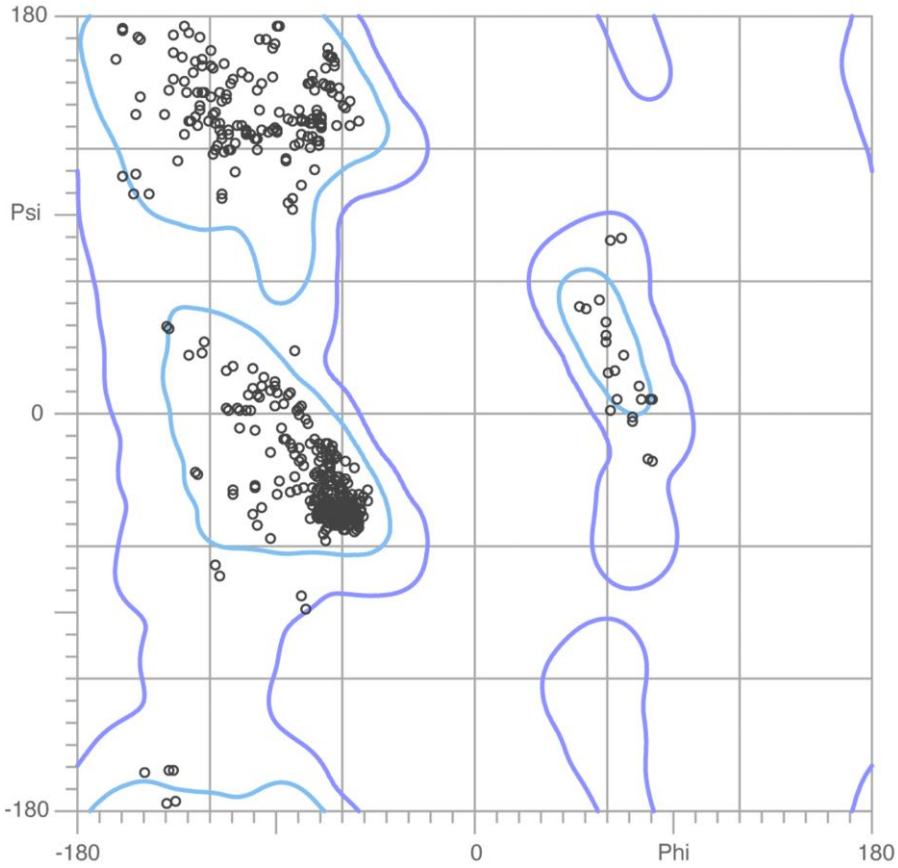

Figure 3.16. Ramachandran plot of LIMK1 structure. 96.7% of all residues in chain are in the most favored region and 0.2% in allowed regions. No residue is in the disallowed region.

Table 3.10. Data collection and refinement statistics of LIMK1 kinase domain structure.

Data collection	
Beam line	I03 Diamond
Wavelenght (Å)	0.976
Resolution range (Å)	43.78-1.65 (1.74–1.65)
Space group	$C222_1$
Cell dimensions	
(*a*, *b*, *c*) (Å)	106.2, 128.0, 131.4
(α, β, γ) (°)	90.0°, 90.0°,90.0°
Unique reflections	105650 (15293)
Overall redundancy	4.1 (4.1)
Completeness (%)	98.7 (98.5)
R_{merge} **(%)**	6.8 (60.8)
$I / \sigma(I)$	11.0 (2.2)
Refinement	
R_{factor} **(%)**	15.7
R_{free} **(%)**	18.1
R.m.s. deviations	
Bond lengths (Å)	0.016
Bond angles (°)	1.6
No of protein atoms	4756
No of ligands atoms	170
No of water molecule	580
Average *B*-factors (Å^2)	
Protein	31
Ligands	41
Water molecules	41
Ramachandran plot	
Favoured regions (%)	96.7
Allowed regions (%)	0.2

* Data in parentheses refer to highest-resolution shell

3.2.1.9 Overall structure of the LIMK1 kinase domain

Crystal structure of LIMK1 in complex with staurosporine belongs to the orthorhombic C 2 2 2_1 space group with unit cell dimensions of a=106.2, b=128.0, c=131.4 Å and α= β= γ= 90°. The asymmetric unit contains two molecules, which differ primarily in the conformation of their phosphate-binding loop (P-loop). The structure adopts the canonical bilobal kinase architecture as shown in Figure 3.17C.

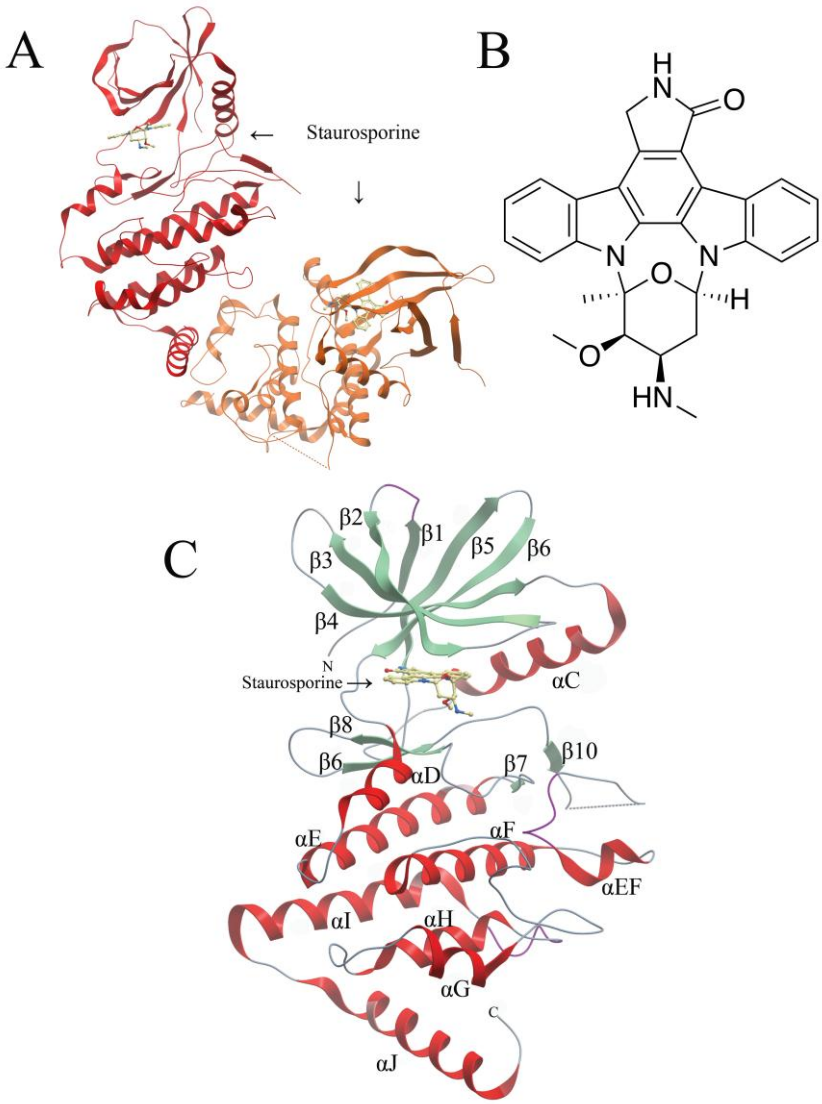

Figure 3.17. Structure of LIMK1 in complex with the staurosporine inhibitor. (A) Structures of the two LIMK1 chains in the asymmetric unit, colored in red (chain A) and orange (chain B). Proteins are shown in ribbon diagram, and staurosporine molecules are in stick representation. (B) Chemical structure of staurosporine. (C) Structural overview: the main secondary structure elements and the NH2 and COOH termini of the protein are labeled.

The N-terminal lobe consists of six β strands with a single α helix (αC) insertion between β4 and β5. The C-terminal lobe contains mostly α helices, exhibiting eight α helixes and four β strands. Both LIMK1 molecules are well defined by electron density, with the exception of part of the activation loop (residues 487-506). This loop is often flexible in unphosphorylated kinases, and typically becomes ordered only upon phosphorylation due to additional hydrogen bond formation with the catalytic region.

The structure of LIMK1 superimposes with 2.8 Å root mean squared deviation (rmsd) over 251 Cα atoms with the c-Src structure (pdb id 1YI6), and with 2.5 Å rsmd over 250 Cα atoms with the Epha3 structure (pdb id 2QO9). Both proteins belong to the tyrosine kinase (TK) family and shares 32% and 29% sequence identity to LIMK1, respectively. The majority of the secondary structure elements of the three kinase structures are superimposed closely, showing some typical structural features of an active kinase such as the Lys (β3)-Glu (αC) pair which forms a characteristic polar contact (Figure 3.18) and the DFG motif (Asp-Phe-Gly) positioned at the N-terminus of the activation loop (A loop) (Figure 3.19C).

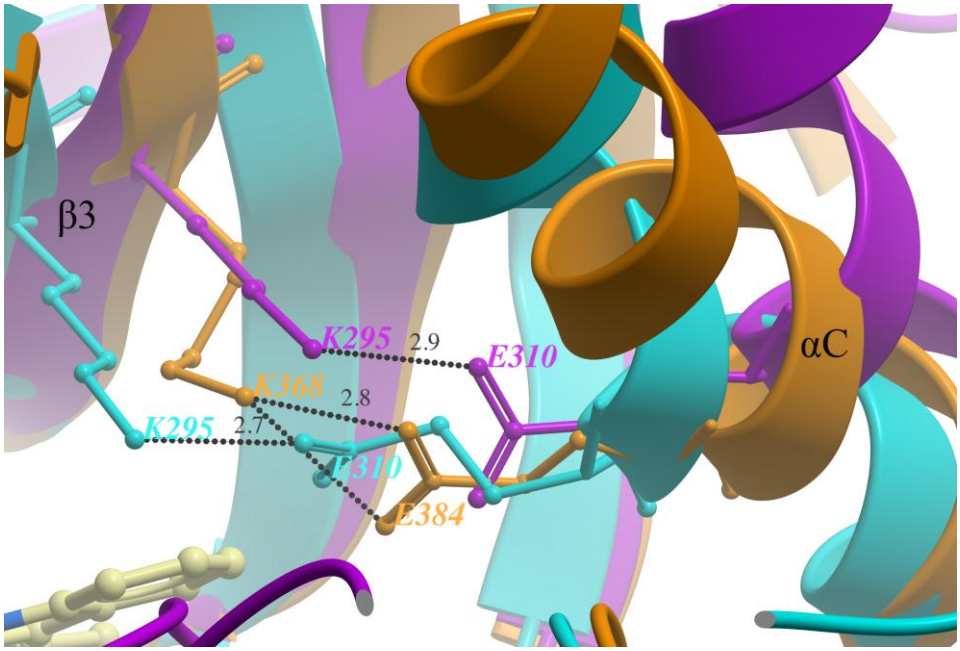

Figure 3.18. Superimposition of LIMK1 (gold) with c-Src kinase (cyan) and the human EphA3 kinase (purple) that were used as search models in MR displaying the characteristic β3-αC salt bridge.

Despite a closed N- and C-lobe conformation to form a hydrophobic pocket and accommodate the ATP adenine ring, there are no other indications to assess that the structure of LIMK1 is clearly in an active conformation. The largest difference between these three structures is in the N-lobe especially at αC helix, which is a common regulatory element associated with the kinase activation. This is seen as a significant movement of αC between the three structures (Figure 3.19D and E). The multiple sequence alignment (Figure 3.15) and structure superimposition underline that the most characteristics protein kinase motifs, such as the glycine rich loop, the hinge region (Figure 3.19G) and the DFG motifs (Figure 3.19C), are conserved between the human kinome. Furthermore, the motif DLSNDHN of LIMK1 differs from the DLAARN and DLRAAN motifs of the aligned kinases (Figure 3.19B). Interestingly, unique and unexpected architectures of kinase C-lobe is observed in the LIMK1 structure. These are the displacement of the typical αG helix (Figure 3.19F), which usually packs against the kinase substrate pocket, and an additional C-terminal αJ helix (Figure 3.19H), which packs below and perpendicular to αH.

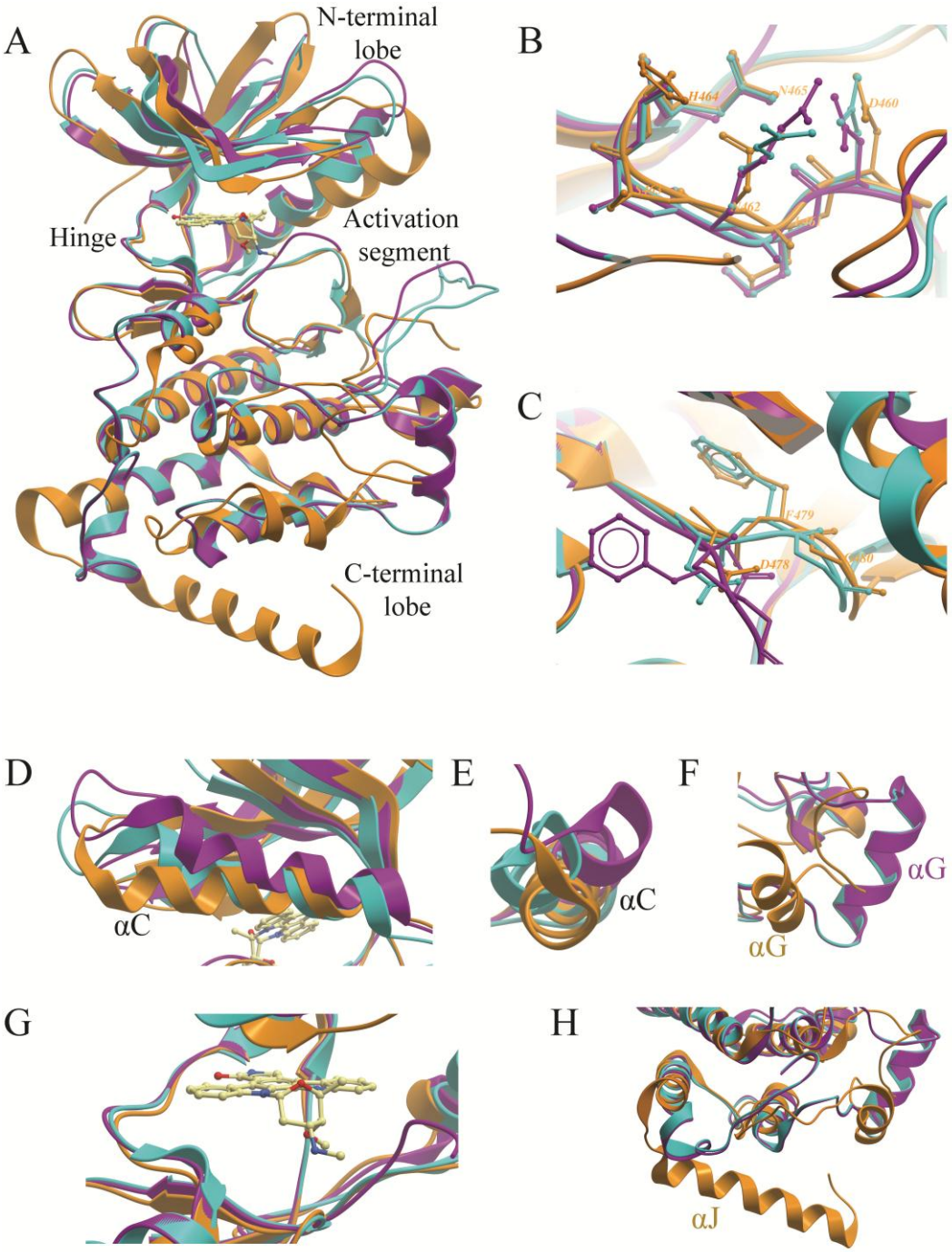

Figure 3.19. Superimposition of LIMK1 (gold) with c-Src kinase (cyan) and the human EphA3 kinase (purple). (A) Overall view of the catalytic domain. (B) diagnostic sequence motifs; LIMK1 motif labelled. (C) DFG motif. (D and E) Different views of the αC helices. (F) Displacement of the LIMK1 αG-helix compared to the models ones. (G) Hinge region and binding pocket. (H) Additional αJ-helix at the C-terminal of LIMK1.

3.2.1.10 Docking of LIMK1 kinase inhibitors

LIMK1 has emerged as an important drug target in cancer research. As previously described (§ 3.2.1.3), a thermal stability shift assay identified several LIMK1 inhibitors of interest for further characterization. K00993a induced a Tm shift of 8.19°C and reversine (K2703a) of 8.11°C. These shifts were significantly higher than the shift observed for staurosporine (3.94°C), indicating higher affinity. Since crystallization trials with these two inhibitors only yielded crystalline precipitates, they were analysed further by molecular docking taking advantage of the existing LIMK1 crystal structure as a template (pdb id 3S95). ICM-Pro (Molsoft) was used for docking. It establishes two pockets or boxes around the ligand binding site (which can be adjusted with user-defined parameters). Reversine has been previously crystallized with the Aurora B kinase (pdb id 2VGO) and provided a quality control check confirming the correct docking solution in pocket 2 (Table 3.11).

Table 3.11 Identified binding pocket solutions.

pocket	Volume	Area	Hydro phobicity	Buried ness	DLID	Radius	Nons phericity
1	191.3	216.7	0.4718	0.709	-0.9569	3.574	1.35
2	178.6	202.7	0.5316	0.6538	-1.089	3.494	1.321

The compounds K00993a and K02703a were imported and converted from 2D to 3D. Energy maps of the environment within the docking box were generated. Interactive docking was used to dock the two analogs. During the energy optimization of the ligands, a conformation set of low energy states was created and the best energy scored. Several solutions were suggested, as shown in Table 3.12. The most probable conformations belonging to the most populated cluster with lowest energy were selected.

Table 3.12. Statistics for K2703a and K993a docking solutions.

	ConfNum	Score	VlsScore	Strain	Steric	Torsion	Electro	Hbond	Hydroph	Surface
K2703a	1	-30.18	-34	3.829	-27.86	1	4.468	-5.976	-6.703	13.22
	3	-27.18	-31.82	4.64	-27.51	1	6.675	-5.871	-6.587	13.26
	2	-21.55	-23.6	2.052	-29.11	1	9.166	-2.808	-7.427	14.59
	5	-20.89	-23.41	2.519	-26.63	1	7.728	-2.953	-7.429	13.29
	4	-10.7	-13.1	2.404	-27.17	1	11.68	0	-7.583	14.46
	ConfNum	**Score2**	**VlsScore**	**Strain**	**Steric**	**Torsion**	**Electro**	**Hbond**	**Hydroph**	**Surface**
K993a	1	-33.76	-41.72	7.955	-26.21	1	-0.4337	-7.181	-6.199	8.67
	2	-23.71	-39.33	15.61	-30.57	1	3.245	-5.92	-6.632	10.57
	3	-13.9	-24.26	10.36	-30.52	1	6.421	-0.7749	-6.609	10.4
	3	-5.888	-15.37	9.485	-27.11	1	9.121	0	-7.103	13.16

3.2.1.11 Expression and purification of human cofilin 1 and PAK4

Cofilin 1 (CFL1) was expressed in *E. coli* Rosetta cells as a C-terminally His_6-tagged protein, while PAK4 was GST-tagged and expressed and purified separately. PAK4 cells were disrupted through high pressure cell disrupter at 25 KPsi and incubated in batch with GST slurry for 1 hour at 4°C. The protein was then eluted with 15 mM reduced glutathione. The fractions corresponding to elution peaks were analysed by SDS-PAGE, indicating a 99% pure protein.

Briefly, CFL1 cells were disrupted by sonication as described in § 2.2.5, purified by Ni^{2+}affinity chromatography and eluted with an increasing imidazole gradient. The His_6-tag was then removed from the cofilin 1 fusion protein by TEV enzymatic cleavage. The tag-free protein was purified by size exclusion chromatography in a sephadex S75 column (Figure 3.20A) and the collected fractions were given a final clean up step by reverse IMAC purification. SDS-PAGE analysis assessed the homogeneity and purity of the sample (Figure 3.20B).

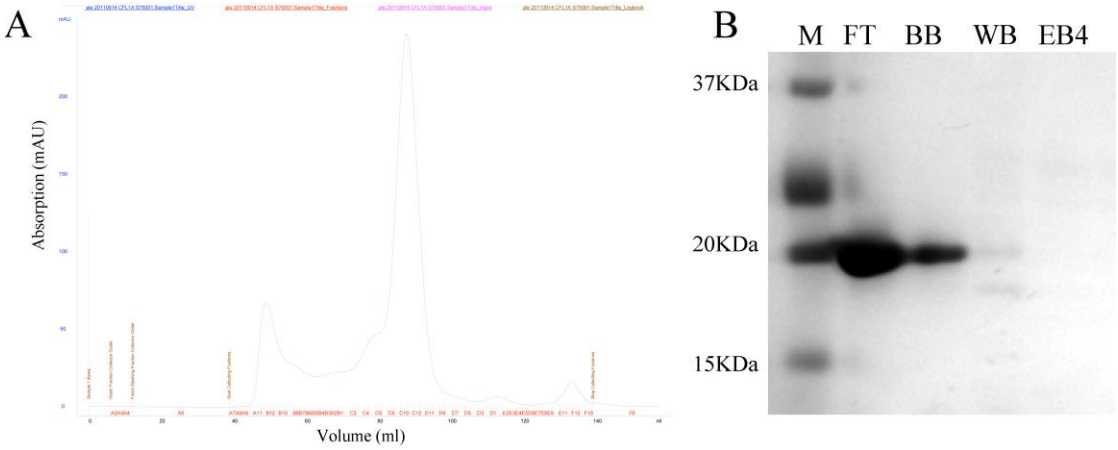

Figure 3.20. Size exclusion elution profile of CLF1, which was monitored at 280 nm (blu curve). The fractions of the main peak were pooled and loaded on a Ni-rebinding gravity column. Fractions were collected as flow trough (FT) and eluted with an increased imidazole gradient: 5mM in binding buffer (BB), 30mM in wash buffer (WB) and 250mM in the elution buffer number 4 (EB4).

3.2.1.12 Mapping of phosphorylation sites by LC-MSMS

The goal of this experiment was, in first place, to confirm *in vitro* that PAK4 is able to phosphorylate LIMK1 and that LIMK1 phosphorylates CFL1 in the presence of ATP. Furthermore, we aimed to map the phosphorylation sites of the involved proteins. To advance this purpose, different reactions were set up incubating (i) LIMK1, (ii) PAK4 with LIMK1 and (iii) LIMK1 with CLF1 in the presence of ATP, $MgCl_2$ and $MnCl_2$. Both reactions were analysed by LC-MS to measure the intact masses. As shown in Fig. 3.21, LIMK1 was partially phosphorylated by PAK4 and LIMK1 was also able to fully phosphorylate CFL1.

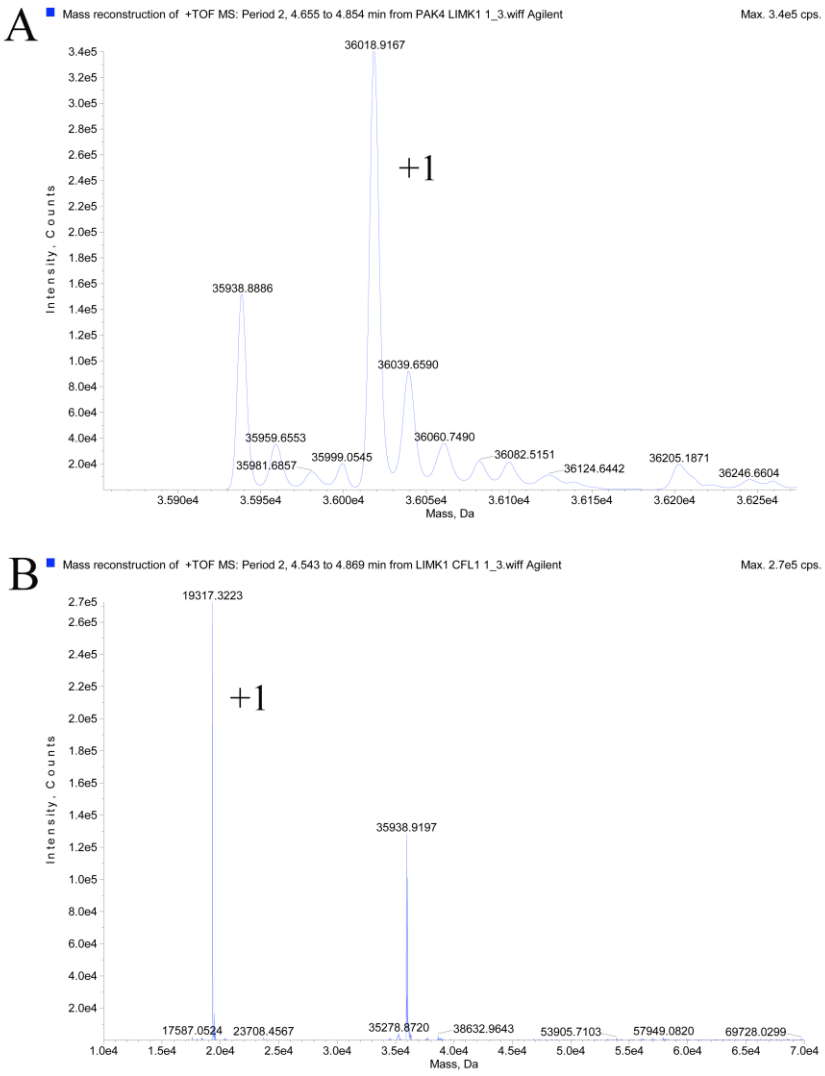

Figure 3.21. Intact mass spectrum of LIMK1 incubated in the presence of ATP with (A) PAK4 and (B) CFL1 evidencing its phosphorylation. "+1" indicates that one phosphorylation sites is occupied, corresponding to an increase of 80 Da.

This second experiment indicates a capability of LIMK1 to autophosphorylate, and also shows that in the presence of the kinase inhibitor LIMK1 is only partially phosphorylated, but still capable to phosphorylate CFL1. To map the phosphorylation sites of PAK4, LIMK1 and CFL1 the proteins were digested by trypsin and chymotrypsin generating a pool of phosphopeptides (§ Section 2.4.3). Since the detection of phosphopeptides by MSMS is often hindered by suppression effects, phosphopeptide enrichment prior to mass spectrometric analysis was applied. The unphosphorylated peptides were removed by metal affinity chromatography using

TiO_2/ZrO_2 enrichment, which selectively allows isolation of single phosphorylated peptides. The phosphopeptides that are negatively charged bound the positively charged metal ions by electrostatic interactions. TiO_2/ZrO_2 enrichment worked extremely well: 90 to 100% of the phosphopeptides were observed in all elutions.

The peptides ions were fragmented by CID and ETD, the data processed by the Mascot software. The analysis revealed a LIMK1 tryptic monophosphopeptide YpTVVGNPYMAPEMINGR with definitive phosphorylation at Thr2 present in all samples. This result is consistent with the intact mass observations of phosphorylation states 0 and 1 for LIMK1. There is a potential site ambiguity between Tyr507 and Thr508 for LIMK1, which spectral analysis does not resolve. However, there are some evidences, which support Thr508 as LIMK1 phosphorylation site: first the software gives Tyr507 and Thr508 equal scores once, and gives Thr508 a higher score twice. In second place, phosophothreonine is more common than phosphotyrosine. To conclude, LIMK1 and PAK4 are homologues and LIMK1 Thr508 is in the homologous position as PAK4 Ser474, which is its identified phosphorylation site. In fact, PAK4 tryptic monophosphopeptide pSLVGTPYMAPELISR showed a definitive phosphorylation at Ser1. Cofilin was the only protein generating peptides upon both trypsin and chymotrypsin digestion. CFL1 chymotryptic monophosphopeptide ApSGVASDGVIKVF and tryptic monophosphopeptide ApSGVASDGVIK indicated a definitive phosphorylation at Ser2 (Figure 3.22), which corresponds to Ser3 in the mature protein.

A

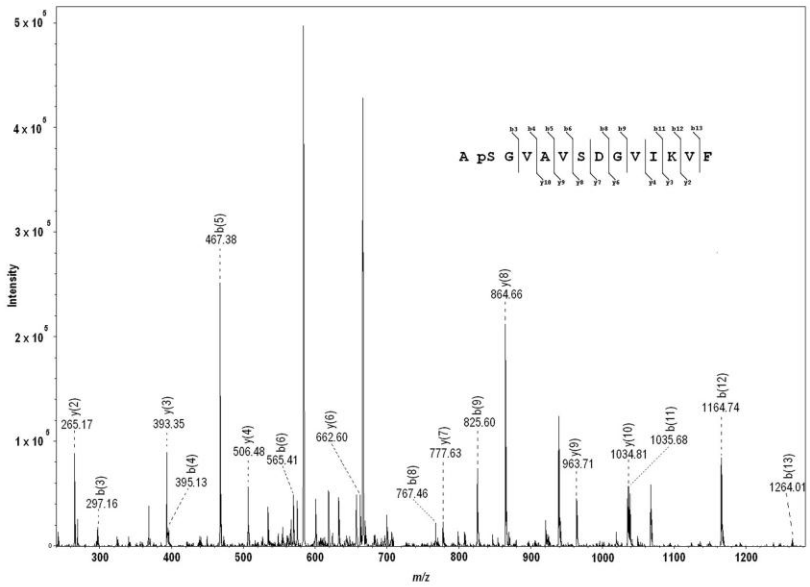

B

Delta	Miss	Score	Expect	Rank	Unique	Peptide
-0.0566	0	(14)	43	3	U	M.ASGVAVSDGVIK.V + Phospho (ST)
-0.0039	0	(28)	1.9	1	U	M.ASGVAVSDGVIK.V + Phospho (ST)
0.0161	0	(31)	0.86	1	U	M.ASGVAVSDGVIK.V + Phospho (ST)
0.0234	0	(25)	3.3	1	U	M.ASGVAVSDGVIK.V + Phospho (ST)
0.0361	0	(31)	0.91	1	U	M.ASGVAVSDGVIK.V + Phospho (ST)
0.0561	0	(41)	0.082	1	U	M.ASGVAVSDGVIK.V + Phospho (ST)
0.0561	0	(34)	0.44	1	U	M.ASGVAVSDGVIK.V + Phospho (ST)
0.0761	0	(26)	2.5	1	U	M.ASGVAVSDGVIK.V + Phospho (ST)
0.0961	0	(23)	5.1	1	U	M.ASGVAVSDGVIK.V + Phospho (ST)
0.0961	0	49	0.013	1	U	M.ASGVAVSDGVIK.V + Phospho (ST)
0.1034	0	(25)	28	1	U	M.ASGVAVSDGVIK.V + Phospho (ST)
0.1161	0	(31)	0.93	1	U	M.ASGVAVSDGVIK.V + Phospho (ST)
0.1161	0	(37)	0.24	1	U	M.ASGVAVSDGVIK.V + Phospho (ST)
0.1161	0	(23)	5.8	1	U	M.ASGVAVSDGVIK.V + Phospho (ST)

Top scoring peptide matches to query 210
Cmpd 177, +MSn(591.84), 9.1 minBTSpecNo=177
Score greater than 32 indicates homology
Score greater than 43 indicates identity

Score	Expect	Delta	Hit	Protein	Peptide
49.3	0.013	0.0961	2	CFL1A-c001	M.ASGVAVSDGVIK.V
16.1	27	-0.8384			K.IRSHMMANK.Y
14.5	40	-0.9235			K.VYMGEMGRLK.S
13.1	54	-0.7470			R.TAPLTPTSR.E
12.9	57	2.1201			R.ISLARAVYK.D
12.0	70	2.0642			R.LRITADGNLK.V
11.5	78	1.2030			K.FMAYPSQGGK.V
11.4	81	0.1412			K.MGLDMCQAIK.Q
11.3	82	0.1412			K.MGLDMCQAIK.Q
11.2	84	2.1693			K.SFGASGGYIGGK.K

Figure 3.22. Evidence for the monophosphopeptides from CID data. (A) MSMS spectrum of the CFL1 phosphopeptide ApSGVASDGVIKVF showing matched fragment ions. (B) The Mascot scores for the peptide of CFL1.

3.2.2 Characterization of the N-terminal regulatory domains of LIMK1 (LIM-LIM-PDZ and LIM-LIM)

3.2.2.1 Expression and Purification

LIM-LIM-PDZ (Glu18-His258) was recombinantly expressed as an N-terminally His_6-tagged protein while the LIM-LIM domains were C-terminally His_6-tagged protein in *E. coli*. Culture conditions were optimized to give a good expression yield by cultivating cells at 18°C overnight in LB medium. For the LIM-LIM domains, two constructs were tested, a longer (Glu18-Ser172) and a shorter one (Glu18-Leu151). Upon cell disruption by sonication and centrifugation of cell debris, the fused proteins were present in the supernatant fraction. A five step purification process was necessary to obtain the required protein purity to perform crystallization trials. The His_6-tagged proteins were purified by IMAC chromatography and the tags removed by incubation with TEV protease overnight. A size exclusion chromatography was applied followed by a second run of Ni^{2+}affinity chromatography. The proteins were then concentrated and diluted into a low salt buffer to be purified through a cation exchange column, assuming a pI of all the cleaved proteins of around 5. The shorter LIM-LIM construct has the tendency to easily aggregate compared to the longest one; for this reason it was not included in further studies.

3.2.2.2 Solubility buffer screen

The LIM-LIM-PDZ construct was generated with the purpose to better investigate the molecular mechanism of BMPRII-tail signalling through LIMK1. To pursue this goal, binding affinity measurements to define and validate the peptide array data mapping the putative BMPRII docking site had to be undertaken. ITC experiments were planned, unfortunately it seems that the ITC buffer, poor in salt content, was not ideal for the LIM-LIM-PDZ protein, which had the tendency to aggregate and precipitate during the dialysis process. A buffer screen was set up to identify more optimal buffer conditions to keep the protein in solution, as described in § 2.4.10. The drops were scored, assigning values from 1, which indicates a positive result where the protein is soluble, to -1, which indicates protein precipitation. It was, then, calculated which conditions were maintaining the LIM-LIM-PDZ construct in solution: the protein

solubility was enhanced under neutral pH and in the presence of arginine as well as glycerol, which were then introduced to all the further experiments (Table 3.13).

Table 3.13. Solubility screen output. Drops are scored as 1 or -1 for soluble or drops containing precipitate, respectively. The highest solubility goes from green to red, which represents precipitate.

pH	**pH4**	**pH5**	**pH6**	**pH7**	**pH8**	**pH9**
	-0,4662524	-0,2984015	-0,1305507	0,2051511	0,4289522	0,2611013
Salt	**no salt**		**0.1 NaCl**	**0.6 NaCl**		**0.5 KOAc**
	0,0535915		0,0434782	0,0434782		-0,1481647
Additive 1	**none**	**Glycerol**	**glucose**	**trehalose**	**PEG300**	**PEG4000**
	-0,0172315	0,1600068	-0,0172315	0,0418479	-0,1353904	0,0418479
Additive 2	**none**	**ARG**	**EDTA**	**Cyclodex**	**Urea**	
	-0,097725	0,2553477	-0,1481647	0,0535915	-0,0788110	
detergent	**Nodet**		**TX100**	**NDSB**		
	-0,004730		0,0649892	-0,0028985		
Metal ions	**No metal**			**metal**		
	-0,0107676			0,0107676		

3.2.2.3 Identification of LIMK1-BMPRII interactions by peptide array

For determination of BMPRII interaction sites, the SPOT synthesis technology was used, which allows parallel synthesis and screening of a large number of cellulose membrane-bound peptides. Cellulose-bound peptide arrays representing the complete BMPRII tail domain sequence were screened for binding to the LIM-LIM-PDZ domain construct of LIMK1. The peptide array was performed as described in § 2.4.5. To avoid non-specific binding, the membrane was first blocked for 2 hours in TBS buffer containing 0.15 M saccharose prior to the addition of the protein at 0.4 μM final concentration. The membrane was then washed 3 times with buffer and incubated with anti-His antibody for 1hour. Finally, the membrane was washed a further three times and incubated with anti-Rabbit HRP-conjugated antibody (Santa Cruz). The membrane was developed using a chemiluminescence substrate and a Lumi-Imager. The analysis and quantification of the spot signal intensities were executed with the Genespotter software.

Eighteen signal spots were found with good intensities, covering a BMPRII-tail region, which was also identified from independent research groups as the putative docking site (Table 3.14). Although at present it is impossible to predict the exact

LIM binding domain, were identified two small hydrophobic sidechains. It is expected that the binding mode will resemble that of the LMO4:Ldb1 complex (pdb id 1RUT) and this can provide a useful model for experimental design (Deane et al, 2004). These side chains are separated by a linker and occupy the apolar pocket in each LIM domain. The BMPRII-tail putative sequence, SNLKQVETGVAKMNTINAA (amino acids 777-795) was then aligned with the sequence of other known LIM binding domain peptide sequences in the PDB to search for any common elements. As shown in Figure 3.23, the presence of small and hydrophobic amino acids is also conserved in sequence, which was later synthesized by GenScript.

Table 3.14. BMPRII-tail 15-mers peptides and the correlatives intensities.

Peptide sequences	Intensity
TTNVAQSIGPTPVCL	strong
VAQSIGPTPVCLQLT	strong
SIGPTPVCLQLTEED	weak
PTPVCLQLTEEDLET	weak
VCLQLTEEDLETNKL	strong
HKSNLKQVETGVAKM	very strong
NLKQVETGVAKMNTI	very strong
QVETGVAKMNTINAA	very strong
TGVAKMNTINAAEPH	weak
AKMNTINAAEPHVVT	null
NTINAAEPHVVTVTM	weak
NAAEPHVVTVTMNGV	weak
EPHVVTVTMNGVAGR	strong
VVTVTMNGVAGRNHS	strong
VTMNGVAGRNHSVNS	strong
GGRTNSNNNNSNPCS	strong
PCSEQDVLAQGVPST	strong
PGPSKPRRAQRPNSL	very strong

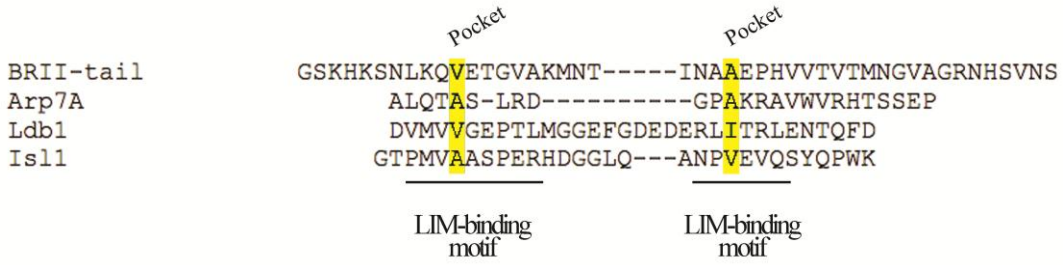

Figure 3.23. Structure-based alignment of the tandem LIM domain ligands indicating the apolar pocket interacting residues (green) in the LIM binding motifs.

3.2.2.4 Isothermal Titration Calorimetry

ITC experiments were accomplished to validate whether the LIMKtide1 peptide sequence SNLKQVETGVAKMNTINAA (KP0156a) of BMPRII-tail actually binds to the LIMK1 N-terminal regulatory domain. LIM-LIM-PDZ and LIM-LIM domains were expressed and purified as previously reported. Prior to the ITC experiment the proteins were dialyzed overnight against 50 mM Hepes, 150 mM NaCl, 0.5 mM TCEP, pH 7.5 to avoid secondary heat effects due to mixing of buffers during the calorimetric experiments. The concentration of LIM-LIM-PDZ and LIM-LIM were 250 μM and 100 μM, respectively and the titrant concentration was 1:10 of the titrated. The experiments were performed at 15°C and the peptide LIMKtide1 was titrated in 20 injections of 15 μl each.

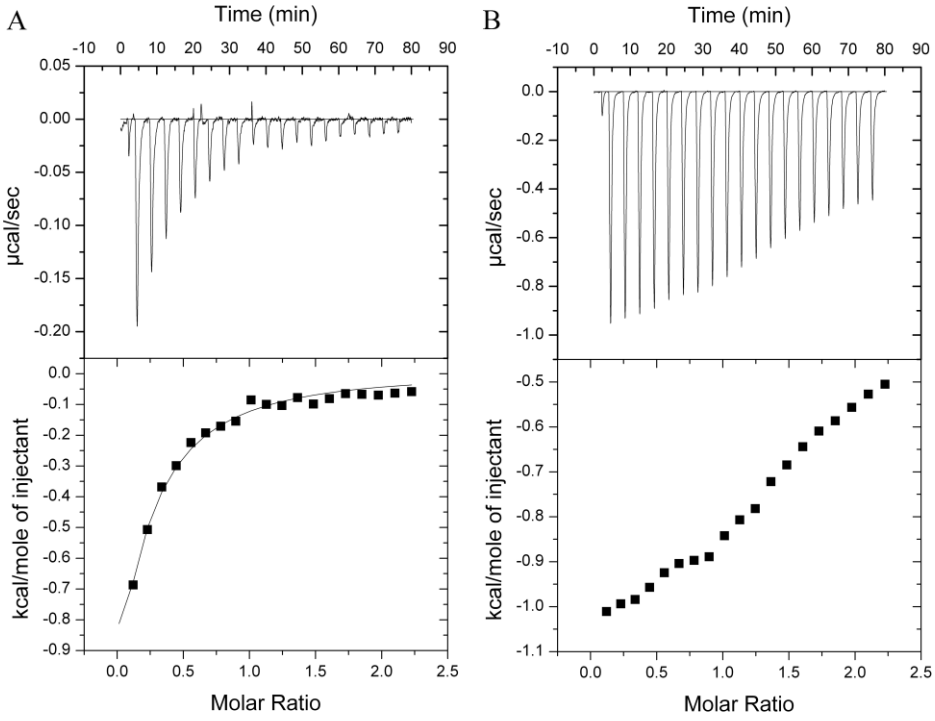

Figure 3.24. ITC experiments performed to characterize thermodynamically the role of LIM-LIM and LIM-LIM-PDZ. (A) ITC data for the interaction LIM-LIM/ KP0156a ; (B) ITC data for the interaction LIM-LIM-PDZ/ KP0156a.

The dissociation constant (Kd) of ~ 60μM determined for LIM-LIM suggests that the binding was very weak (Figure 3.24). In the case of LIM-LIM-PDZ, the protein

unfortunately aggregated and, since it was not possible to know at which point of the sigmoidal curve the reaction was, the data of this experiment could not be properly analysed.

3.2.2.5 Crystallization of the LIMK1 regulatory domains

Crystallization of the N-terminal region of LIMK1 was undertaken for both LIM-LIM-PDZ and LIM-LIM constructs. The crystallization was performed using vapour diffusion experiments with several commercial sparse matrix screens. The protein of interest was mixed in 2:1, 1:1 and 1:2 ratio concentration with the reservoir solution to 150 nl final volume drops taking advantage of a Mosquito (TTP Labtech) robotic crystallization device. Crystallization plates were incubated at 4°C and 20°C and systematically inspected over a period of few months using a Minstrel™ HT crystal imaging system (Rigaku). The experiments set up are described in Table 3.15.

Table 3.15. Crystallization experiment condition for LIM-LIM-PDZ and LIM-LIM.

Construct	Concentration	Peptide	Peptide concentration	Screen	Temperature
LIM-LIM-PDZ	12.8 mg/ml			LFS4 JCSG4 HCS HIN	20°C
LIM-LIM-PDZ	12.8 mg/ml			LFS4 JCSG4 HCS HIN	4°C
LIM-LIM-PDZ	12 mg/ml	KP0156a	0.5 mM	LFS4 JCSG4	20°C
LIM-LIM	6 mg/ml	KP0156a	1 mM	LFS4	20°C
LIM-LIM	6 mg/ml			LFS4	20°C
LIM-LIM	21 mg/ml	KP0156a	1 mM	HCS	20°C
LIM-LIM	21 mg/ml			HCS	20°C

LIM-LIM-PDZ was concentrated in the presence of the LIMKtide1 (KP0156a) to 12 mg/ml and several sparse matrix screens were set up at 4°C and 20°C; microcrystals and crystalline precipitate were found in 0.2 Na formate, 20 % (w/v) PEG 3350, 10 % ethylene glycol (Figure 3.25A). Phase separation was observed in 0.20 KSCN, 20 % (w/v) PEG 3350(Figure 3.25B).

Additionally, the LIM-LIM protein was concentrated to 21 mg/ml and screened against HCS sparse matrix screen, in the presence of LIMKtide1 (KP0156a) at 20°C. Furthermore, the LIM-LIM fraction which was titrated against the LIMKtide1 during the ITC experiment (see § 3.2.2.4) was recovered and concentrated up to 6 mg/ml; the complex was then used to perform a crystallization screen using LFS4 potential conditions at 20°C. None of these attempts gave promising indication of crystal formation.

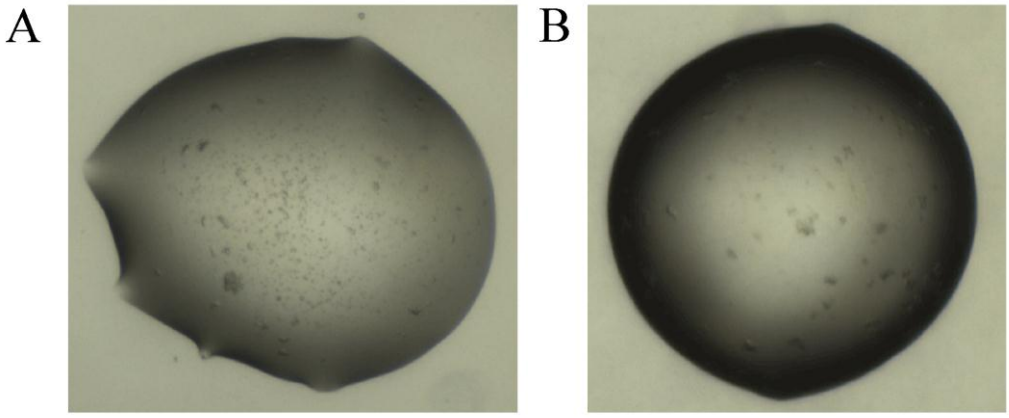

Figure 3.25. Crystallization of LIM-LIM-PDZ domains concentrated in the presence of the peptide KP0156a. (A) microcrystals grown on a LFS4 condition and (B) phase separation in JCSG4.

4 Discussion

The work presented in this Ph.D. thesis aimed to investigate the three dimensional structures of cGMP-dependent kinase I (cGKI) and LIM kinase 1 (LIMK1), which both interact with the long cytoplasmic tail of BMPRII (Schwappacher et al, 2009; Foletta et al, 2003) generating different mechanisms. Coexpression of cGKI with BMPRII-tail mutants rescues some effects of PAH through enhancement of the BMP signaling pathway, suggesting that the downstream activity of cGKI is an important regulator of PAH and vasodilation (Schwappacher et al, 2009). LIMK1 also colocalizes with the BMPRII tail and phosphorylates cofilin, which determines actin polymerization in cell division and movement. Notably, LIMK1 is associated with many pathological processes such as tumour cell invasion, metastasis and HIV-1 infection (Foletta et al, 2003; Manetti, 2011). The functional consequences of the BMPRII-LIMK1 interaction are still controversial.

Breafly, the main conclusions of my Ph.D. study are below describes.

4.1 cGKI

Malfunction of BMP signaling is involved in several developmental disorders like fibrosis, cancer and vascular diseases. It was demonstrated that cGMP-dependent protein kinase I (cGKI) has a pivotal role in BMP signaling enhancing Smad pathway at multiple levels. The activated cGKI is able to specifically interact with the tail domain of BMPRII, to phosphorylate it and to trigger a phosphorylation cascade, which then regulates the Smad pathway. cGKI interacts with activated R-Smad/co-Smad complexes and translocates with them to the nucleus to regulate BMP gene transcription. In an effort to characterize their binding to BMPRII and to solve their structures, different full length and truncated forms of the human cGKI isoform β were cloned and tested for expression. The full length cGKIβ as well as successive truncations lacking the N-terminal leucine zipper or central cGMP-binding domains was expressed in Sf9 cells and purified for crystallization purposes. Interestingly, the purified proteins analysed by SDS PAGE and by time-of-flight mass spectrometry (MS TOF) were found to have a mass 80 Da higher than predicted corresponding to a single autophosphorylation site, indicating constitutive enzyme activity during expression.

To begin the investigations of receptor crosstalk, cGKIβ constructs were tested for binding and/or phosphorylation of a peptide array prepared from overlapping regions of the BMPRII-tail. A specific BMPRII-tail sequence, which if deleted destroys the BMPRII-tail/cGKIβ interaction on a SPOT analysis, was identified. Two peptides GEKNRNSIY (aa 581- aa 589) and EPHVVTVTMNG (aa 797- aa 888) of the BMPRII tail domain, which are located at the N-terminal and middle tail region, were synthesized. To validate their potential interaction with cGKIβ, biophysical analysis in solution was planned. Unfortunately the peptides were rich in hydrophobic residues and precipitated, limiting the experimental success.

Nevertheless, cGKIβ kinase activity was confirmed against both peptides, as well as the consensus peptide RKRSRAE. Using an NADH-coupled assay it was found that cGKIβ protein was functional and that the kinase activity was strictly dependent on cGMP, as expected. Although putative crystals were obtained in cGKIβ crystal screens, it was not possible to determine protein diffraction as the crystals dissolved before it was time to mount them. However further crystals obtained in a follow up screen did not show protein diffraction at the UK synchrotron. The difficulty in obtaining crystals of cGKIβ can be explained by the presence of multidomains, especially of the two tandem cGMP-binding regions. Probably, conformational changes, which might occur in the presence of cGMP, prevent the formation of crystal nucleation.

4.2 LIMK1

4.2.1 Conformation of the catalytic domain

In the absence of the N-terminal negative regulatory domains, the structure of unphosphorylated LIMK1 catalytic domain is shifted towards an active conformation, as indicated by the closed conformation of the kinase lobes. Helix αC of the N-terminal lobe represents one of the most conserved regulatory elements of kinase function. The αC helix is anchored in the proximity of the ATP binding site through the long 2.8 Å αC-β3 salt bridge between the conserved Lys368 and Glu384 forming a critical element of the active site (Figure 4.1A).

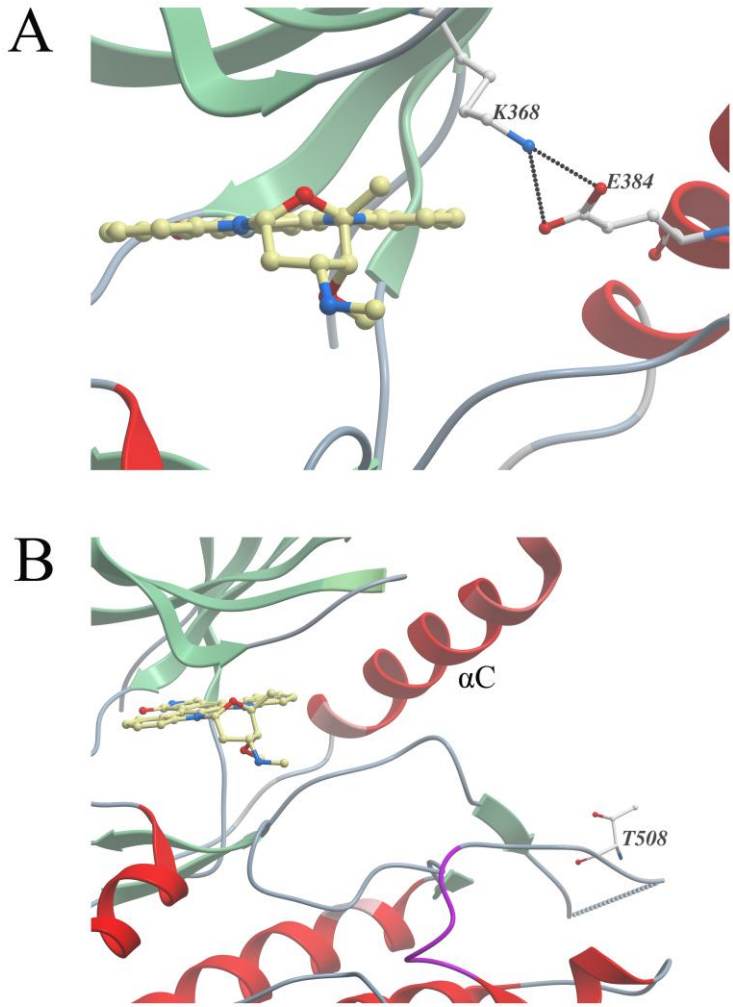

Figure 4.1. Activation site region: (A) salt bridge between K368-E385 that allowed a correct positioning of the αC helix; (B) absence of phosphorylation in the activation loop residue T508. Staurosporine is represented in yellow.

Another conserved loop is represented by the P-loop, which sits above the ATP binding groove and contains a glycine-rich motif. The glycine-rich P-loop has been suggested to play a role in the conformational plasticity of the ATP-binding site. Upon ATP binding, the loop closes down and residues within the loop form hydrogen bonds to the ATP phosphate, while it becomes flexible and opens in the absence of ATP. Superimposition of the two LIMK1 molecules present in the asymmetric unit shows that they differ mostly in the P-loop conformation; a displacement is observed in the glycine-rich P-loop leading to variable closure of the two lobes (Figure 4.2).

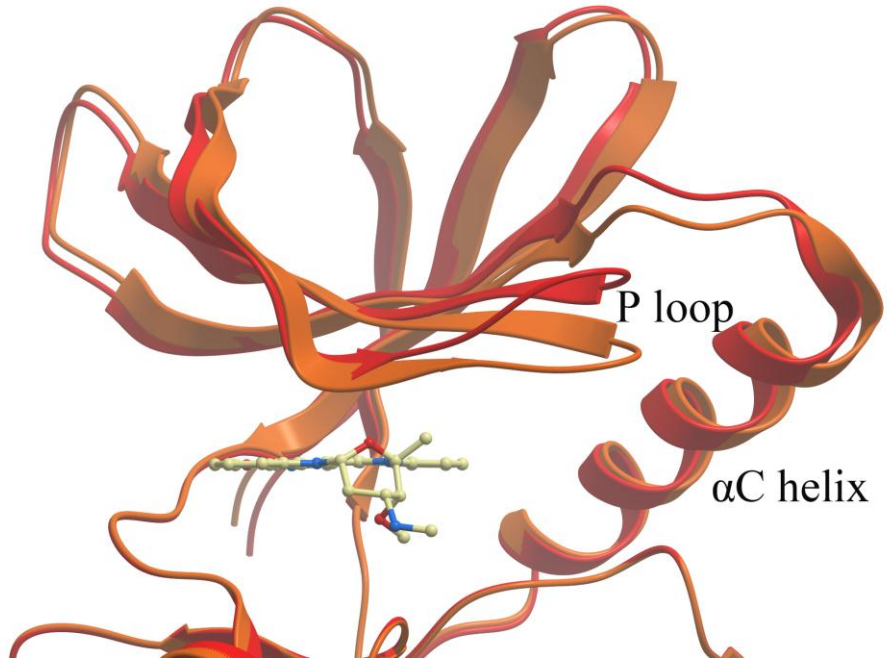

Figure 4.2. Superimposition of the amino terminal small lobe of LIMK1 chain A (red) and chain B (orange) indicating a shift of the P loop.

Despite a closed conformation of the N- and C-lobes, the phosphorylation site Tyr508 in the activation loop was not phosphorylated, making no other contacts within the kinase domain (Figure 4.1 B). Since the phosphorylation of key residues in the activation segment is required to stabilize a conformation suitable for substrate binding, a significant part of the activation loop (A loop) of both molecules is not defined in the electron density, and consequentially not modelled. This region contains an unusual basic insertion including the sequence RSLKKPDRKKR.

4.2.2 Staurosporine binding mode

LIMK1 was crystallized in the presence of staurosporine, an alkaloid originally isolated in 1977 from the bacterium *Streptomyces staurosporeus.* Staurosporine is a typical ATP-competitive kinase inhibitor, which binds to many kinases with high affinity. This promiscuity has precluded its clinical use, but has made it a valuable research tool. In the crystal structure, staurosporine is bound to the active site in the typical ATP-mimetic manner, stabilizing the structural changes that trigger closure of the kinase lobes. The inhibitor forms three hydrogen bonds (Figure 4.3A), two of which anchor the lactam moiety to the kinase hinge and mimic the hydrogen bonding

pattern of the adenine base in protein kinases. The lactam carbonyl oxygen accepts a hydrogen bond from the main-chain amide of Ile416, while the lactam amide nitrogen donates a hydrogen bond to the carbonyl oxygen of residue Glu414. The distances are both 2.8 Å (Figure 4.3 A).

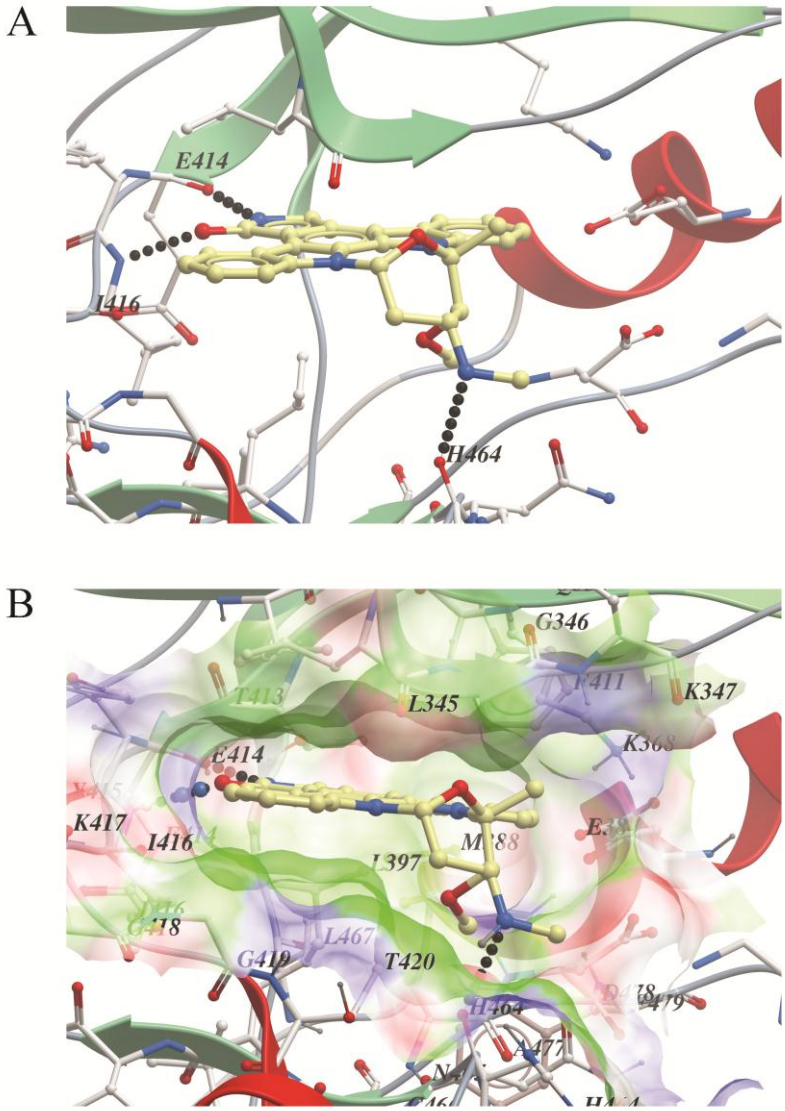

Figure 4.3. Staurosporine binding in the ATP pocket. (A) Staurosporine forms two hydrogen bonds to E414 and I416 within the hinge and one with H464; (B) Staurosporine fills the space of the ATP binding pocket, providing a large interaction surface. The surface of LIMK1 is shown semi-transparent and coloured blue (H-bond donor), red (H-bond acceptor), or green (other residues).

Specificity of kinase inhibitors is strongly determined by the hinge gatekeeper residue. In LIMK1 the gatekeeper residue is a small threonine (Thr413), which allows the access to the back of the binding pocket, providing scope for inhibitor

development here. A further hydrogen bond is observed between the pyranose N-H of staurosporine and the carbonyl oxygen of His464 showing an excellent fit of the ATP-binding pocket.

High inhibitor specificity is one of the limiting factors in the success of a new drug development. Due to this reason alternative small molecules, which are already in clinical trials against cell metastasis, were identified by DSF screening. Molecular docking solutions, using the existing LIMK1 structure (pdb id 3S95) offer a reasonable docking model for both of the examined inhibitors and offer an exciting lead for further chemistry. The results are presented in Figure 4.4. Both K02703a and K00993a, indicated a type I ATP-competitive inhibitor binding mode, showing two hydrogen bonds to the kinase hinge region. The NH at position 9 of the K02703a (reversine) purine ring donates a hydrogen bond to the carbonyl oxygen of Ile414. Furthermore, the NH of the aniline donates a hydrogen bond to the carbonyl oxygen of Glu414. Unfortunately, compound K00993a is confidential and its chemical structure cannot be revealed. Nevertheless, inhibitor design for drug targets in a kinase family is aided by additional structural knowledge of the family; there is clearly a lot to learn about the LIM kinase family since this is the first structure to be solved.

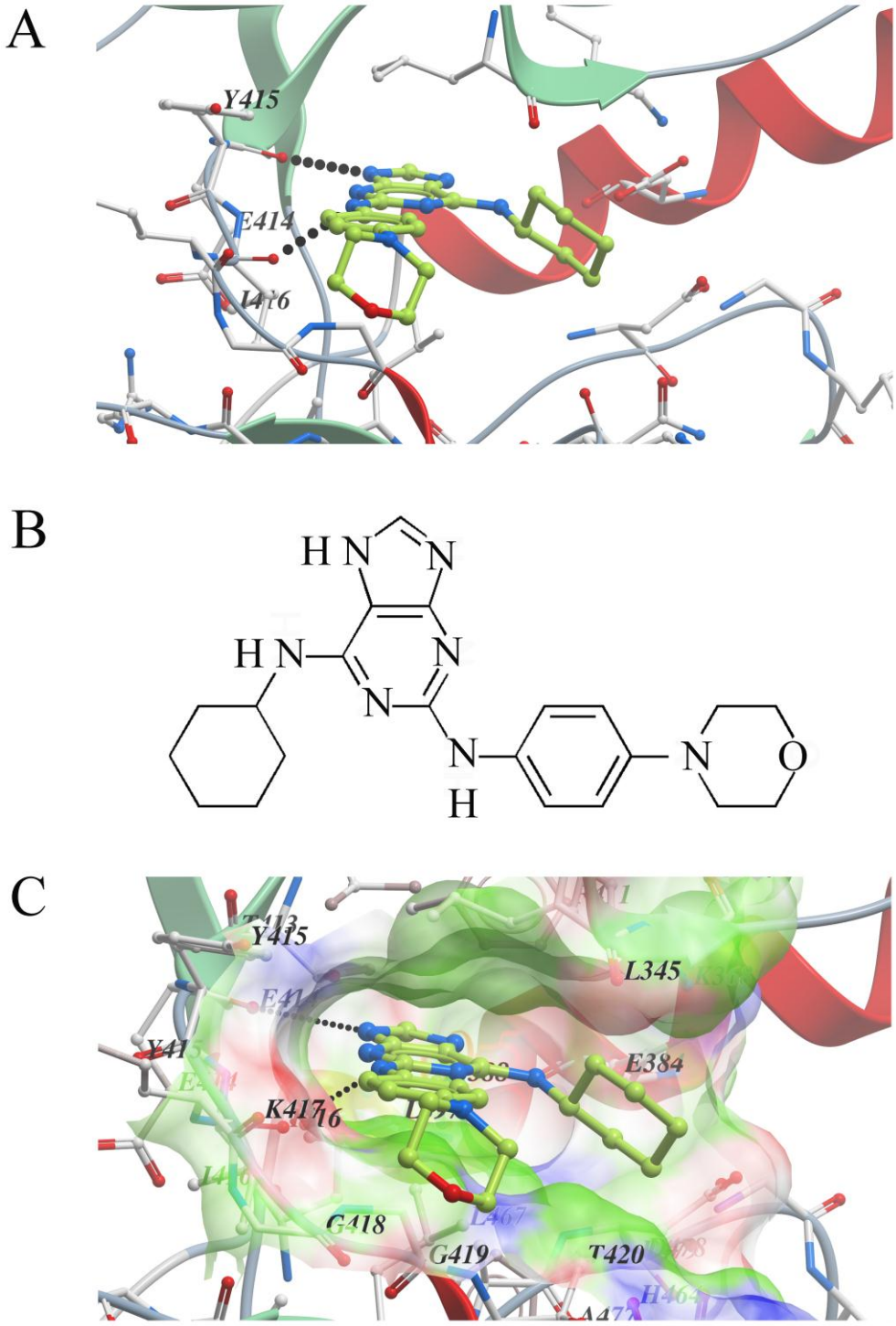

Figure 4.4. Docking of reversine (K02703a) into LIMK1. The modelled structure is represented in yellow. (A) Interactions of the inhibitor in the binding pocket, where it forms the typical hydrogen bonds to the kinase hinge region. (B) Chemical structure of reversine (K02703a). (C) K02703a fitting into the shape of the ATP binding site.

4.2.3 Structure features in cofilin regulation

LIM domain kinase 1 (LIMK1) controls the delicate balance between phosphorylated and unphosphorylated cofilin. Consequently, LIMK1 activity is regulated by a number of positive and negative regulators. Moreover, LIMK1 represents a promising target for the design of inhibitors with application in tumour metastasis. Therefore, one of the exciting outcomes of this research was to solve the structure of LIMK1 kinase domain, which has implications for the regulation of the actin cytoskeleton and anti-metastatic drug development. The crystal structure, solved at 1.65 Å, reveals a unique and unexpected architecture of the kinase C-lobe, showing the displacement of the typical αG helix and an additional C-terminal αJ helix, which is placed differently to other kinases (Figure 4.5A). The αG helix usually packs against the kinase substrate pocket, while, at the same position, in the LIMK1 structure there is a loop insertion (Figure 4.5B). Therefore, this loop might represent a docking site for substrate recognition and it raises the exciting possibility that this is an evolved LIMK feature that facilitates the specific recruitment of cofilin. In addition, the presence of an unusually positioned αJ helix at the end of the C lobe is the second most significant difference (Figure 4.5C). In LIMK1, this helix packs below and perpendicular to the αH helix and may form a docking site for protein-protein interaction or stabilize the kinase in the absence of the usual αG helix. This kinase-substrate binding is unusual as it is likely to be predominantly a protein-protein rather than protein-peptide interaction. The loop sequence, which replaces it, is conserved only in LIMK1/2 and in the testicular protein kinases (TESK1/2). Cofilin is uniquely regulated by both the LIMK and TESK families, suggesting that this atypical structural feature could be a docking site for cofilin protein interaction (Toshima et al, 2001).

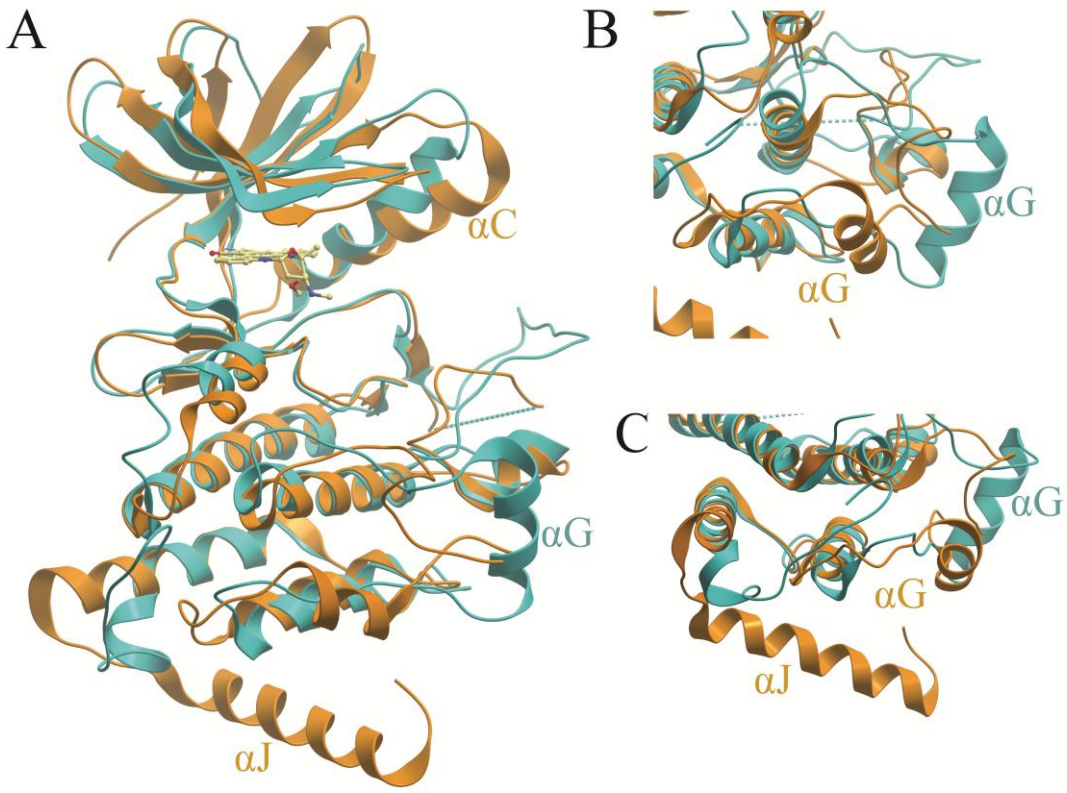

Figure 4.5. (A) Structural superimposition of LIMK1 (gold) and c-Src (cyan); (B) Superimposition showing the displacement of the αG helix from the canonical position close to the activation loop; (C) The additional αJ helix of LIMK1 is a unique feature of this kinase.

4.2.4 LIMK1 activation

During this study, it was possible to demonstrate that the crystallized LIMK1 construct was catalytically active, as supported by the closed conformation of the two lobes in the kinase structure. This is consistent with literature describing the LIM-LIM domains (absent in the present crystal structure) as a negative regulatory element (Nagata et al, 1999). During this work, the human PAK4 and cofilin were also expressed to investigate these activities by mass spectrometry. PAK4 phosphorylation of LIMK1 was observed at the activation loop residue Thr508, providing one potential kinase activation mechanism. In turn, LIMK1 phosphorylation of cofilin was detected on Ser3, the known physiological site.

For determination of BMPRII interaction sites, binding data have been collected on LIMK1, which produced several strong positive spots on a BMPRII-tail peptide array. A putative LIMK1-interacting peptide region from the array was assigned to a

specific region of less than 20 amino acids, SNLKQVETGVAKMNTINAA (aa 777-aa 796). However, isothermal titration calorimetry (ITC) measurements showed a weak binding with Kd = 60 µM. Higher affinity might be expected for physiological interaction. It is possible that the synthesized peptide was too short and therefore missed some critical interactions. In addition, it is possible that there may be multiple BMPRII interaction sites contributing further avidity.

Initial crystallization trials were also undertaken for the LIM-LIM and LIM-LIM-PDZ domains, which mediate BMPRII interaction. Both constructs had a tendency to aggregate, but a screen for different buffer/additive combinations identified an improved buffer pH condition and additive. Early crystal screens yielded promising crystalline precipitates, which would require further optimization.

5 Summary

The aim of this Ph.D. research was to understand the structural basis of cGMP-dependent protein kinase Iβ (cGKIβ) involved in pulmonary arterial hypertension (PAH), and of LIM Kinase 1 (LIMK1) as a key drug target for cancer metastasis. It was suggested that the downstream activity of cGKI is a pivotal regulator of PAH and vasodilation, and its interaction with BMP receptor II (BMPRII) tail region can recover PAH effects. BMPRII tail is also a docking site for LIMK1, which determines the balance between actin polymerization and depolymerisation. Therefore, the identification and structure determination of LIMK1 is of particular significance. Moreover, we investigated docking sites on the BMPRII tail for both cGKIβ and LIMK1 to provide new insight into signaling mechanisms and also to identify specific chemical inhibitors with potential for therapeutic development.

During this work, bacterial and baculoviral expression systems were established generating high yields of the target proteins and to determine their kinase activity *in vitro*. Interestingly, cGKIβ thermal stability and inhibitor binding were changed by cGMP. It is possible to speculate that the binding of cGMP to the cGMP-binding domains leads to large conformational changes affecting the accessibility of the ATP binding pocket. Furthermore, putative interaction sites in BMPRII using peptide arrays were also identified and validated indicating that cGKIβ shows high affinity binding to the N-terminal region of BMPRII-tail (GEKNRNSIY, aa 581- aa 589). cGKIβ binds also another tail region (EPHVVTVTMNG, aa 797- aa 888) with a weaker affinity, due to BMPRII-tail secondary structure. In addition, binding data showed that peptide SNLKQVETGVAKMNTINAA (aa 777- aa 796) is a BMPRII-tail docking site for the N-terminal region of LIMK1. In the present work, the first X-ray crystal structure of LIMK1 kinase domain was determined at 1.65 Å resolution in complex with the promiscuous inhibitor staurosporine. Small molecule kinase inhibitors, with potential application against tumour cell invasion and metastasis, were used as template for molecular docking (pdb id 3S95), obtaining reliable docking solution. LIMK1 kinase domain is shifted towards an active kinase domain conformation, this evidence is also supported from enzymatic kinase activity studies, showing its ability to directly phosphorylate cofilin 1.

6 Zusammenfassung

Das Ziel der vorliegenden Arbeit war die Strukturanalyse der cGMP-abhängigen Proteinkinase Iβ (cGKIβ) sowie der LIM Kinase I (LIMKI).

Es wird vermutet, dass der Aktivität der cGKIβ eine Schlüsselrolle bei der pulmonären arteriellen Hypertension (PAH) und der Blutgefäßerweiterung zukommt: cGKIβ bindet an den BMPRII-Tail. Die Überexpression von cGKIβ verringert die durch Mutationen im *BMPRII* hervorgerufene PAH. Demzufolge war die Analyse der cGKIβ-BMPRII-Interaktionsstellen von besonderer Bedeutung.

Die Aufklärung der LIMK1-Struktur ist ebenfalls von größter Wichtigkeit: Die LIMK1-BMPRII-Interaktion beeinflusst die Phosphorylierung von Cofilin und damit die Polymerisation von Aktin sowie die Struktur des Cytoskeletts. Außerdem ist LIMK1 an der Metastasierung von Tumoren beteiligt. Struktur und Interaktionsstellen von LIMK1 und BMPRII oder cGKIβ und BMPRII ermöglichen neue Einblicke in die molekularen Mechanismen der Signaltransduktion und die Entwicklung von therapeutischen Maßnahmen.

Im Rahmen dieser Arbeit wurden bakterielle und baculovirale Expressionssysteme etabliert, die eine hohe Ausbeute der beiden Kinasen cGKIβ und LIMKI und die *in vitro* Analyse ihrer Aktivität ermöglichen. Interessanterweise, ändert sich in Gegenwart von cGMP die thermische Stabilität von cGKIβ und die Bindung von cGKIβ an Inhibitoren. Das lässt vermuten, dass die Bindung von cGMP an die cGMP-Bindungsdomänen Konformationsänderungen der cGKI verursacht, die den Zugang zur ATP-Bindungstasche beeinflussen. Außerdem wurden durch den Peptid-Array mögliche cGKIβ-BMPRII-Interaktionsstellen identifiziert und validiert: cGKI zeigte eine hohe Affinität zur N-terminalen Region des BMPRII-Tails (GEKNRNSIY, aa 581- aa 589) und aufgrund der Sekundärstruktur des BMPRII-Tails eine geringere Affinität zur Tail-Region (EPHVVTVTMNG, aa 797- aa 888).

Darüber hinaus konnte anhand von Bindungsdaten das Peptid SNLKQVETGVAKMNTINAA (aa 777- aa 796) als die Bindungsregion des BMPRII-Tails an die N-terminale Region der LIMK1 identifiziert werden. Durch diese Arbeit wurde außerdem die Röntgenstruktur der Kinase-Domäne von LIMK1 im Komplex mit dem Inhibitor Stauroporine (Auflösung 1,65 Å) aufgeklärt (pdb id

3S95). Kleine Molekül-Kinase-Inhibitoren, die das Potential haben, die Metastasierung und Invasion von Tumoren zu hemmen, wurden zur Simulation der molekularen Bindung benutzt. Dabei zeigte sich, dass die LIMK1 Kinase-Domäne in eine aktive Kinase-Domäne umgewandelt wird. Bestätigt wird dieses Ergebnis durch enzymatische Kinase-Studien, in denen die Fähigkeit Cofilin 1 zu phosphorylieren untersucht wurde.

7 Appendix

7.1 The theory of X-ray crystallography

Unveiling the structure of a macromolecule can benefit understanding its function. X-ray crystallography is one of powerful techniques to determine the molecular structures of proteins at atomic resolution. Since the technique was employed in this study, this part is to provide a brief theory of protein crystallography, including the crystal growth process, an introduction to the phase problem and model building and refinement.

7.1.1 Protein crystallization

Protein crystals are a regular, ordered arrangement of protein molecules in repeating lattice held together by weak intermolecular interactions. Crystals of macromolecules are typically fragile due to a high solvent content of approximately 50%, which presents in large solvent channels. Several crystallization techniques have been developed, such as vapour-diffusion techniques, batch crystallization, dialysis and free-interface diffusion. Since the vapour-diffusion method was employed in this study, it will be described here.

This technique is based on the vapour diffusion process between a crystallization drop, formed by a mixture of protein and precipitant solution, and a precipitant reservoir in a closed system. Upon equilibration, the loss of water from the crystallization drop causes an increase in concentration of precipitant and protein in the drop, giving a supersaturated protein solution (Figure 7.1). Once the supersaturation state is reached, an ordered assembly of several protein molecules triggers crystal nucleation. This process also leads to a slight decrease of the protein concentration in the drop, and hence the protein solubility shifts back to the metastable state where crystal growth occurs. Crystal growth stops when the protein concentration reaches the solubility curve. In this work, all crystallizations using the vapour diffusion method were set up in a sitting drop system using a robotic dispenser and 96-well plates. The advantage of use a robotic dispenser is that it is capable of dispensing small drops. Crystallization drops were set at the final volume of 150-200 nL and at three protein: precipitant volume ratios (1:1; 2:1; 3:1) for each crystallization condition.

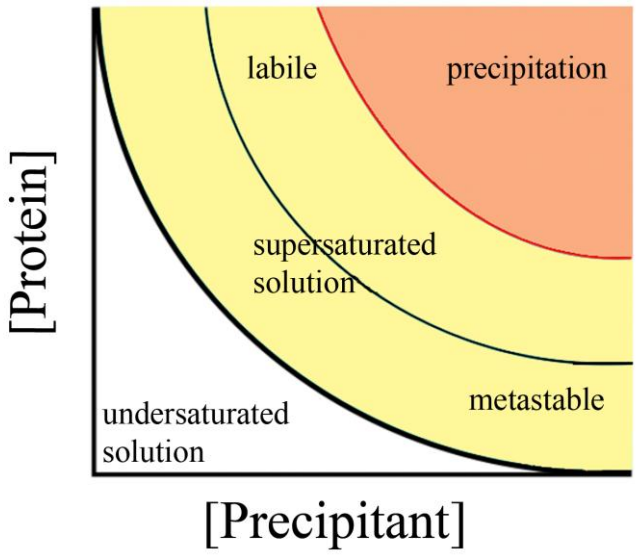

Figure 7.1. Crystallization phase diagram showing the solubility of a protein as a function of protein and precipitant concentrations.

7.1.2 Crystallization cocktails

Precipitating agents are mixed to the protein stock solution in order to reduce the solubility of the protein and reach the supersaturated state. Crystallization precipitants are grouped into several classes: inorganic salts, low molecular weight alcohols as isopropanol and MPD and organic polymers, such as polyethylene glycols (PEGs). Additives, such as ions, detergents and cofactors, may also be included in the crystallization reagents. Combinations of chemicals from each class at different concentration levels give various crystallization cocktails that decrease the protein solubility in the vapour-diffusion crystallization experiments.

7.1.3 Introduction to the phase problem

A diffraction experiment can be described as the reflections of X-rays from parallel lattice planes, called Miller indices annotated as h, k, l. As the crystal is formed by an ordered repetition of the smallest unit, known as the asymmetric unit, which can contain one or multiple protein molecules, the scattering phenomenon of X-rays by protein molecule can be amplified. A crystal lattice diffracts the X-rays focused on the crystal, and leads to interference of scattered X-rays with one another both

constructively or destructively, in which the former results sharp spots, called reflections. This process is described by the Bragg's law:

$$2\, d_{hkl} \sin\theta = n\lambda$$

Equation 7.1

This demonstrates a correlation between scattering angle (θ) and the interplanar spacing d_{hkl} between lattice planes h, k, l in a crystal. Reflection spots in a diffraction pattern occur when n is an integer, providing that the wavelength of the X-ray (λ) is constant. During diffraction data collection, the crystal has to be rotated within the X-ray beam so that the most of all possible reflections can be recorded. A data collection strategy in terms of angular degrees of rotation required for a complete data set depends on the crystal point group. Crystal properties, such as unit cell dimensions and Bravais lattice type, are then determined during the indexing process. The intensity of each diffraction spot (I) is calculated by measuring the difference between the reflections and background intensities. The diffraction intensity is equal to the square of the structure factor amplitude.

$$I(h,k,l) = |F(h,k,l)|^2$$

Equation 7.2

At the end of this processing, all diffraction images are integrated to assign the same crystal parameters, including the h, k, l values, and then scaled. Once the scaling process is completed, the images in the data set are merged and a list of coordinates and intensities of all reflections are generated.

The correlation of the contribution of each atom in the crystals to the reflection hkl can be expressed in the form of the structure factors ($F_{h,k,l}$) using the Fourier equation:

$$F_{hkl} = \sum_{j=1}^{n} f_j e^{\,2\pi i(hxj+kyj+lzj)}$$

Equation 7.3

where F_{hkl} is the structure factor for reflection will indices h, k, l, f_j is the scattering factor of atom j, which include the amplitude of its contribution, and x_j, y_j, z_j is the coordinates of atom j in the unit cell, which establish the phase of its contribution

$2\pi i(hx_j + ky_j + lz_j)$. In order to calculate the structure factors, the amplitude of the X-ray wave, diffraction position and phase of the X-ray wave are required. The first two factors are determined directly from the diffraction data collection, but the phase information cannot be measured from the diffraction experiment. The missing of this information is called the "phase problem".

To determine the macromolecule structure, three dimensional electron density map is required and can be derived from the Fourier transform, which allows the conversion of the reciprocal space as a set of structure factors to electron density at position x, y and z in real space ($\rho(x,y,z)$):

$$\rho(x,y,z) = 1/V \sum_{h}\sum_{k}\sum_{l} |F_{h,k,l}| e^{-2\pi i(hx+ky+lz) - \alpha calc(h,k,l)}$$

Equation 7.4

where V is the unit cell volume, $|F_{h,k,l}|$ is the structure factor amplitude and $\alpha_{calc}(h,k,l)$ is the phase angle which has to be determined.

Different methods have been developed to derive the phase information, and these include:

1. Experimental substructure phasing: This method includes single isomorphous replacement (SIR), multiple isomorphous replacement (MIR) and single-wavelenght or multi-wavelenght anomalus dispersion (SAD or MAD) and their combinations: SIRAS (single isomorphous replacement with anomalous scattering) and MIRAS (multiple isomorphous replacement with anomalous scattering). The techniques are based on the differences in the diffraction patterns between collected datasets. One dataset has to be collected from native crystals and the others from derivatized crystals (heavy atoms ions, seleniomethionine, sulphur or naturally bound metal ion).

2. Molecular replacement (MR): this method has been frequently used over the last ten years, in fact, 70% of all the macromolecular structures deposited on PDB were solved with this method (Evans and McCoy, 2008). Since MR was used throughout this work it will be described in details in the next section.

7.1.4 Molecular replacement method for the solution of the phase problem

In order to use molecular replacement to determine the phase information, a three-dimensional structure of a homologue protein with at least 25-30% sequence identity to the target protein is a prerequisite. This homologue structure is called a search model and it has to be rotated and translated for fitting into in its final position as described by the equation:

$$\vec{X}' = [C]\overrightarrow{X} + \vec{t}$$

Equation 7.5

where $\vec{X}$ is the set of position vectors indicating the coordinates of the model's atoms and $\overrightarrow{X'}$ is the set of position vectors upon the rotation of the model, according to the rotation matrix [C], and the translation by the translation vector $\vec{t}$. Six parameters have to be determined to place the model in its final position in the unit cell, and these are three-rotational parameters, the Euler's angles and three-translational, x, y, and z. The rotation function evaluates the correlation between the Patterson maps of both oriented molecules and the target molecule, when possible orientations are found then the translational function is performed. At the end of the rotational and translational search the phases can be calculated and an initial electron density map can be obtained. Best orientation and position in the unit cell is given by the agreement between the structure factors of the search model $|F_{calc}|$ and the observed amplitude $|F_{obs}|$ obtained from the experimental diffraction intensities of the target protein expressed as R-factor:

$$R_{fact} = \frac{\sum |F_{obs}| - |F_{calc}|}{\sum |F_{obs}|}$$

Equation 7.6

7.1.5 Structure refinement and quality of the model

Structure determination is the process consisting of interpretation of electron density map, called model building which involves assigning correct atoms into each position, and structure refinement. Several cycles of structure refinement and model building are necessary to examine whether the real-space-fitted target model is in close

agreement with the experimental diffraction data. The R-factor (R_{fact}) is used to measure the agreement between the structure factor amplitudes calculated from the model and the observed structure factor amplitudes. However, the R-factor may induce bias towards the model, resulting in an increase in the calculated structure factor amplitudes and as a consequent a decrease in the R-factor value. Hence, the free R-factor (R_{free}) is used as another independent parameter to determine the quality of the model by measuring the fits of the model to omitted reflections (~5%) that are not included in the structure refinement:

$$R_{free} = \frac{\sum_{(free\ set)} (|F_{obs}| - |F_{calc}|)}{\sum_{(free\ set)} |F_{obs}|}$$

Equation 7.7

A point of convergence is an indication for an end of model building and refinement that the model cannot be improved anymore. This is indicated by stable R-factor values (both R_{fact} and R_{free}) at the end of refinement process. Furthermore, the difference in both R values should be in between 3-6%.

7.2 Crystallization follow up screens

7.2.1 cGKI-sp-z001

	1	2	3	4	5	6	7	8	9	10	11	12
A	7.2 pH SPG 37% (v/v) MPD	7.2 pH SPG 40% (v/v) MPD	7.2 pH SPG 43% (v/v) MPD	7.2 pH SPG 46% (v/v) MPD	7.2 pH SPG 49% (v/v) MPD	7.2 pH SPG 52%(v/v) MPD	7.2 pH SPG 55% (v/v) MPD	7.2 pH SPG 58% (v/v) MPD	7.2 pH SPG 61% (v/v) MPD	7.2 pH SPG 64% (v/v) MPD	7.2 pH SPG 67% (v/v) MPD	7.2 pH SPG 70% (v/v) MPD
B	7.6 pH SPG 37%(v/v) MPD	7.6 pH SPG 40% (v/v) MPD	7.6 pH SPG 43% (v/v) MPD	7.6 pH SPG 46% (v/v) MPD	7.6 pH SPG 49% (v/v) MPD	7.6 pH SPG 52% (v/v) MPD	7.6 pH SPG 55% (v/v) MPD	7.6 pH SPG 58% (v/v) MPD	7.6 pH SPG 61% (v/v) MPD	7.6 pH SPG 64% (v/v) MPD	7.6 pH SPG 67% (v/v) MPD	7.6 pH SPG 70% (v/v) MPD
C	8pH SPG 37% (v/v) MPD	8pH SPG 40% (v/v) MPD	8pH SPG 43% (v/v) MPD	8pH SPG 46% (v/v) MPD	8pH SPG 49% (v/v) MPD	8pH SPG 52% (v/v) MPD	8pH SPG 55% (v/v) MPD	8pH SPG 58% (v/v) MPD	8pH SPG 61% (v/v) MPD	8pH SPG 64% (v/v) MPD	8pH SPG 67% (v/v) MPD	8pH SPG 70% (v/v) MPD
D	8.4 pH SPG 37% (v/v) MPD	8.4 pH SPG 40% (v/v) MPD	8.4 pH SPG 43% (v/v) MPD	8.4 pH SPG 46% (v/v) MPD	8.4 pH SPG 49% (v/v) MPD	8.4 pH SPG 52% (v/v) MPD	8.4 pH SPG 55% (v/v) MPD	8.4 pH SPG 58% (v/v) MPD	8.4 pH SPG 61% (v/v) MPD	8.4 pH SPG 64% (v/v) MPD	8.4 pH SPG 67% (v/v) MPD	8.4 pH SPG 70% (v/v) MPD

	1	2	3	4	5	6	7	8	9	10	11	12
E	8.8 pH SPG 37% (v/v) MPD	8.8 pH SPG 40% (v/v) MPD	8.8 pH SPG 43% (v/v) MPD	8.8 pH SPG 46% (v/v) MPD	8.8 pH SPG 49% (v/v) MPD	8.8 pH SPG 52% (v/v) MPD	8.8 pH SPG 55% (v/v) MPD	8.8 pH SPG 58% (v/v) MPD	8.8 pH SPG 61% (v/v) MPD	8.8 pH SPG 64% (v/v) MPD	8.8 pH SPG 67% (v/v) MPD	8.8 pH SPG 70% (v/v) MPD
F	37% (v/v) MPD 7.5 pH tris	40% (v/v) MPD 7.5 pH tris	43% (v/v) MPD 7.5 pH tris	46% (v/v) MPD 7.5 pH tris	49% (v/v) MPD 7.5 pH tris	52% (v/v) MPD 7.5 pH tris	55% (v/v) MPD 7.5 pH tris	58% (v/v) MPD 7.5 pH tris	61% (v/v) MPD 7.5 pH tris	64% (v/v) MPD 7.5 pH tris	67% (v/v) MPD 7.5 pH tris	70% (v/v) MPD 7.5 pH tris
G	37% (v/v) MPD 8pH tris	40% (v/v) MPD 8pH tris	43% (v/v) MPD 8pH tris	46% (v/v) MPD 8pH tris	49% (v/v) MPD 8pH tris	52% (v/v) MPD 8pH tris	55% (v/v) MPD 8pH tris	58% (v/v) MPD 8pH tris	61% (v/v) MPD 8pH tris	64% (v/v) MPD 8pH tris	67% (v/v) MPD 8pH tris	70% (v/v) MPD 8pH tris
H	37% (v/v) MPD 8.5 pH tris	40% (v/v) MPD 8.5 pH tris	43% (v/v) MPD 8.5 pH tris	46% (v/v) MPD 8.5 pH tris	49% (v/v) MPD 8.5 pH tris	52% (v/v) MPD 8.5 pH tris	55% (v/v) MPD 8.5 pH tris	58% (v/v) MPD 8.5 pH tris	61% (v/v) MPD 8.5 pH tris	64% (v/v) MPD 8.5 pH tris	67% (v/v) MPD 8.5 pH tris	70% (v/v) MPD 8.5 pH tris

7.2.2 LIMK1-sp-z001

	1	2	3	4	5	6	7	8	9	10	11	12
A	14% (v/v) jeff600 7 pH HEPES	17% (v/v) jeff600 7 pH HEPES	20% (v/v) jeff600 7 pH HEPES	23% (v/v) jeff600 7 pH HEPES	26% (v/v) jeff600 7 pH HEPES	29% (v/v) jeff600 7 pH HEPES	14% (v/v) MPD 7.7 pH tris	17% (v/v) MPD 7.7 pH tris	20% (v/v) MPD 7.7 pH tris	23% (v/v) MPD 7.7 pH tris	26% (v/v) MPD 7.7 pH tris	29% (v/v) MPD 7.7 pH tris
B	14% (v/v) jeff600 7.3 pH HEPES	17% (v/v) jeff600 7.3 pH HEPES	20% (v/v) jeff600 7.3 pH HEPES	23% (v/v) jeff600 7.3 pH HEPES	26% (v/v) jeff600 7.3 pH HEPES	29% (v/v) jeff600 7.3 pH HEPES	14% (v/v) MPD 8.0 pH tris	17% (v/v) MPD 8.0 pH tris	20% (v/v) MPD 8.0 pH tris	23% (v/v) MPD 8.0 pH tris	26% (v/v) MPD 8.0 pH tris	29% (v/v) MPD 8.0 pH tris
C	14% (v/v) jeff600 7.6 pH HEPES	17% (v/v) jeff600 7.6 pH HEPES	20% (v/v) jeff600 7.6 pH HEPES	23% (v/v) jeff600 7.6 pH HEPES	26% (v/v) jeff600 7.6 pH HEPES	29% (v/v) jeff600 7.6 pH HEPES	14% (v/v) MPD 8.3 pH tris	17% (v/v) MPD 8.3 pH tris	20% (v/v) MPD 8.3 pH tris	23% (v/v) MPD 8.3 pH tris	26% (v/v) MPD 8.3 pH tris	29% (v/v) MPD 8.3 pH tris
D	14% (v/v) jeff600 7.9 pH HEPES	17% (v/v) jeff600 7.9 pH HEPES	20% (v/v) jeff600 7.9 pH HEPES	23% (v/v) jeff600 7.9 pH HEPES	26% (v/v) jeff600 7.9 pH HEPES	29% (v/v) jeff600 7.9 pH HEPES	14% (v/v) MPD 8.9 pH tris	17% (v/v) MPD 8.9 pH tris	20% (v/v) MPD 8.9 pH tris	23% (v/v) MPD 8.9 pH tris	26% (v/v) MPD 8.9 pH tris	29% (v/v) MPD 8.9 pH tris

	1	2	3	4	5	6	7	8	9	10	11	12
E	4.0 pH Acetate	4.0 pH Acetate	4.0 pH Acetate	4.0 pH Acetate	4.0 pH Acetate	4.0 pH Acetate	18 % (w/v) PEG 3.3k	18% (w/v) PEG 3.3k	18% (w/v) PEG 3.3k	18% (w/v) PEG 3.3k	18% (w/v) PEG 3.3k	18% (w/v) PEG 3.3k
							0.15M NaCl	0.2 M NaCl	0.15 M NaCl	0.2 M NaCl	0.15 M NaCl	0.2 M NaCl
	0.6M NaK phosphate	0.8M NaK phosphate	1.0M NaK phosphate	1.2M NaK phosphate	1.4M NaK phosphate	1.6M NaK phosphate	5.5pH bis-tris	5.5pH bis-tris	5.8pH bis-tris	5.8pH bis-tris	6.2pH bis-tris	6.2pH bis-tris
F	4.3 pH Acetate)	4.3 pH Acetate	4.3 pH Acetate	4.3 pH Acetate	4.3 pH Acetate	4.3 pH Acetate	23 % (w/v) PEG 3.3k	23% (w/v) PEG 3.3k	2% (w/v) PEG 3.3k	23% (w/v) PEG 3.3k	23% (w/v) PEG 3.3k	23% (w/v) PEG 3.3k
							0.15 M NaCl	0.2 M NaCl	0.15 M NaCl	0.2 M NaCl	0.15 M NaCl	0.2 M NaCl
	0.6M NaK phosphate	0.8M NaK phosphate	1.0M NaK phosphate	1.2M NaK phosphate	1.4M NaK phosphate	1.6M NaK phosphate	5.5pH bis-tris	5.5pH bis-tris	5.8pH bis-tris	5.8pH bis-tris	6.2pH bis-tris	6.2pH bis-tris
G	4.6 pH Acetate	4.6 pH Acetate	4.6 pH Acetate	4.6 pH Acetate	4.6 pH Acetate	4.6 pH Acetate	28 % (w/v) PEG 3.3k	28% (w/v) PEG 3.3k	28% (w/v) PEG 3.3k	28% (w/v) PEG 3.3k	28% (w/v) PEG 3.3k	28% (w/v) PEG 3.3k
							0.15 M NaCl	0.2 M NaCl	0.15 M NaCl	0.2 M NaCl	0.15 M NaCl	0.2 M NaCl
	0.6M NaK phosphate	0.8M NaK phosphate	1.0M NaK phosphate	1.2M NaK phosphate	1.4M NaK phosphate	1.6M NaK phosphate	5.5 pH bis-tris	5.5 pH bis-tris	5.8 pH bis-tris	5.8 pH bis-tris	6.2 pH bis-tris	6.2 pH bis-tris
H	4.9 pH Acetate	4.9 pH Acetate	4.9 pH Acetate	4.9 pH Acetate	4.9 pH Acetate	4.9 pH Acetate	33 % (w/v) PEG 3.3k	33%(w/v) PEG 3.3k	33%(w/v) PEG 3.3k	33%(w/v) PEG 3.3k	33%(w/v) PEG 3.3k	33%(w/v) PEG 3.3k
							0.15 M NaCl	0.2 M NaCl	0.15 M NaCl	0.2 M NaCl	0.15 M NaCl	0.2 M NaCl
	0.6M NaK phosphate	0.8M NaK phosphate	1.0M NaK phosphate	1.2M NaK phosphate	1.4M NaK phosphate	1.6M NaK phosphate	5.5 pH bis-tris	5.5 pH bis-tris	5.8 pH bis-tris	5.8 pH bis-tris	6.2 pH bis-tris	6.2 pH bis-tris

7.2.3 LIMK1-sp-z002

	1	2	3	4	5	6	7	8	9	10	11	12
A	12% (v/v) MPD	12% (v/v) MPD	12% (v/v) MPD	12% (v/v) MPD	12% (v/v) jeff600	12% (v/v) jeff600	20% (w/v) PEG 3.3k 0.125 M NaCl	20% (w/v) PEG 3.3k 0.125 M NaCl	20% (w/v) PEG 3.3k 0.125 M NaCl	20% (w/v) PEG 3.3k 0.125 M NaCl	20% (w/v) PEG 3.3k 0.125 M NaCl	20% (w/v) PEG 3.3k 0.125 M NaCl
	7.0 pH tris	7.25 pH tris	7.50 pH tris	7.75 pH tris	7.3 pH tris	7.7 pH tris	5.5 pH bis-tris	5.8 pH bis-tris	6.3 pH bis-tris	6.6 pH bis-tris	6.9 pH bis-tris	7.2 pH bis-tris
B	15% (v/v) MPD	15% (v/v) MPD	15% (v/v) MPD	15% (v/v) MPD	15% (v/v) jeff600	15% (v/v) jeff600	25% (w/v) PEG 3.3k 0.125 M NaCl	25% (w/v) PEG 3.3k 0.125 M NaCl	25% (w/v) PEG 3.3k 0.125 M NaCl	25% (w/v) PEG 3.3k 0.125 M NaCl	25% (w/v) PEG 3.3k 0.125 M NaCl	25% (w/v) PEG 3.3k 0.125 M NaCl
	7.0 pH tris	7.25 pH tris	7.50 pH tris	7.75 pH tris	7.3 pH tris	7.7 pH tris	5.5 pH bis-tris	5.8 pH bis-tris	6.3 pH bis-tris	6.6 pH bis-tris	6.9 pH bis-tris	7.2 pH bis-tris
C	17% (v/v) MPD	17% (v/v) MPD	17% (v/v) MPD	17% (v/v) MPD	17% (v/v) jeff600	17% (v/v) jeff600	30% (w/v) PEG 3.3k 0.125 M NaCl	30% (w/v) PEG 3.3k 0.125 M NaCl	30% (w/v) PEG 3.3k 0.125 M NaCl	30% (w/v) PEG 3.3k 0.125 M NaCl	30% (w/v) PEG 3.3k 0.125 M NaCl	30% (w/v) PEG 3.3k 0.125 M NaCl
	7.0 pH tris	7.25 pH tris	7.50 pH tris	7.75 pH tris	7.3 pH tris	7.7 pH tris	5.5 pH bis-tris	5.8 pH bis-tris	6.3 pH bis-tris	6.6 pH bis-tris	6.9 pH bis-tris	7.2 pH bis-tris
D	21% (v/v) MPD	21% (v/v) MPD	21% (v/v) MPD	21% (v/v) MPD	21% (v/v) jeff600	21% (v/v) jeff600	20% (w/v) PEG 3.3k 0.175 M NaCl	20% (w/v) PEG 3.3k 0.175 M NaCl	20% (w/v) PEG 3.3k 0.175 M NaCl	20% (w/v) PEG 3.3k 0.175 M NaCl	20% (w/v) PEG 3.3k 0.175 M NaCl	20% (w/v) PEG 3.3k 0.175 M NaCl
	7.0 pH tris	7.25 pH tris	7.50 pH tris	7.75 pH tris	7.3 pH tris	7.7 pH tris	5.5 pH bis-tris	5.8 pH bis-tris	6.3 pH bis-tris	6.6 pH bis-tris	6.9 pH bis-tris	7.2 pH bis-tris

	1	2	3	4	5	6	7	8	9	10	11	12
E	24% (v/v) MPD	24% (v/v) MPD	24% (v/v) MPD	24% (v/v) MPD	24% (v/v) jeff600	24% (v/v) jeff600	25% (w/v) PEG 3.3k	25% (w/v) PEG 3.3k	25% (w/v) PEG 3.3k	25% (w/v) PEG 3.3k	25% (w/v) PEG 3.3k	25% (w/v) PEG 3.3k
							0.175 M NaCl	0.175 M NaCl	0.175 M NaCl	0.175 M NaCl	0.175 M NaCl	0.175 M NaCl
	7.0 pH tris	7.25 pH tris	7.50 pH tris	7.75 pH tris	7.3 pH tris	7.7 pH tris	5.5 pH bis-tris	5.8 pH bis-tris	6.3 pH bis-tris	6.6 pH bis-tris	6.9 pH bis-tris	7.2 pH bis-tris
F	27% (v/v) MPD	27% (v/v) MPD	27% (v/v) MPD	27% (v/v) MPD	27% (v/v) jeff600	27% (v/v) jeff600	30% (w/v) PEG 3.3k	30% (w/v) PEG 3.3k	30% (w/v) PEG 3.3k	30% (w/v) PEG 3.3k	30% (w/v) PEG 3.3k	30% (w/v) PEG 3.3k
							0.175 M NaCl	0.175 M NaCl	0.175 M NaCl	0.175 M NaCl	0.175 M NaCl	0.175 M NaCl
	7.0 pH tris	7.25 pH tris	7.50 pH tris	7.75 pH tris	7.3 pH tris	7.7 pH tris	5.5 pH bis-tris	5.8 pH bis-tris	6.3 pH bis-tris	6.6 pH bis-tris	6.9 pH bis-tris	7.2 pH bis-tris
G	15% (v/v) MPD	15% (v/v) MPD	15% (v/v) MPD	15% (v/v) MPD	15% (v/v) jeff600	15% (v/v) jeff600	20% (w/v) PEG 3.3k	20% (w/v) PEG 3.3k	20% (w/v) PEG 3.3k	20% (w/v) PEG 3.3k	20% (w/v) PEG 3.3k	20% (w/v) PEG 3.3k
							0.12 M NaCl	0.12 M NaCl	0.12 M NaCl	0.12 M NaCl	0.12 M NaCl	0.12 M NaCl
	0.05 M NaK phosphate	0.05 M NaK phosphate	0.05 M NaK phosphate	0.05 M NaK phosphate	0.05 M NaK phosphate	0.05 M NaK phosphate	0.05 M NaK phosphate	0.05 M NaK phosphate	0.05 M NaK phosphate	0.05 M NaK phosphate	0.05 M NaK phosphate	0.05 M NaK phosphate
	7.0 pH tris	7.25 pH tris	7.50 pH tris	7.75 pH tris	7.3 pH tris	7.7 pH tris	5.5 pH bis-tris	5.8 pH bis-tris	6.3 pH bis-tris	6.6 pH bis-tris	6.9 pH bis-tris	7.2 pH bis-tris
H	22% (v/v) MPD	22% (v/v) MPD	22% (v/v) MPD	22% (v/v) MPD	22% (v/v) jeff600	22% (v/v) jeff600	25% (w/v) PEG 3.3k	25% (w/v) PEG 3.3k	25% (w/v) PEG 3.3k	25% (w/v) PEG 3.3k	25% (w/v) PEG 3.3k	25% (w/v) PEG 3.3k
							0.12 M NaCl	0.12 M NaCl	0.12 M NaCl	0.12 M NaCl	0.12 M NaCl	0.12 M NaCl
	0.05 M NaK phosphate	0.05 M NaK phosphate	0.05 M NaK phosphate	0.05 M NaK phosphate	0.05 M NaK phosphate	0.05 M NaK phosphate	0.05 M NaK phosphate	0.05 M NaK phosphate	0.05 M NaK phosphate	0.05 M NaK phosphate	0.05 M NaK phosphate	0.05 M NaK phosphate
	7.0 pH tris	7.25 pH tris	7.50 pH tris	7.75 pH tris	7.3 pH tris	7.7 pH tris	5.5 pH bis-tris	5.8 pH bis-tris	6.3 pH bis-tris	6.6 pH bis-tris	6.9 pH bis-tris	7.2 pH bis-tris

7.2.4 LIMK1-sp-z003

	1	2	3	4	5	6	7	8	9	10	11	12
A	12.5% (v/v) MPD 6.5pH bis-tris	22.5% (v/v) MPD 6.5pH bis-tris	32.5% (v/v) MPD 6.5pH bis-tris	12.5% (v/v) MPD 7pH tris	22.5% (v/v) MPD 7pH tris	32.5% (v/v) MPD 7pH tris	12.5% (v/v) jeff600 6.5pH bt-prop	22.5% (v/v) jeff600 6.5pH bt-prop	32.5% (v/v) jeff600 6.5pH bt-prop	12.5% (v/v) jeff600 7pH HEPES	22.5% (v/v) jeff600 7pH HEPES	32.5% (v/v) jeff600 7pH HEPES
B	15% (v/v) MPD 6.5pH bis-tris	25% (v/v) MPD 6.5pH bis-tris	35% (v/v) MPD 6.5pH bis-tris	15% (v/v) MPD 7pH tris	25% (v/v) MPD 7pH tris	35% (v/v) MPD 7pH tris	15% (v/v) jeff600 6.5pH bt-prop	25% (v/v) jeff600 6.5pH bt-prop	35% (v/v) jeff600 6.5pH bt-prop	15% (v/v) jeff600 7pH HEPES	25% (v/v) jeff600 7pH HEPES	35% (v/v) jeff600 7pH HEPES
C	17.5% (v/v) MPD 6.5pH bis-tris	27.5% (v/v) MPD 6.5pH bis-tris	37.5% (v/v) MPD 6.5pH bis-tris	17.5% (v/v) MPD 7pH tris	27.5% (v/v) MPD 7pH tris	37.5% (v/v) MPD 7pH tris	17.5% (v/v) jeff600 6.5pH bt-prop	27.5% (v/v) jeff600 6.5pH bt-prop	37.5% (v/v) jeff600 6.5pH bt-prop	17.5% (v/v) jeff600 7pH HEPES	27.5% (v/v) jeff600 7pH HEPES	37.5% (v/v) jeff600 7pH HEPES
D	20% (v/v) MPD 6.5pH bis-tris	30% (v/v) MPD 6.5pH bis-tris	40% (v/v) MPD 6.5pH bis-tris	20% (v/v) MPD 7pH tris	30% (v/v) MPD 7pH tris	40% (v/v) MPD 7pH tris	20% (v/v) jeff600 6.5pH bt-prop	30% (v/v) jeff600 6.5pH bt-prop	40% (v/v) jeff600 6.5pH bt-prop	20% (v/v) jeff600 7pH HEPES	30% (v/v) jeff600 7pH HEPES	40% (v/v) jeff600 7pH HEPES

	1	2	3	4	5	6	7	8	9	10	11	12
E	12.5% (v/v) MPD	22.5% (v/v) MPD	32.5% (v/v) MPD	12.5% (v/v) MPD	22.5% (v/v) MPD	32.5% (v/v) MPD	12.5% (v/v) jeff600	22.5% (v/v) jeff600	32.5% (v/v) jeff600	12.5% (v/v) jeff600	22.5% (v/v) jeff600	32.5% (v/v) jeff600
	7.25 pH tris	7.25 pH tris	7.25 pH tris	7.5 pH tris	7.5 pH tris	7.5 pH tris	7.25 pH HEPES	7.25 pH HEPES	7.25 pH HEPES	7.5 pH HEPES	7.5 pH HEPES	7.5 pH HEPES
F	15% (v/v) MPD	25% (v/v) MPD	35% (v/v) MPD	15% (v/v) MPD	25% (v/v) MPD	35% (v/v) MPD	15% (v/v) jeff600	25%(v/v) jeff600	35% (v/v) jeff600	15% (v/v) jeff600	25% (v/v) jeff600	35% (v/v) jeff600
	7.25 pH tris	7.25 pH tris	7.25 pH tris	7.5 pH tris	7.5 pH tris	7.5 pH tris	7.25 pH HEPES	7.25 pH HEPES	7.25 pH HEPES	7.5 pH HEPES	7.5 pH HEPES	7.5 pH HEPES
G	17.5% (v/v) MPD	27.5% (v/v) MPD	37.5% (v/v) MPD	17.5% (v/v) MPD	27.5% (v/v) MPD	37.5% (v/v) MPD	17.5% (v/v) jeff600	27.5% (v/v) jeff600	37.5% (v/v) jeff600	17.5% (v/v) jeff600	27.5% (v/v) jeff600	37.5% (v/v) jeff600
	7.25 pH tris	7.25 pH tris	7.2 5pH tris	7.5pH tris	7.5pH tris	7.5pH tris	7.25 pH HEPES	7.25 pH HEPES	7.25 pH HEPES	7.5 pH HEPES	7.5 pH HEPES	7.5 pH HEPES
H	20% (v/v) MPD	30% (v/v) MPD	40% (v/v) MPD	20% (v/v) MPD	30% (v/v) MPD	40% (v/v) MPD	20% (v/v) jeff600	30% (v/v) jeff600	40% (v/v) jeff600	20% (v/v) jeff600	30% (v/v) jeff600	40% (v/v) jeff600
	7.25 pH tris	7.25 pH tris	7.25 pH tris	7.5 pH tris	7.5 pH tris	7.5 pH tris	7.25 pH HEPES	7.25 pH HEPES	7.25 pH HEPES	7.5 pH HEPES	7.5 pH HEPES	7.5 pH HEPES
E	12.5% (v/v) MPD	22.5% (v/v) MPD	32.5% (v/v) MPD	12.5% (v/v) MPD	22.5% (v/v) MPD	32.5% (v/v) MPD	12.5% (v/v) jeff600	22.5% (v/v) jeff600	32.5% (v/v) jeff600	12.5% (v/v) jeff600	22.5% (v/v) jeff600	32.5% (v/v) jeff600

7.2.5 LIMK1-sp-z004

	1	2	3	4	5	6	7	8	9	10	11	12
A	14% (w/v) PEG 3.3k 0.1M K3 citr	17% (w/v) PEG 3.3k 0.1M K3 citr	20% (w/v) PEG 3.3k 0.1M K3 citr	23% (w/v) PEG 3.3k 0.1M K3 citr	26% (w/v) PEG 3.3k 0.1M K3 citr	29% (w/v) PEG 3.3k 0.1M K3 citr	14% (w/v) PEG 3.3k 0.1M Na malate	17% (w/v) PEG 3.3k 0.1M Na malate	20% (w/v) PEG 3.3k 0.1M Na malate	23% (w/v) PEG 3.3k 0.1M Na malate	26% (w/v) PEG 3.3k 0.1M Na malate	29% (w/v) PEG 3.3k 0.1M Na malate
B	14% (w/v) PEG 3.3k 0.15 M K3 citr	17% (w/v) PEG 3.3k 0.15 M K3 citr	20% (w/v) PEG 3.3k 0.15 M K3 citr	23% (w/v) PEG 3.3k 0.15 M K3 citr	26% (w/v) PEG 3.3k 0.15 M K3 citr	29% (w/v) PEG 3.3k 0.15 M K3 citr	14% (w/v) PEG 3.3k 0.15 M Na malate	17% (w/v) PEG 3.3k 0.15 M Na malate	20% (w/v) PEG 3.3k 0.15 M Na malate	23% (w/v) PEG 3.3k 0.15 M Na malate	26% (w/v) PEG 3.3k 0.15 M Na malate	29% (w/v) PEG 3.3k 0.15 M Na malate
C	14%(w/v) PEG 3.3k 0.2M K3 citr	17% (w/v) PEG 3.3k 0.2M K3 citr	20% (w/v) PEG 3.3k 0.2M K3 citr	23% (w/v) PEG 3.3k 0.2M K3 citr	26% (w/v) PEG 3.3k 0.2M K3 citr	29% (w/v) PEG 3.3k 0.2M K3 citr	14% (w/v) PEG 3.3k 0.2M Na malate	17% (w/v) PEG 3.3k 0.2M Na malate	20% (w/v) PEG 3.3k 0.2M Na malate	23% (w/v) PEG 3.3k 0.2M Na malate	26% (w/v) PEG 3.3k 0.2M Na malate	29% (w/v) PEG 3.3k 0.2M Na malate
D	14% (w/v) PEG 3.3k 0.25 M K3 citr	17%(w/v) PEG 3.3k 0.25 M K3 citr	20%(w/v) PEG 3.3k 0.25 M K3 citr	23%(w/v) PEG 3.3k 0.25 M K3 citr	26%(w/v) PEG 3.3k 0.25 M K3 citr	29%(w/v) PEG 3.3k 0.25 M K3 citr	14%(w/v) PEG 3.3k 0.25 M Na malate	17%(w/v) PEG 3.3k 0.25 M Na malate	20%(w/v) PEG 3.3k 0.25 M Na malate	23%(w/v) PEG 3.3k 0.25 M Na malate	26%(w/v) PEG 3.3k 0.25 M Na malate	29%(w/v) PEG 3.3k 0.25 M Na malate

	1	2	3	4	5	6	7	8	9	10	11	12
E	20% (w/v) PEG 4k 0.1M (amm)(ac) 0.019 M bt-prop 0.081 M Na citr	33% (w/v) PEG 4k 0.1M (amm)(ac) 0.019 M bt-prop 0.081 M Na citr	26% (w/v) PEG 4k 0.2M (amm)(ac) 0.019 M bt-prop 0.081 M Na citr	23% (w/v) PEG 4k 0.15 M (amm)(ac) 0.019 M bt-prop 0.081 M Na citr	20% (w/v) PEG 4k 0.1M (amm)(ac) 0.009 M bt-prop 0.091 M Na citr	33% (w/v) PEG 4k 0.1M (amm)(ac) 0.009 M bt-prop 0.091 M Na citr	26% (w/v) PEG 4k 0.2M (amm)(ac) 0.009 M bt-prop 0.091 M Na citr	23% (w/v) PEG 4k 0.15 M (amm)(ac) 0.009 M bt-prop 0.091 M Na citr	20% (w/v) PEG 4k 0.1M (amm)(ac) 0.002 M bt-prop 0.098 M Na citr	33% (w/v) PEG 4k 0.1M (amm)(ac) 0.002 M bt-prop 0.098 M Na citr	26% (w/v) PEG 4k 0.2M (amm)(ac) 0.002 M bt-prop 0.098 M Na citr	23% (w/v) PEG 4k 0.15 M (amm)(ac) 0.002 M bt-prop 0.098 M Na citr
F	23% (w/v) PEG 4k 0.1M (amm)(ac) 0.019 M bt-prop 0.081 M Na citr	17% (w/v) PEG 4k 0.2M (amm)(ac) 0.019 M bt-prop 0.081 M Na citr	29% (w/v) PEG 4k 0.2M (amm)(ac) 0.019 M bt-prop 0.081 M Na citr	26% (w/v) PEG 4k 0.15 M (amm)(ac) 0.019 M bt-prop 0.081 M Na citr	23% (w/v) PEG 4k 0.1M (amm)(ac) 0.009 M bt-prop 0.091 M Na citr	17% (w/v) PEG 4k 0.2M (amm)(ac) 0.009 M bt-prop 0.091 M Na citr	29% (w/v) PEG 4k 0.2M (amm)(ac) 0.009 M bt-prop 0.091 M Na citr	26% (w/v) PEG 4k 0.15 M (amm)(ac) 0.009 M bt-prop 0.091 M Na citr	23% (w/v) PEG 4k 0.1M (amm)(ac) 0.002 M bt-prop 0.098 M Na citr	17% (w/v) PEG 4k 0.2M (amm)(ac) 0.002 M bt-prop 0.098 M Na citr	29% (w/v) PEG 4k 0.2M (amm)(ac) 0.002 M bt-prop 0.098 M Na citr	26% (w/v) PEG 4k 0.15 M (amm)(ac) 0.002 M bt-prop 0.098 M Na citr
G	26% (w/v) PEG 4k 0.1M (amm)(ac) 0.019 M bt-prop 0.081 M Na citr	20% (w/v) PEG 4k 0.2M (amm)(ac) 0.019 M bt-prop 0.081 M Na citr	33% (w/v) PEG 4k 0.2M (amm)(ac) 0.019 M bt-prop 0.081 M Na citr	29% (w/v) PEG 4k 0.15 M (amm)(ac) 0.019 M bt-prop 0.081 M Na citr	26% (w/v) PEG 4k 0.1M (amm)(ac) 0.009 M bt-prop 0.091 M Na citr	20% (w/v) PEG 4k 0.2M (amm)(ac) 0.009 M bt-prop 0.091 M Na(citr	33% (w/v) PEG 4k 0.2M (amm)(ac) 0.009 M bt-prop 0.091 M Na citr	29% (w/v) PEG 4k 0.15 M (amm)(ac) 0.009 M bt-prop 0.091 M Na citr	26% (w/v) PEG 4k 0.1M (amm)(ac) 0.002 M bt-prop 0.098 M Na citr	20% (w/v) PEG 4k 0.2M (amm)(ac) 0.002 M bt-prop 0.098 M Na citr	33% (w/v) PEG 4k 0.2M (amm)(ac) 0.002 M bt-prop 0.098 M Na citr	29% (w/v) PEG 4k 0.15 M (amm)(ac) 0.002 M bt-prop 0.098 M Na citr
H	29% (w/v) PEG 4k 0.1M (amm)(ac) 0.019 M bt-prop 0.081 M Na citr	23% (w/v) PEG 4k 0.2M (amm)(ac) 0.019 M bt-prop 0.081 M Na citr	20% (w/v) PEG 4k 0.15 M (amm)(ac) 0.019 M bt-prop 0.081 M Na citr	33% (w/v) PEG 4k 0.15 M (amm)(ac) 0.019 M bt-prop 0.081 M Na citr	29% (w/v) PEG 4k 0.1M (amm)(ac) 0.009 M bt-prop 0.091 M Na citr	23% (w/v) PEG 4k 0.2M (amm)(ac) 0.009 M bt-prop 0.091 M Na citr	20% (w/v) PEG 4k 0.15 M (amm)(ac) 0.009 M bt-prop 0.091 M Na citr	33% (w/v) PEG 4k 0.15 M (amm)(ac) 0.009 M bt-prop 0.091 M Na citr	29% (w/v) PEG 4k 0.1M (amm)(ac) 0.002 M bt-prop 0.098 M Na(itr	23% (w/v) PEG 4k 0.2M (amm)(ac) 0.002 M bt-prop 0.098 M Na citr	20% (w/v) PEG 4k 0.15 M (amm)(ac) 0.002 M bt-prop 0.098 M Na citr	33% (w/v) PEG 4k 0.15 M (amm)(ac) 0.002 M bt-prop 0.098 M Na citr

8 Bibliobraphy

Abagyan, R.A., Totrov, M.M., and Kuznetsov, D.A. Icm: A New Method For Protein Modeling and Design: Applications To Docking and Structure Prediction From The Distorted Native Conformation J. Comp. Chem. 15, 488-506.

Abdollah, S., M. Macias-Silva, T. Tsukazaki, H. Hayashi, L. Attisano, and J.L. Wrana. 1997. TbetaRI phosphorylation of Smad2 on Ser465 and Ser467 is required for Smad2-Smad4 complex formation and signaling. *J Biol Chem*. 272:27678-85.

Acevedo, K., N. Moussi, R. Li, P. Soo, and O. Bernard. 2006. LIM kinase 2 is widely expressed in all tissues. *J Histochem Cytochem*. 54:487-501.

Attisano L, Lee-Hoeflich ST. The Smads. Genome Biol. 2001; 2(8): reviews 3010.

Attisano, L., and J.L. Wrana. 2002. Signal transduction by the TGF-beta superfamily. *Science*. 296:1646-7.

Attisano, L., J. Carcamo, F. Ventura, F.M. Weis, J. Massague, and J.L. Wrana. 1993. Identification of human activin and TGF beta type I receptors that form heteromeric kinase complexes with type II receptors. *Cell*. 75:671-80.

Attisano, L., J.L. Wrana, E. Montalvo, and J. Massague. 1996. Activation of signalling by the activin receptor complex. *Mol Cell Biol*. 16:1066-73.

Bagheri-Yarmand R, Mazumdar A, Sahin AA, Kumar R. LIM kinase 1 increases tumor metastasis of human breast cancer cells via regulation of the urokinase-type plasminogen activator system.Int J Cancer. 2006 Jun 1;118(11):2703-10.

Bassing, C.H., J.M. Yingling, D.J. Howe, T. Wang, W.W. He, M.L. Gustafson, P. Shah, P.K. Donahoe, and X.F. Wang. 1994. A transforming growth factor beta type I receptor that signals to activate gene expression. *Science*. 263:87-9.

Bellamy TC, Garthwaite J. Pharmacology of the nitric oxide receptor, soluble guanylyl cyclase, in cerebellar cells. Br J Pharmacol. 2002 May;136(1):95-103.

Bengtsson, L., R. Schwappacher, M. Roth, J.H. Boergermann, S. Hassel, and P. Knaus. 2009. PP2A regulates BMP signalling by interacting with BMP receptor complexes and by dephosphorylating both the C-terminus and the linker region of Smad1. *J Cell Sci*. 122:1248-57.

Boehning D, Snyder SH. Novel neural modulators. Annu Rev Neurosci. 2003;26:105-31;

Butt AY, Dinh-Xuan AT, Pepke-Zaba J, Cremona G, Clelland CA, Higenbottam TW. In vitro pulmonary vasorelaxant effect of the phosphodiesterase inhibitor enoximone. Angiology. 1993 Apr;44(4):289-94.

Canalis E, Economides AN, Gazzerro E. Bone morphogenetic proteins, their antagonists, and the skeleton. Endocr Rev. 2003 Apr;24(2):218-35.

Casteel DE, Smith-Nguyen EV, Sankaran B, Roh SH, Pilz RB, Kim C. A crystal structure of the cyclic GMP-dependent protein kinase Iβ dimerization/docking domain reveals molecular details of isoform-specific anchoring. J Biol Chem. 2010 Oct 22;285(43):32684-8.

Casteel DE, Zhuang S, Gudi T, Tang J, Vuica M, Desiderio S, Pilz RB. cGMP-dependent protein kinase I beta physically and functionally interacts with the transcriptional regulator TFII-I. J Biol Chem. 2002 Aug 30;277(35):32003-14.

Chan, M.C., P.H. Nguyen, B.N. Davis, N. Ohoka, H. Hayashi, K. Du, G. Lagna, and A. Hata. 2007. A novel regulatory mechanism of the bone morphogenetic protein (BMP) signaling pathway involving the carboxyl-terminal tail domain of BMP type II receptor. *Mol Cell Biol*. 27:5776-89.

Chen, D., M. Zhao, and G.R. Mundy. 2004. Bone morphogenetic proteins. *Growth Factors*. 22:233-41.

Cheng, H., W. Jiang, F.M. Phillips, R.C. Haydon, Y. Peng, L. Zhou, H.H. Luu, N. An, B. Breyer, P. Vanichakarn, J.P. Szatkowski, J.Y. Park, and T.C. He. 2003. Osteogenic activity of the fourteen types of human bone morphogenetic proteins (BMPs). *J Bone Joint Surg Am*. 85-A:1544-52.

Chu DM, Francis SH, Thomas JW, Maksymovitch EA, Fosler M, Corbin JD. Activation by autophosphorylation or cGMP binding produces a similar apparent conformational change in cGMP-dependent protein kinase. J Biol Chem. 1998 Jun 5;273(23):14649-56.

Dan, C., A. Kelly, O. Bernard, and A. Minden. 2001. Cytoskeletal changes regulated by the PAK4 serine/threonine kinase are mediated by LIM kinase 1 and cofilin. *J Biol Chem*. 276:32115-21.

Davila M, Jhala D, Ghosh D, Grizzle WE, Chakrabarti R. Expression of LIM kinase 1 is associated with reversible G1/S phase arrest, chromosomal instability and prostate cancer. Mol Cancer. 2007 Jun 8;6:40.

Davis IW, Leaver-Fay A, Chen VB, Block JN, Kapral GJ, Wang X, Murray LW, Arendall WB 3rd, Snoeyink J, Richardson JS, Richardson DC. MolProbity: all-atom contacts and structure validation for proteins and nucleic acids. Nucleic Acids Res. 2007 Jul;35(Web Server issue):W375-83.

Dawson TM, Snyder SH. Gases as biological messengers: nitric oxide and carbon monoxide in the brain. J Neurosci. 1994 Sep;14(9):5147-59.

Deane JE, Ryan DP, Sunde M, Maher MJ, Guss JM, Visvader JE, Matthews J.M. Tandem LIM domains provide synergistic binding in the LMO4:Ldb1 complex. EMBO J. (2004); 23(18), 3589–3598.

Deng Z, Haghighi F, Helleby L, Vanterpool K, Horn EM, Barst RJ, Hodge SE, Morse JH, Knowles JA. Fine mapping of PPH1, a gene for familial primary pulmonary hyper- tension, to a 3 cM region on chromosome 2q33. Am J Respir Cr it Care Med 2000;161:1055-9.

Derynck R., Zhang YE. Smad-dependent and Smad-independent pathways in TGF-beta family signalling. Nature. 2003 Oct 9;425(6958):577-84.

Ebner, R., R.H. Chen, S. Lawler, T. Zioncheck, and R. Derynck. 1993. Determination of type I receptor specificity by the type II receptors for TGF-beta or activin. *Science*. 262:900-2.

Edwards, D.C., L.C. Sanders, G.M. Bokoch, and G.N. Gill. 1999. Activation of LIM-kinase by Pak1 couples Rac/Cdc42 GTPase signalling to actin cytoskeletal dynamics. *Nat Cell Biol*. 1:253-9.

Emsley P, Cowtan K. Coot: model-building tools for molecular graphics. Acta Crystallogr D Biol Crystallogr. 2004 Dec;60(Pt 12 Pt 1):2126-32.

Evans P. Scaling and assessment of data quality. Acta Crystallogr D Biol Crystallogr. 2006 Jan;62(Pt 1):72-82.

Evans P and McCoy A. An introduction to molecular replacement. Acta Crystallogr D Biol Crystallogr 64: 1-10.

Feng, X.H., and R. Derynck. 1997. A kinase subdomain of transforming growth factor-beta (TGF-beta) type I receptor determines the TGF-beta intracellular signaling specificity. *Embo J*. 16:3912-23.

Feng, X.H., and R. Derynck. 2005. Specificity and versatility in tgf-beta signaling through Smads. *Annu Rev Cell Dev Biol*. 21:659-93.

Foletta, V.C., M.A. Lim, J. Soosairajah, A.P. Kelly, E.G. Stanley, M. Shannon, W. He, S. Das, J. Massague, and O. Bernard. 2003. Direct signaling by the BMP type II receptor via the cytoskeletal regulator LIMK1. *J Cell Biol*. 162:1089-98.

Foletta, V.C., N. Moussi, P.D. Sarmiere, J.R. Bamburg, and O. Bernard. 2004. LIM kinase 1, a key regulator of actin dynamics, is widely expressed in embryonic and adult tissues. *Exp Cell Res*. 294:392-405.

Franzen, P., P. ten Dijke, H. Ichijo, H. Yamashita, P. Schulz, C.H. Heldin, and K. Miyazono. 1993. Cloning of a TGF beta type I receptor that forms a heteromeric complex with the TGF beta type II receptor. *Cell*. 75:681-92.

Friebe A., Koesling D. Regulation of nitric oxide-sensitive guanylyl cyclase.Circ Res. 2003 Jul 25;93(2):96-105.

Garthwaite J, Boulton CL. Nitric oxide signaling in the central nervous system. Annu Rev Physiol. 1995;57:683-706.

Garthwaite J. Concepts of neural nitric oxide-mediated transmission. Eur J Neurosci. 2008 Jun;27(11):2783-802.

Gilboa L, Nohe A, Geissendörfer T, Sebald W, Henis YI, Knaus P. Bone morphogenetic protein receptor complexes on the surface of live cells: a new oligomerization mode for serine/threonine kinase receptors. Mol Biol Cell. 2000 Mar;11(3):1023-35.

Gonzalez, L., Jr., Woolfson, D. N., and Alber, T. Buried polar residues and structural specificity in the GCN4 leucine zipper. (1996) Nat. Struct. Biol. 3, 1011–1018.

Goyal, P., D. Pandey, and W. Siess. 2006. Phosphorylation-dependent regulation of unique nuclear and nucleolar localization signals of LIM kinase 2 in endothelial cells. *J Biol Chem*. 281:25223-30.

Greenblatt MB, Shim JH, Zou W, Sitara D, Schweitzer M, Hu D, Lotinun S, Sano Y, Baron R, Park JM, Arthur S, Xie M, Schneider MD, Zhai B, Gygi S, Davis R, Glimcher LH. The p38 MAPK pathway is essential for skeletogenesis and bone homeostasis in mice.Am J Transl Res. 2010 May 10;2(3):248-53.

Gudi T, Lohmann SM, Pilz RB. Regulation of gene expression by cyclic GMP-dependent protein kinase requires nuclear translocation of the kinase: identification of a nuclear localization signal. Mol Cell Biol. 1997 Sep;17(9):5244-5254.

Goujon, M, McWilliam H, Li W, Valentin F, Squizzato S, Paern J, Lopez R. A new bioinformatics analysis tools framework at EMBL-EBI. Nucleic acids research, 2010. 38(Web Server issue): p. W695- 9.

Gouet P, Courcelle E, Stuart DI, Métoz F. ESPript: analysis of multiple sequence alignments in PostScript. Bioinformatics, 1999. 15(4): p. 305- 8.

Hassel, S., A. Eichner, M. Yakymovych, U. Hellman, P. Knaus, and S.Souchelnytskyi. 2004. Proteins associated with type II bone morphogenetic protein receptor (BMPR-II) and identified by two-dimensional gel electrophoresis and mass spectrometry. *Proteomics*. 4:1346-58.

Hassel, S., M. Yakymovych, U. Hellman, L. Ronnstrand, P. Knaus, and S. Souchelnytskyi. 2006. Interaction and functional cooperation between the serine/threonine kinase bone morphogenetic protein type II receptor with the tyrosine kinase stem cell factor receptor. *J Cell Physiol*. 206:457-67.

Hayashi, M., T. Imamura, and K. Miyazono. 2005. BMP receptors and signal transduction. *Nippon Rinsho*. 63 Suppl 10:399-403.

Heldin CH, Miyazono K, ten Dijke P. TGF-beta signalling from cell membrane to nucleus through SMAD proteins. Nature. 1997 Dec 4;390(6659):465-71.

Hiraoka J, Okano I, Higuchi O, Yang N, Mizuno K. Self-association of LIM-kinase 1 mediated by the interaction between an N-terminal LIM domain and a C-terminal kinase domain. FEBS Lett. 1996 Dec 9;399(1-2):117-21.

HofmannF. The biology of cyclic GMP-dependent protein kinases. J Biol Chem. 2005 Jan 7;280(1):1-4. Epub 2004 Nov 15.

Jin, W., C. Yun, H.S. Kim, and S.J. Kim. 2007. TrkC binds to the bone morphogenetic protein type II receptor to suppress bone morphogenetic protein signaling. *Cancer Res*. 67:9869- 77.

Kobayashi, M., M. Nishita, T. Mishima, K. Ohashi, and K. Mizuno. 2006. MAPKAPK-2- mediated LIM-kinase activation is critical for VEGF-induced actin remodeling and cell migration. *Embo J*. 25:713-26.

Koesling D, Russwurm M, Mergia E, Mullershausen F, Friebe A. Nitric oxide-sensitive guanylyl cyclase: structure and regulation. Neurochem Int. 2004 Nov;45(6):813-9.

Kretzschmar M, Doody J, Massagué J. Opposing BMP and EGF signalling pathways converge on the TGF-beta family mediator Smad1. Nature. 1997 Oct 9;389(6651):618-22.

Krumenacker JS, Hanafy KA, Murad F. Regulation of nitric oxide and soluble guanylyl cyclase. Brain Res Bull. 2004 Feb 15;62(6):505-15.

Kuo JF, Greengard P. An assay method for cyclic AMP and cyclic GMP based upon their abilities to activate cyclic AMP-dependent and cyclic GMP-dependent protein kinases. Adv Cyclic Nucleotide Res. 1972;2:41-50.

Lee-Hoeflich, S.T., C.G. Causing, M. Podkowa, X. Zhao, J.L. Wrana, and L. Attisano. 2004. Activation of LIMK1 by binding to the BMP receptor, BMPRII, regulates BMP- dependent dendritogenesis. *Embo J*. 23:4792-801.

Leslie AG. The integration of macromolecular diffraction data. Acta Crystallogr D Biol Crystallogr. 2006 Jan;62(Pt 1):48-57.

Li DY, Brooke B, Davis EC, Mecham RP, Sorensen LK, Boak BB, Eichwald E, Keating MT (1998) Elastin is an essential determinant of arterial morphogenesis. Nature 393:276-280

Li R, Soosairajah J, Harari D, Citri A, Price J, Ng HL, Morton CJ, Parker MW, Yarden Y, Bernard O. Hsp90 increases LIM kinase activity by promoting its homo-dimerization. FASEB J 2006;20:E417–E425.

Liu, F., F. Ventura, J. Doody, and J. Massague. 1995. Human type II receptor for bone morphogenic proteins (BMPs): extension of the two-kinase receptor model to the BMPs. *Mol Cell Biol*. 15:3479-86.

Lo, R.S., Y.G. Chen, Y. Shi, N.P. Pavletich, and J. Massague. 1998. The L3 loop: a structural motif determining specific interactions between SMAD proteins and TGF-beta receptors. *Embo J*. 17:996-1005.

Machado RD, Rudarakanchana N, Atkinson C, Flanagan JA, Harrison R, Morrell NW, Trembath RC. 2003. Functional interaction between BMPR-II and Tctex-1, a light chain of Dynein, is isoform-specific and disrupted by mutations underlying primary pulmonary hypertension. *Hum Mol Genet*. 12:3277-86.

Manetti F. LIM kinases are attractive targets with many macromolecular partners and only a few small molecule regulators. Med Res Rev. 2011 Jan 16.

McCoy AJ, Grosse-Kunstleve RW, Paul D. Storoni LC, Read RJ. Likelihood-enhanced fast translation functions. Acta Crystallogr D Biol Crystallogr. 2005 Apr;61(Pt 4):458-64.

Meyer-Lindenberg, A., C.B. Mervis, and K.F. Berman. 2006. Neural mechanisms in Williams syndrome: a unique window to genetic influences on cognition and behaviour. *Nat Rev Neurosci*. 7:380-93.

Misra, U.K., R. Deedwania, and S.V. Pizzo. 2005. Binding of activated alpha2-macroglobulin to its cell surface receptor GRP78 in 1-LN prostate cancer cells regulates PAK-2-dependent activation of LIMK. *J Biol Chem*. 280:26278-86.

Mizuno, K., I. Okano, K. Ohashi, K. Nunoue, K. Kuma, T. Miyata, and T. Nakamura. 1994. Identification of a human cDNA encoding a novel protein kinase with two repeats of the LIM/double zinc finger motif. *Oncogene*. 9:1605-12.

Müller U. The nitric oxide system in insects. Prog Neurobiol. 1997 Feb;51(3):363-81.

Murshudov GN, Vagin AA, Dodson EJ. Refinement of macromolecular structures by the maximum-likelihood method. Acta Crystallogr D Biol Crystallogr. 1997 May 1;53(Pt 3):240-55.

Nagata, K., K. Ohashi, N. Yang, and K. Mizuno. 1999. The N-terminal LIM domain negatively regulates the kinase activity of LIM-kinase 1. *Biochem J*. 343 Pt 1:99-105.

Niesen FH, Berglund H, Vedadi M. The use of differential scanning fluorimetry to detect ligand interactions that promote protein stability. Nat Protoc. 2007;2(9):2212-21.

Nishitoh, H., H. Ichijo, M. Kimura, T. Matsumoto, F. Makishima, A. Yamaguchi, H. Yamashita, S. Enomoto, and K. Miyazono. 1996. Identification of type I and type II serine/threonine kinase receptors for growth/differentiation factor-5. *J Biol Chem*. 271:21345-52.

Nishiya N, Sabe H, Nose K, Shibanuma M. The LIM domains of hic-5 protein recognize specific DNA fragments in a zinc-dependent manner in vitro. Nucleic Acids Res. 1998 Sep 15; 26(18):4267-73.

Nohe A, Hassel S, Ehrlich M, Neubauer F, Sebald W, Henis YI, Knaus P. The mode of bone morphogenetic protein (BMP) receptor oligomerization determines different BMP-2 signaling pathways. J Biol Chem. 2002 Feb 15; 277(7):5330-8.

Nohno, T., T. Ishikawa, T. Saito, K. Hosokawa, S. Noji, D.H. Wolsing, and J.S. Rosenbaum. 1995. Identification of a human type II receptor for bone morphogenetic protein-4 that forms differential heteromeric complexes with bone morphogenetic protein type I receptors. *J Biol Chem*. 270:22522-6.

Okano I, Hiraoka J, Otera H, Nunoue K, Ohashi K, Iwashita S, Hirai M, Mizuno K. Identification and characterization of a novel family of serine/threonine kinases containing two N-terminal LIM motifs. J Biol Chem. 1995 Dec 29; 270(52):31321-30.

Olson MF, Sahai E. The actin cytoskeleton in cancer cell motility. Clin Exp Metastasis. 2009; 26(4):273-87.

Ørstavik S, Natarajan V, Taskén K, Jahnsen T, Sandberg M. Characterization of the human gene encoding the type I alpha and type I beta cGMP-dependent protein kinase (PRKG1). Genomics. 1997 Jun 1;42(2):311-8.

Osborne BW, Wu J, McFarland CJ, Nickl CK, Sankaran B, Casteel DE, Woods VL Jr, Kornev AP, Taylor SS, Dostmann WR. Crystal structure of cGMP-dependent protein

kinase reveals novel site of interchain communication. Structure. 2011 Sep 7;19(9):1317-27.

Osyczka AM, Leboy PS. Bone morphogenetic protein regulation of early osteoblast genes in human marrow stromal cells is mediated by extracellular signal-regulated kinase and phosphatidylinositol 3-kinase signaling. Endocrinology. 2005 Aug;146(8):3428-37.

Painter J, Merritt EA. Optimal description of a protein structure in terms of multiple groups undergoing TLS motion. Acta Crystallogr D Biol Crystallogr. 2006 Apr;62(Pt 4):439-50.

Perrakis A, Morris R, Lamzin VS. Automated protein model building combined with iterative structure refinement. Nat Struct Biol. 1999 May;6(5):458-63.

Podkowa M, Zhao X, Chow CW, Coffey ET, Davis RJ, Attisano L. Microtubule stabilization by bone morphogenetic protein receptor-mediated scaffolding of c-Jun N-terminal kinase promotes dendrite formation. Mol Cell Biol. 2010 May;30(9):2241-50.

Proschel, C., M.J. Blouin, N.J. Gutowski, R. Ludwig, and M. Noble. 1995. Limk1 is predominantly expressed in neural tissues and phosphorylates serine, threonine and tyrosine residues in vitro. *Oncogene*. 11:1271-81.

Resing KA, Johnson RS, Walsh KA. Mass Spectrometric Analysis of 21 Phosphorylation Sites in the Internal Repeat of Rat Profilaggrin, Precursor of an Intermediate Filament Associated Protein. *Biochemistry*, 1995, *34* (29), pp 9477–9487

Rosenzweig, B.L., T. Imamura, T. Okadome, G.N. Cox, H. Yamashita, P. ten Dijke, C.H. Heldin, and K. Miyazono. 1995. Cloning and characterization of a human type II receptor for bone morphogenetic proteins. *Proc Natl Acad Sci U S A*. 92:7632-6.

Sachdev, P., S. Menon, D.B. Kastner, J.Z. Chuang, T.Y. Yeh, C. Conde, A. Caceres, C.H. Sung, and T.P. Sakmar. 2007. G protein beta gamma subunit interaction with the dynein light- chain component Tctex-1 regulates neurite outgrowth. *Embo J*. 26:2621-32.

Schmierer, B., and C.S. Hill. 2007. TGFbeta-SMAD signal transduction: molecular specificity and functional flexibility. *Nat Rev Mol Cell Biol*. 8:970-82.

Schwappacher, R., J. Weiske, E. Heining, V. Ezerski, B. Marom, Y.I. Henis, O. Huber, and P. Knaus. 2009. Novel crosstalk to BMP signalling: cGMP-dependent kinase I modulates BMP receptor and Smad activity. *Embo J*. 28:1537-50.

Scott RW, Hooper S, Crighton D, Li A, König I, Munro J, Trivier E, Wickman G, Morin P, Croft DR, Dawson J, Machesky L, Anderson KI, Sahai EA, Olson MF. LIM kinases are required for invasive path generation by tumor and tumor-associated stromal cells. J Cell Biol. 2010 Oct 4;191(1):169-85.

Shi, Y., and J. Massague. 2003. Mechanisms of TGF-beta signaling from cell membrane to the nucleus. *Cell*. 113:685-700.

Shim JH, Greenblatt MB, Xie M, Schneider MD, Zou W, Zhai B, Gygi S, Glimcher LH. TAK1 is an essential regulator of BMP signalling in cartilage. EMBO J. 2009 Jul 22;28(14):2028-41.

Smith, WC, Harland RM. Expression cloning of noggin, a new dorsalizing factor localized to the Spemann organizer in Xenopus embryos. Cell, 1992. 70(5): p. 829-40.

Soosairajah, J., S. Maiti, O. Wiggan, P. Sarmiere, N. Moussi, B. Sarcevic, R. Sampath, J.R. Bamburg, and O. Bernard. 2005. Interplay between components of a novel LIM kinase- slingshot phosphatase complex regulates cofilin. *Embo J*. 24:473-86.

Souchelnytskyi, S., K. Tamaki, U. Engstrom, C. Wernstedt, P. ten Dijke, and C.H. Heldin. 1997. Phosphorylation of Ser465 and Ser467 in the C terminus of Smad2 mediates interaction with Smad4 and is required for transforming growth factor-beta signaling. *J Biol Chem*. 272:28107-15.

ten Dijke, P. 2006. Bone morphogenetic protein signal transduction in bone. *Curr Med Res Opin*. 22 Suppl 1:S7-11.

ten Dijke, P., and C.S. Hill. 2004. New insights into TGF-beta-Smad signalling. *Trends Biochem Sci*. 29:265-73.

ten Dijke, P., H. Yamashita, T.K. Sampath, A.H. Reddi, M. Estevez, D.L. Riddle, H. Ichijo, C.H. Heldin, and K. Miyazono. 1994. Identification of type I receptors for osteogenic protein-1 and bone morphogenetic protein-4. *J Biol Chem*. 269:16985-8.

Toshima J, Toshima JY, Amano T, Yang N, Narumiya S, Mizuno K. Cofilin Phosphorylation by Protein Kinase Testicular Protein Kinase 1 and Its Role in Integrin-mediated Actin Reorganization and Focal Adhesion Formation. Mol Biol Cell. (2001); 12(4): 1131-45.

Tursun, B., A. Schluter, M.A. Peters, B. Viehweger, H.P. Ostendorff, J. Soosairajah, A. Drung, M. Bossenz, S.A. Johnsen, M. Schweizer, O. Bernard, and I. Bach. 2005. The ubiquitin ligase Rnf6 regulates local LIM kinase 1 levels in axonal growth cones. *Genes Dev*. 19:2307-19.

Urist, M.R. 1965. Bone: formation by autoinduction. *Science*. 150:893-9.

Vedadi M, Niesen FH, Allali-Hassani A, Fedorov OY, Finerty PJ Jr, Wasney GA, Yeung R, Arrowsmith C, Ball LJ, Berglund H, Hui R, Marsden BD, Nordlund P, Sundstrom M, Weigelt J, Edwards AM. Chemical screening methods to identify ligands that promote protein stability, protein crystallization, and structure determination. Proc Natl Acad Sci U S A. 2006 Oct 24;103(43):15835-40.

Vorster PJ, Guo J, Yoder A, Wang W, Zheng Y, Xu X, Yu D, Spear M, Wu Y. LIM kinase 1 modulates cortical actin and CXCR4 cycling and is activated by HIV-1 to initiate viral infection. J Biol Chem. 2011 Apr 8;286(14):12554-64.

Wall ME, Francis SH, Corbin JD, Grimes K, Richie-Jannetta R, Kotera J, Macdonald BA, Gibson RR, Trewhella J. *Mechanisms associated with cGMP binding and activation of cGMP-dependent protein kinase*. Proc Natl Acad Sci U S A, 2003. 100(5): p. 2380-5.

West, J., K. Fagan, W. Steudel, B. Fouty, K. Lane, J. Harral, M. Hoedt-Miller, Y. Tada, J. Ozimek, R. Tuder, and D.M. Rodman. 2004. Pulmonary hypertension in transgenic mice expressing a dominant-negative BMPRII gene in smooth muscle. *Circ Res*. 94:1109-14.

Wieser, R., L. Attisano, J.L. Wrana, and J. Massague. 1993. Signaling activity of transforming growth factor beta type II receptors lacking specific domains in the cytoplasmic region. *Mol Cell Biol*. 13:7239-47.

Wong, W.K., J.A. Knowles, and J.H. Morse. 2005. Bone morphogenetic protein receptor type II C-terminus interacts with c-Src: implication for a role in pulmonary arterial hypertension. *Am J Respir Cell Mol Biol*. 33:438-46.

Wrana, J.L., L. Attisano, J. Carcamo, A. Zentella, J. Doody, M. Laiho, X.F. Wang, and J. Massague. 1992. TGF beta signals through a heteromeric protein kinase receptor complex. *Cell*. 71:1003-14.

Wrana, J.L., L. Attisano, R. Wieser, F. Ventura, and J. Massague. 1994. Mechanism of activation of the TGF-beta receptor. *Nature*. 370:341-7.

Wrana, J.L. 2000. Crossing Smads. *Sci STKE*. 2000:re1.

Wu, M.Y., and C.S. Hill. 2009. Tgf-beta superfamily signaling in embryonic development and homeostasis. *Dev Cell*. 16:329-43.

Yamaguchi K, Nagai S, Ninomiya-Tsuji J, Nishita M, Tamai K, Irie K, Ueno N, Nishida E, Shibuya H, Matsumoto K XIAP, a cellular member of the inhibitor of apoptosis protein family, links the receptors to TAB1-TAK1 in the BMP signaling pathway. (1999) EMBO J. 18, 179 –187.

Yanagita, M. 2009. BMP modulators regulate the function of BMP during body patterning and disease progression. *Biofactors*. 35:113-9.

Yang X, Yu K, Hao Y, Li DM, Stewart R, Insogna KL, Xu T. LATS1 tumour suppressor affects cytokinesis by inhibiting LIMK1. Nat Cell Biol. 2004 Jul;6(7):609-17.

Yoshioka K, Foletta V, Bernard O, Itoh K. A role for LIM kinase in cancer invasion. A role for LIM kinase in cancer invasion. Proc Natl Acad Sci U S A. 2003 Jun 10;100(12):7247-52.

Zhang K. Y. J., Cowtan K., Main P. (1997) Combining constraints for electron-density modification. Methods in Enzymology, 277, 53-64.

9 Curriculum Vitae

For reasons of data protection,
the curriculum vitae is not included in the online version.